Next-to-soft factorization and unitarity in Drell-Yan processes

Domenico Bonocore

Cover illustration by: Federica Poerio
Printed by: Proefschriftmaken.nl || Uitgeverij BOXPress.
ISBN: 978-94-629-5484-7

This work was supported by the Research Executive Agency (REA) of the European Union under the Grant Agreements number PITN-GA-2010-264564 (LHCPhenoNet) and PITN-GA- 2012-316704 (HIGGSTOOLS) and is part of the research programme of the Foundation for Fundamental Research on Matter (FOM), which is part of the Netherlands Organisation for Scientific Research (NWO), programme 104 “Theoretical Particle Physics in the Era of the LHC” and programme 156 “Higgs as Probe and Portal”.

Next-to-soft factorization and unitarity in Drell-Yan processes

ACADEMISCH PROEFSCHRIFT

ter verkrijging van de graad van doctor
aan de Universiteit van Amsterdam
op gezag van de Rector Magnificus
prof. dr. D.C. van den Boom
ten overstaan van een door het College voor Promoties ingestelde commissie,
in het openbaar te verdedigen in de Aula der Universiteit
op woensdag 18 mei 2016, te 11:00 uur

door

Domenico Bonocore

geboren te Genua, Italië

Promotiecommissie:

Promotor:	prof. dr. E.L.M.P. Laenen	Universiteit van Amsterdam
Copromotor:	dr. C.D. White	University of Glasgow
Overige leden:	prof. dr. W.J.P. Beenakker	Universiteit van Amsterdam
	prof. dr. S.C.M. Bentvelsen	Universiteit van Amsterdam
	prof. dr. R. Fleischer	Vrije Universiteit Amsterdam
	prof. dr. L. Magnea	University of Turin
	prof. dr. P.J.G. Mulders	Vrije Universiteit Amsterdam
	prof. dr. E.P. Verlinde	Universiteit van Amsterdam
	dr. W.J. Waalewijn	Universiteit van Amsterdam

Faculteit der Natuurwetenschappen, Wiskunde en Informatica

This thesis is based on the following publications

- Domenico Bonocore, E. Laenen, L. Magnea, L. Vernazza and C. D. White
  "*The method of regions and next-to-soft corrections in Drell-Yan production*"
  Phys.Lett. **B742** (2015) 375–382, arXiv:1410.6406 [hep-ph],

- Domenico Bonocore, E. Laenen, L. Magnea, S. Melville, L. Vernazza and C. D. White
  "*A factorization approach to next-to-leading-power threshold logarithms*"
  JHEP **1506** (2015) 008, arXiv:1503.05156 [hep-ph],

- Domenico Bonocore, E. Laenen and R. Rietkerk
  "*Unitarity methods for Mellin moments of Drell-Yan cross sections*"
  arXiv:1603.05252 [hep-ph],

and the following conference proceedings

- Domenico Bonocore
  "*Universal structure of Drell-Yan beyond threshold*"
  to appear on PoS RADCOR **2015**, (2015), arXiv:1512.05364 [hep-ph],

- Domenico Bonocore, E. Laenen, L. Magnea, S. Melville, L. Vernazza and C. D. White
  "Next-to-leading power threshold logarithms: a status report"
  to appear on PoS RADCOR **2015**, (2015), arXiv:1602.01988 [hep-ph].

Contents

CHAPTER 1

Introduction

Perturbative calculations in quantum field theories, and Quantum Chromodynamics (QCD) in particular, are the cornerstone in current research in high energy physics. Experiments at hadron colliders demand maximally precise calculations to reduce the theoretical uncertainty on observables. The combination of experimental and theoretical efforts to reduce these uncertainties is key to making discoveries in collider physics, and is highly important to extract maximum information from reactions involving e.g. the recently discovered Higgs boson [1,2].

Among the ample recent progress directly significant for phenomenology (for a recent review see e.g. [3–5]) we mention a precise determination of parton distribution functions and their uncertainties [6,7], the development of jet algorithms and the study of internal jet substructures [8], the automation of event generators at NLO [9] and towards NNLO [10–12] and the develpment of new tools for hard partonic scattering higher order [13–15] (that most notably culminated in the computation of the Higgs cross-section at the impressive N^3LO accuracy [16]).

This field is often regarded as a somewhat technical area, where it is difficult to develop new interesting insights and the only aim is extending precision to ever more digits. Although this is the driving force of this field, there is more structure than meets the eye. Indeed, though the study of perturbative quantum field theories is quite old, it continues to be an active area in revealing new elegant mathematical structures.

For instance, the search for an efficient evaluation of Feynman diagrams led to the introduction in physics of so-called symbol technology [13]. This, together with the recently improved approach of using differential equations [14, 17], was key in the classification of functions in the result of Feynman diagrams in terms of generalized polylogarithms [13]. Unitarity methods [18–22] have been very successful for processes with large number of external legs [23] and led to a number of studies of scattering

amplitudes from more formal point of view, both in gauge and gravity theories [24–30].

Therefore, the field of perturbative calculations is an active area that is relevant both for phenomenology and for more formal applications. In this context, this thesis aims at investigating different aspects of perturbative QCD considering the specific case of the Drell-Yan process.

Drell-Yan processes

The Drell-process is one of the most well-studied processes and is the prototype for many other processes at hadron colliders. It describes the creation of a lepton-antilepton pair of invariant mass Q^2 through

$$h_1 + h_2 \to \ell + \bar{\ell} + X \,, \tag{1.1}$$

where h_1 and h_2 are two hadrons and X represents any other non-measured final states. The production mechanism happens through the creation of an intermediate state of invariant mass Q^2. As shown in Fig. 1.1 for the muon-antimuon case, this can be quite generally a meson or an electroweak boson. However, in this thesis we will focus on the case of the production of an off-shell photon $\gamma^*(Q^2)$, without explicitly including its subsequent decay into the lepton pair. Moreover, we will restrict our analysis to the quark-antiquark channel of the partonic cross-section.

To stress the relevance of this process, we note that the original work of Drell and Yan [32] was the first application in hadronic interactions of the parton model, originally developed for Deep Inelastic Scattering (DIS). Moreover, it was the theoretical interpretation behind more than one breakthrough discovery in particle physics and served as a benchmark for the experimental confirmation of the Standard Model. For instance, it led to the Nobel prize discovery of the J/Ψ particle at Brookhaven National Laboratory in 1974, through the analysis of proton-nucleus collisions of the form $p + \text{Be} \to e^+ + e^- + X$ that proved the existence of the charm quark [33]. In 1977 at Fermilab it led to discovery of the Y particle through proton-nucleus collisions of the form $p + \text{Cu/Pt} \to \mu^+ + \mu^- + X$, which proved the existence of the bottom quark [34]. Then, in 1983 it led to the Nobel prize discovery of the $W^\pm$ and Z bosons at the Super Proton Synchrotron via proton-antiproton collisions [35–38]. Nowadays it is a benchmark process for the physics at the Large Hadron Collider (LHC), as it provides valuable information on precision measurements of the properties of the $W^\pm$ and Z bosons, and constitutes a sensitive test for many new physics models.

From the computational point of view, the relevance of QCD corrections for this process was soon realized and the first next-to-leading order (NLO) inclusive cross-section appeared in 1979 [39]. More that ten years passed until the next-to-next-to-leading

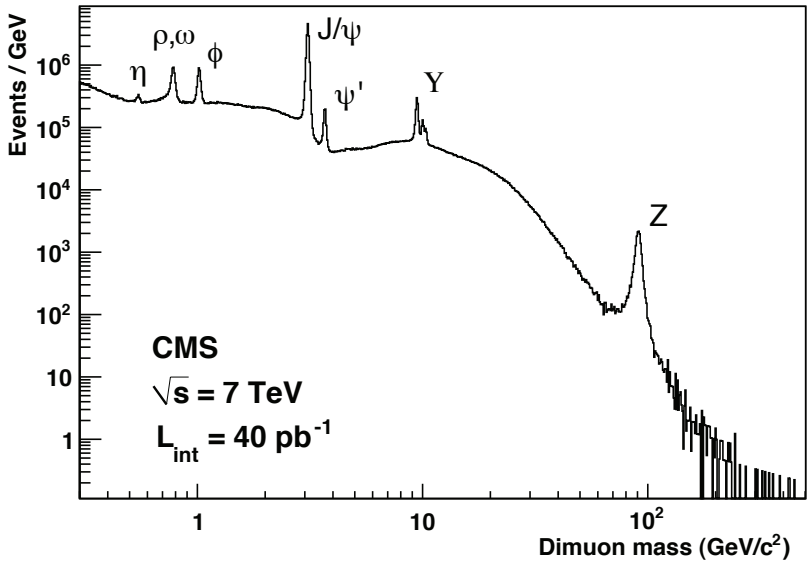

Figure 1.1: Cross-section measured in the CMS detector at the LHC in the $\mu^+\mu^-$ channel as a function of the $\mu^+\mu^-$ invariant mass [31]. In the peaks we note the resonant production of the mesons η, ϕ, J/Ψ and Y and of the Z boson.

order (NNLO) matrix elements were published [40, 41], and even more years for rapidity distributions [42], while fully differential distributions at NNLO were computed only in the last decade [43, 44]. The importance of these computations goes beyond the pure application in Drell-Yan measurements as they provides important tools also for other processes, most notably for the Higgs boson production via gluon-fusion, which it shares many features with.

This thesis

Despite this long history, in this thesis we will show that the Drell-Yan process can still reveal surprising new insights in theoretical developments for perturbative quantum field theory. In particular, we will use it as a case study to investigate two different aspects of perturbative QCD: all-order corrections and "next-to-soft" factorization [45–48], and the issue of unitarity and the development of new methods for fixed-order computations [49].

As we will discuss in detail in the following chapters, soft and collinear radiation originates logarithms that in the Drell-Yan case depend on a variable $z = Q^2/s$, where s is the incoming partonic center-of-mass energy squared and z measures the distance to threshold $s \to Q^2$. These logarithms (called threshold logarithms) might damage the pre-

dictivity of perturbation theory and need to be resummed to all orders. Much is known about this resummation at leading power (LP) while no systematic framework is known at next-to-leading power (NLP). In this thesis, we will tackle this issue by investigating soft and collinear radiation at subleading power, known as "next-to-soft". Focusing on the NNLO Drell-Yan cross-section, we will investigate these next-to-soft corrections with three different approaches: the use diagrammatic techniques, the expansion by regions and the soft-collinear factorization formula. The final result of this process will be the definition of a next-to-soft factorization formalism with predictive power for all NLP threshold logarithms.

At the same time the Drell-Yan process shows also interesting insights from the point of view of developing new methods for fixed order computation. Indeed, the inclusiveness of a cross-section in terms of QCD radiation might make its analytic structure relatively simpler and hence suggests the search for alternative methods for its computation. This is certainly the case for the fully inclusive DIS, where the optical theorem and the operator product expansion made possible a three-loop calculation more than a decade ago. Processes like Drell-Yan or Higgs production, even though they are only one-particle inclusive, possess a quite simple structure since the kinematics is contained in one single dimensionless variable. We will then be able to generalize the use of unitarity from DIS to the Drell-Yan case, which will require moving from the optical theorem to the more general use of unitary cuts.

The structure of this thesis is as follows. In Chapter 2 we review the basis of soft-collinear factorization, referring in particular to the case of the quark form factor, which will be relevant in the application to the Drell-Yan case. Then, in Chapter 3 we present a first attempt to organize next-to-soft corrections by means of diagrammatic techiniques. In Chapter 4, which is based on [45], we present a calculation based on the so-called method of regions, by means of which is it possible to analyze the entire soft and collinear logarithmic structure of the NNLO cross-section. However, though powerful, it does not give any information toward higher orders. This step will instead be achieved in Chapter 5, based on [46], by means of the soft-collinear factorization formula derived in Chapter 2. Finally, in Chapter 6, which is based on [49], we will develop a new method to compute NNLO Drell-Yan corrections making use of unitarity in Mellin space.

CHAPTER 2

Soft and collinear factorization

A central theme in this thesis is the analysis of soft and collinear singularities, from here on occasionally referred to collectively as infrared (IR) singularities. These plague QCD perturbation theory giving rise to large logarithms that need to be resummed to all orders. The standard procedure to achieve this resummation usually passes through factorization. This can be understood referring to the perhaps more familiar ultraviolet (UV) renormalization: when operators are multiplicatively renormalizable, it is possible to write an evolution equation whose solution resums all logarithms involving the renormalization scale. Following the same strategy, we can factorize soft and collinear emissions from the hard part of the process in terms of universal functions. Upon writing an evolution equation for these, we can eventually get an all-order formula where the contributions of soft and collinear origin are resummed.

This approach is nowadays a well-establish field, where many results have been obtained for various cross-sections. Many of the insights in this area were developed in the context of factorization for full QCD, and refer to the work done mainly by Collins, Soper and Sterman in the '80s and '90s [50–53], where factorization theorems for various processes are derived from first principles of QCD. This is the approach followed in this thesis, and its key aspects will be reviewed in this chapter.

An alternative approach that has become very popular in last decade is given by the use of soft-collinear effective field theories (SCET) [54–57]: in that context factorization theorems are elegantly derived at the Lagrangian level, where soft and collinear modes are defined through independent fields and effective operators describe their interaction. Clearly, there are many connections between this and the more traditional diagrammatic approach followed in this thesis.

The goal of this chapter is to introduce the key aspects of soft-collinear factorization that will be relevant for the subsequent chapters of this thesis. In particular, we will

focus on the specific example of the quark form factor which will be central for the investigation of the Drell-Yan process. However, many of the observations are quite general and can be implemented in more complicated cases. We note that even if a proof is presented, we will not aim to be fully comprehensive, but refer the reader to the extensive literature for a more detailed discussion. Specifically, we will follow the approach of [58–61].

The structure of the chapter is as follows. In the first section, we start with very general considerations about Feynman integrals, showing how singularities can be identified. Then, we restrict our analysis to the case of the quark form factor. For this specific case, we will organize singularities to all orders in leading singular regions, and we will see how these can be disentangled by means of diagrammatic techniques. After this set up, we will construct an operator interpretation for these regions. Finally, we will implement this formalism to the one-loop accuracy.

2.1 Singularities of Feynman integrals

Divergences are usually regarded as a troublesome feature of the theory and often that is the case from the merely computational point of view. However, from a more theoretical perspective, scattering amplitudes must be regarded as complex-valued integrals in the complex plane and, in the spirit of Cauchy's theorem, all the information is encoded in their singularity structure. Before discussing how to systematically identify the singularities of a generic diagram, let us recall how these arise in perturbative calculations.

Perhaps the best known singularity is the ultraviolet (UV) divergence. Such divergences are completely under control with standard renormalization techniques and will not be discussed here. But there are other singularities. If we consider for example amplitudes involving massive particles, when the energy is sufficient to produce new particles at rest, divergences known as **threshold** singularities appear. With massless particles, instead, we have to deal with IR divergences.

To illustrate this point, let us consider the scalar propagator

$$\frac{1}{(p+k)^2+i\eta} = \frac{1}{2p\cdot k+i\eta}\,, \tag{2.1}$$

where we assumed that both p and k are on-shell momenta. Let us also assume that p belongs to a fermion and k to a gluon. Infrared singularities arise when the denominator vanishes.

Two cases are possible:

- $k^\mu = 0$ (**soft** singularity)
- $p \cdot k = 0$ (**collinear** singularity)

The case $p^\mu = 0$ is not considered since, as we will see, a fermion never develops a soft singularity by power counting. While the soft singularity is present also after Wick rotating to the euclidean space-time, the collinear singularity is a specific feature of the Minkowski signature. In dimensional regularization with space-time dimension $d = 4 - 2\varepsilon$ each of these give rise to a single pole ε^{-1}, order by order in perturbation theory. Of course the emission can be soft and collinear at the same time, and this would give rise to a double pole ε^{-2}.

However, as we will discuss in detail, the vanishing of a denominator is not a sufficient condition for an actual diagram to be singular: propagators are part of a full integrand with numerator insertions that must be integrated over loop momenta. Hence, some of the singularities might actually be integrable. Let us now make these preliminary considerations more systematic.

We consider a generic graph $G(p_1, \dots, p_E)$ with L-loop, E-external legs and I-internal lines. It can be written as

$$G(p_1, \dots, p_E) = \left(\prod_{j=1}^{L} \int \frac{d^d k_j}{(2\pi)^d} \right) \frac{\mathcal{N}(p_r, k_j)}{\prod_{i=1}^{I} (\ell_i^2 - m_i^2 + i\eta)} \,, \tag{2.2}$$

where $r = (1, \dots, E)$, m_i and $\ell_i = \ell_i(p_r, k_j)$ are respectively the mass and the momentum of the i-th propagator, which is function of the external momenta p_r and loop momenta k_j. Introducing I Feynman parameters x_i this becomes

$$G(p_1, \dots, p_E) = \left(\prod_{i=1}^{I} \int_0^1 dx_i \right) \delta(1 - \sum_{k=1}^{I} x_k) \left(\prod_{j=1}^{L} \int \frac{d^d k_j}{(2\pi)^d} \right) \frac{\widetilde{\mathcal{N}}(p_r, k_j, x_i)}{[\mathcal{D}(p_r, k_j, x_i)]^I} \,, \tag{2.3}$$

where $\widetilde{\mathcal{N}}(p_r, k_j, x_i)$ gathers all numerator factors after the parametrization and

$$\mathcal{D}(p_r, k_j, x_i) = \sum_{i=1}^{I} x_i \left(\ell_i^2 - m_i^2 \right) + i\eta \,. \tag{2.4}$$

Landau [62] found a set of necessary (but not sufficient) conditions for such a general Feynman integral to be divergent. The analysis starts from the observation that the integrand must be read as a function of the complex integration variables (Feynman

parameters x_i and loop momenta k_j^μ). Potential singularities correspond to the zeroes of the denominator

$$\mathcal{D}(p_r, k_j, x_i) = 0 \,. \tag{2.5}$$

However, if the path of integration can avoid this singularity by deforming the contour in the (x_i, k_j^μ) space, then by Cauchy's theorem the integral is not divergent. Thus we have to find the conditions that ensure that such a deformation is not possible in *any* direction of this $(d \times L + I)$-dimensional space.[1] This possibility is realized differently for k_j^μ and x_i integrations:

- Two singularities can merge at the same point and "pinch" the contour (**pinch singularity**). This is possible only for k_j^μ integrations (and not for x_i), since denominators are quadratic in k_j^μ (and linear in x_i) and two zeroes can merge in a single point. The condition for this to happen is

  $$\frac{\partial\, \mathcal{D}(p_r, k_j, x_i)}{\partial\, k_n^\mu} = 0 \,, \tag{2.6}$$

  which combined with Eq. (2.4) gives

  $$\sum_{i=1}^{I} x_i \frac{\partial \ell_i^2(p_r, k_j)}{\partial k_n^\mu} = 0 \,, \tag{2.7}$$

  or more explicitly

  $$\sum_{j \in \text{loop } n} x_j \, \ell_j^\mu \, \sigma_{j,n} = 0 \,, \tag{2.8}$$

  where $\sigma_{j,n}$ is +1 if the line momentum ℓ_j in the loop n flows in the same direction as the loop momentum k_n, -1 if in the opposite direction, zero otherwise.

- The singularity can be located at the end of the integration contour (**endpoint singularity**). For k_j^μ integrations this would correspond to the standard UV divergence which is treated by renormalization and is not of interest here, since each k_j^μ runs from $-\infty$ to $+\infty$. Endpoint singularities instead are relevant for non-UV divergences, specifically for x_i integrations, when

  $$x_i = 0 \,, \tag{2.9}$$

  ($x_i = 1 \; \forall i$ does not fulfill the condition $\mathcal{D} = 0$). However, if $\mathcal{D}$ does not depend on x_i, this condition cannot be applied. In that case we simply demand that

  $$\partial \mathcal{D} / \partial x_i = 0 \,, \tag{2.10}$$

[1] Indeed even if a single variable does not satisfy this condition, we can modify the contour in this subspace.

which amounts to requiring that the corresponding denominator $\ell_i^2 - m_i^2$ vanishes. So in conclusion we can combine 2.9 and 2.10 into

$$x_i \, \frac{\partial \mathcal{D}}{\partial x_i} = 0 \, . \tag{2.11}$$

These considerations constitute the Landau equations: they state that a necessary condition for a Feynman amplitude to be divergent is that its denominator must have a pinch singularity for *all* loop momenta components k_j^μ , and for *every* x_i either must have an endpoint singularity or must not depend on it:

$$\begin{cases} \displaystyle\sum_{j \in \text{loop } n} x_j \, \ell_j^\mu \, \sigma_{j,n} = 0 \qquad \forall \mu, n \, , \\ x_i \, \left(\ell_i^2 - m_i^2 \right) = 0 \qquad \forall i \, . \end{cases} \tag{2.12}$$

Every singularity of a diagram is a solution of these equations. The use of line momenta $\ell = \ell(p_r, k_j)$ hides the fact that many ingredients are involved, and it might not be immediately clear which are the unknowns that these relations must constrain and which the parameters to be kept fixed. In this regard we can distinguish two different classes of solutions:

- solutions that constrain external momenta, which means that the integral is divergent for a particular kinematical configuration. This is the case for **threshold** singularities.
- solutions for a given fixed set of masses and external momenta. This is the case for **soft** and **collinear** singularities.

In Section 2.3 this machinery will become much clearer when we will explicitly solve Landau equations for the one-loop quark form factor. However, at higher orders, finding solutions to Landau equations becomes difficult. Fortunately, thanks to Coleman and Norton [63], there is a much shorter and more intuitive way to solve this problem.

The starting point for the Coleman-Norton prescription is that the Landau equations can be read as a different prescription for on-shell and off-shell lines: for the former $x_i \neq 0$ and we demand $\partial \mathcal{D} / \partial k_j^\mu = 0$, while for the latter simply $x_i = 0$. We can define

$$\Delta s_i^\mu \equiv x_i \ell_i^\mu \, , \tag{2.13}$$

whose spatial component can be interpreted as the displacement done in a proper time $x_i \ell_i^0$ of a classical particle with momentum ℓ_i^μ and four-velocity $v^\mu = (1, \overrightarrow{\ell_i} / \ell_i^0)$. Then the

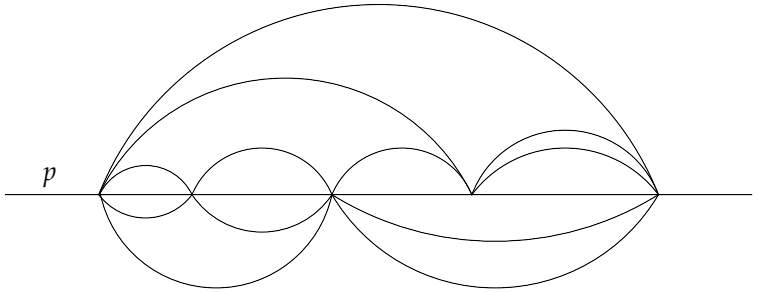

Figure 2.1: A reduced diagram for a 2-point function corresponding to the threshold solution $p^2 = 36m^2$. In the rest frame of the initial particle, there are always 6 particles at rest relative to one another. The trajectories of the massive particles are drawn as separate for clarity, but their relative momenta are zero.

Landau equations become:

$$\begin{cases} \displaystyle\sum_{j\in\text{loop } n} \Delta s_j^\mu \, \sigma_{j,n} = 0 & \text{if} \quad \ell_j^2 = m_j^2 \,, \\ \Delta s_i^\mu = 0 & \text{if} \quad \ell_i^2 \neq m_i^2 \,. \end{cases} \tag{2.14}$$

In this picture the "pinch condition" ($\partial\mathcal{D}/\partial k_j^\mu = 0$) for on-shell lines ($\partial\mathcal{D}/\partial x_i = 0$) is equivalent to the requirement that every loop made out of these corresponds to a closed classical path (in the sense of a free propagation between vertices). Then these on-shell lines make the diagram singular only if the off-shell ones do not propagate ("endpoint condition" $x_i = 0$).

Therefore every singularity of a given diagram can be represented as the original diagram where some lines are kept off-shell (and thus shrunk into a point) and others are kept on-shell and correspond to allowed classical trajectories with the given momenta. Hence the task of finding all possible solutions to Landau equations is now simplified to the graphical exercise of drawing all possible (classically allowed) reduced diagrams.

To see the power of the Coleman-Norton method at every order, let us apply it to the 2-point functions, as shown in Fig. 2.1. The scalar 2-point functions have *only* normal threshold singularities, which correspond to the case when the momentum p satisfy

$$p^2 = n^2 m^2 \,, \tag{2.15}$$

where m is the mass of the scalar fields. This can be easily seen in the reference frame where $p^\mu = \{\sqrt{p^2}, 0, 0, 0\}$: the allowed Coleman-Norton process corresponds to the production of n particles at relative rest among each other. Every further particle created with non-vanishing momentum must be balanced by another one in the opposite

direction, by momentum conservation. But then in a free propagation they cannot meet again, and thus this process is not allowed. We conclude that there are no singularities other than normal thresholds. In the limit $m \to 0$ the spectrum of solutions becomes degenerate and corresponds to collinear solutions: in a semiclassical picture the only way n massless particles can recombine is if they have mutually collinear momenta. Soft divergences instead cannot arise here.

2.2 Leading regions and power counting

The discussion until now has been very general, allowing also for the presence of massive particles. Now we focus on diagrams formed exclusively of massless lines. In this case, solutions to Landau equations will not include threshold singularities but only soft and collinear ones. Their general structure at all orders can be organized by the use of reduced diagrams in the Coleman-Norton picture. Indeed, as we have seen, in a reduced diagram all lines are on-shell and in the massless case they can be either soft or collinear (non-singular lines are off-shell and have been contracted to a point). Now we can introduce some definitions for the elements of such reduced diagrams.

A connected set of massless collinear lines is called a *jet subdiagram*. A set of massless soft lines (not necessarily connected) whose momenta vanish in all the four components is called a *soft subdiagram*. A vertex where lines from different jet subdiagrams meet is called a *hard vertex* while a vertex between a jet and a soft line is called a *soft vertex*. The number of jet subdiagrams must be less or equal to the number of external legs otherwise that would imply external legs colliding at later time. From this follows that there should be only a single hard vertex and that all collinear lines belong to different sets of jet subdiagrams. The remaining lines are soft and can be collected in a single soft subdiagram.

Summarizing, in the massless case a generic n-leg reduced diagram can be decomposed into a single hard vertex connected to one soft subdiagram and n jet subdiagrams that are connected to this soft subdiagram and to the hard vertex. An example is shown in Fig. 2.2. These jet and soft subdiagrams are mutually connected and thus not yet completely independent. If one manages to prove that these connecting lines can be somehow removed, then these subdiagrams are independent and a factorization picture would emerge. This is indeed what we will achieve eventually, and moreover it will be possible to re-define these leading regions as matrix elements of composite operators. Before doing that, we have to get rid of solutions of the Landau equations that do not give rise to a singularity. Indeed most of the lines connecting the subdiagrams correspond to integrable singularities and thus can be removed. To prove this we need a precise IR

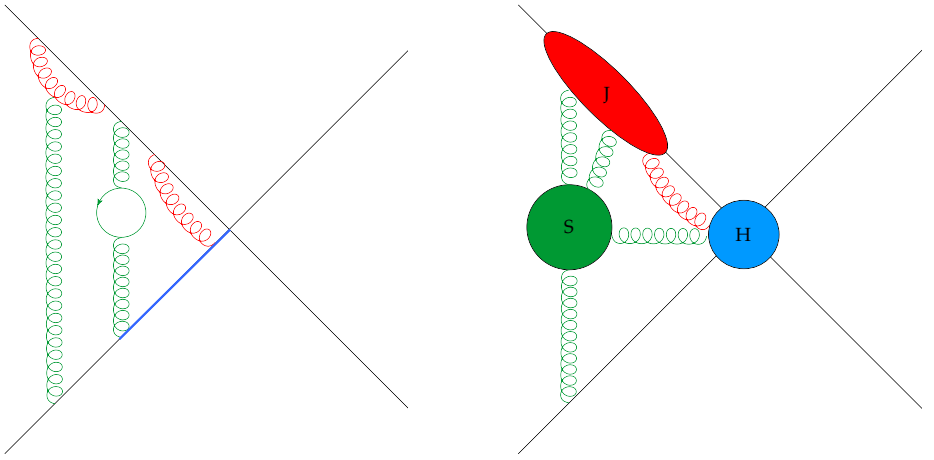

(a) (b)

Figure 2.2: A generic 4-parton amplitude (a). Soft and collinear lines are represented respectively in green and red. Hard (off-shell) lines in blue are shrunk to a point in the corresponding reduced graph (b), which can be represented with massless subgraphs.

power counting.

Indeed, with the Landau equations (and their graphical representation given by the Coleman-Norton picture) we have seen that the vanishing of a denominator in a diagram is not enough to develop a singularity, since some of the singular points can be avoided by modifying the integration contour. Still, Landau equations are a necessary but not sufficient condition for a diagram to be singular. There might be other contributions (e.g. numerator factors or the integration measure) that would make a solution to Landau equation not singular. In order to have full control of this at all orders in perturbation theory we need a systematic power counting of the infrared singularities of a generic diagram, as is well-known for UV divergences.

Given a diagram, every solution $(k_i = \bar{k}_i, x_i = \bar{x}_i)$ to the Landau equations (i.e. every reduced diagram) defines a surface $\mathcal{S}$ in the multidimensional space (k_i, x_i) that we call a *pinch surface*[2]. At a given point of every surface we can distinguish in the k_i subspace two kinds of coordinates: *intrinsic coordinates* k_i^{intr}, which parametrize the surface (and thus assuming that there is only one pinch surface the integration over them would be finite), and *normal coordinates* k_i^{norm}, which are the actual singular ones and whose variation measures how close we are to the singularity surface. Of course the choice of

[2]We call it pinch surface even if it contains also endpoint singularities. This is because the k_j will always be pinched, while the x_i do not have to have an endpoint singularity.

intrinsic and normal coordinates refers to a specified pinch surface: different surfaces have different intrinsic and normal variables and the integration over the intrinsic ones may be divergent when the surface intersect other pinch surfaces.

The power counting analysis starts by rescaling these normal variables with a parameter λ

$$k_i^{\text{norm}} \equiv \lambda^{a_i} \widetilde{k}_i^{\text{norm}} \,, \tag{2.16}$$

such that the singularity is approached for $\lambda \to 0$. We assumed here the possibility that different normal variables can scale with different powers a_i with $i = 1, \ldots, N_{norm}$, where N_{norm} is the number of normal variables. To every surface we can associate an integral, known as the *homogeneous integral*. It is constructed by expanding the denominator of each propagator j to leading power in λ. We call this power A_j with $j = 1, \ldots, N_{lines}$ where N_{lines} is the number of propagators. The integral corresponding to the surface $\mathcal{S}$ then scales as $\lambda^{n_\mathcal{S}}$, where the degree of divergence $n_\mathcal{S}$ is defined as

$$n_\mathcal{S} = \sum_{i=1}^{N_{norm}} a_i - \sum_{j=1}^{N_{lines}} A_j + n_{num} \,. \tag{2.17}$$

The first contribution arises from the normal variables in the measure, the second from denominators and the third from factors in the numerators that produces powers of λ. A sufficient condition for the diagram to be divergent is

$$n_\mathcal{S} \leq 0 \,. \tag{2.18}$$

More precisely, the divergence is logarithmic if $n_\mathcal{S} = 0$ and linear or beyond if $n_\mathcal{S} < 0$.

The reason why counting leading powers of λ is a good way to measure the degree of divergence is that almost always the remaining homogeneous integral is divergent at the same pinch surface $\mathcal{S}$ of the original integral - i.e. no new IR divergence is created (the same is not true for the UV case: spurious UV divergences usually appear in the homogeneous integral, but these do not spoil the power counting of the IR ones).

However, the procedure fails when a subset of normal variables in a subsurface $\mathcal{S}'$ of $\mathcal{S}$ vanishes faster than the others. If this happens, one must repeat the procedure and verify the power counting for $\mathcal{S}'$. Thus, as for the UV power counting, $n_\mathcal{S}$ is only a *superficial degree of divergence*, since there might be sub-divergences not caught by the λ scaling.[3] However, in the cases relevant for this thesis this can be avoided by a suitable

[3] An example is given by the one-loop form factor in QED, when a fermion anti-fermion pair of momenta p and $\bar{p}$ annihilate into a photon and a virtual photon of momentum k is exchanged between them: thanks to the fermion mass m there are no collinear singularities but only soft ones whose pinch surface is $k^\mu = 0$. The corresponding homogeneous integral scales like λ^0 thus implying a logarithmic divergence. However, this integral has a further pinch surface given by $k^0 = 0, \boldsymbol{k} \neq 0$ which corresponds to a threshold singularity when $p \cdot \bar{p} = 2m^2$. At this surface the scaling is λ^{-1} so k^0 vanishes faster than $\boldsymbol{k}$ making the original integral power divergent [58].

choice of coordinates. Moreover, it is generally assumed that, given a set of variables on a pinch surface such that the homogeneous integral has no pinch surface different from the original diagram, the diagram is IR finite if the superficial degree of divergence for *every* set of variables on *every* pinch surface is positive.

The discussion so far has been very general. However, performing a precise IR power counting for a generic n-leg graph requires discussing many aspects that are actually not necessary for the purpose of this thesis. Thus from now on we will focus on the case of the quark form factor: 2 jets and no internal masses. This encodes the fundamental features of the factorization that can be generalized for a generic number of legs and, importantly, is the fundamental building block of the Drell-Yan process we investigate in this thesis.

2.3 The quark form factor

The quark form factor $\Gamma^\mu\left(p_1, p_2\right)$ is defined as the matrix elements of the electromagnetic current j_μ

$$\Gamma^\mu\left(p, \bar{p}\right) \equiv \langle 0|j_\mu(0)|p, \bar{p}\rangle \ , \tag{2.19}$$

which describes the annihilation of a quark-antiquark pair of momenta p and $\bar{p}$ into a photon of invariant mass Q^2 [64, 65]. In a massless theory without any real radiation this is the only scale involved besides the standard renormalization scale μ and one finds $Q^2 = 2p \cdot \bar{p}$, since all energy flows into the photon. The Lorentz algebra can be factorized such that the form factor can be expressed in term of a scalar function $\Gamma\left(\frac{\mu^2}{Q^2}, \alpha_s(\mu), \varepsilon\right)$. Hence one can write

$$\Gamma^\mu\left(p, \bar{p}\right) = -i\,\Gamma\left(\frac{\mu^2}{s}, \alpha_s(\mu), \varepsilon\right)\,\bar{v}(\bar{p})\,\gamma^\mu\,u(p)\ , \tag{2.20}$$

where for simplicity we have set to one the electromagnetic charge. QCD corrections can be decoupled from the electromagnetic vertex. Indeed, gluons do not couple directly to j_μ (unless one consider some effective vertex such as for Higgs production via gluon-fusion). Since the electromagnetic current is conserved, the form factor is a renormalization group invariant. This is consistent with the fact that QCD corrections do not affect the electric charge.

In this section we will first calculate the form factor at one-loop, in order to recall the main ingredients for the calculation, which will be useful for an IR analysis at the integrand level. We will not show the details of the integrations since these are standard one-loop methods. Then we will move to the IR analysis at the integrand level, first at one loop and then to all orders. At the end of this section we will see that the form factor

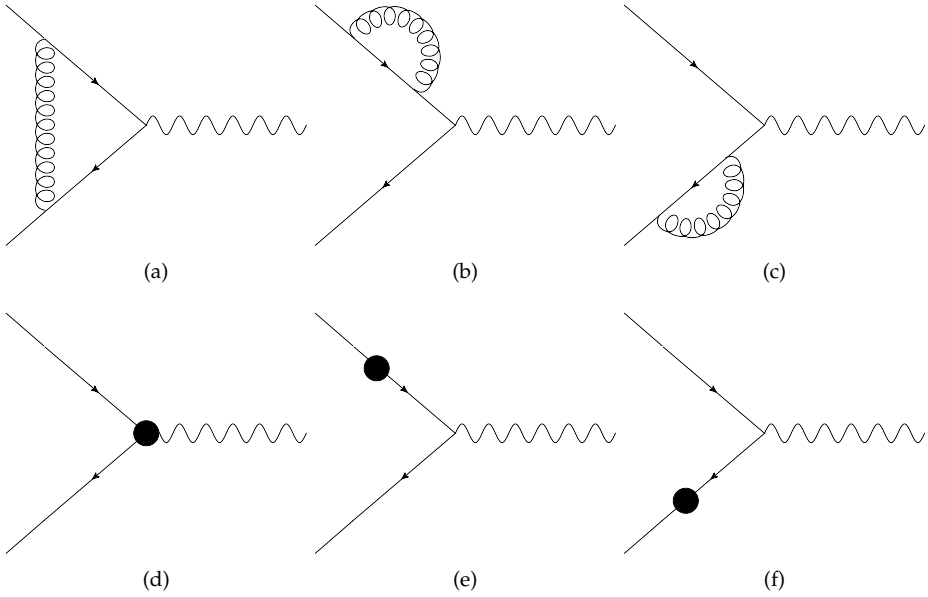

Figure 2.3: Diagrams contributing to the one-loop quark form factor. Solid dots represent UV counterterms.

can be factorized into leading regions that are connected only through longitudinally polarized gluons.

The relevant diagrams $\mathcal{D}_{(a)\text{-}(f)}$ for the computation of the one-loop form factor are depicted in Fig. 2.3. Gluon corrections bring IR divergences, which will will be discussed in detail, but also UV ones. Hence they require the introduction of (standard) UV counterterms. We will work in Feynman gauge.

Let us start with self energy graphs $\mathcal{D}_{(b)}$ and $\mathcal{D}_{(c)}$. Specifically, consider the self-energy correction to the p line of diagram $\mathcal{D}_{(b)}$. This is proportional to the integral

$$\int \frac{d^d k}{(2\pi)^d} \frac{\gamma_\mu (\not{p} - \not{k}) \gamma^\mu}{(p-k)^2 k^2} \,. \tag{2.21}$$

For $p^2 = 0$ the integral is scaleless[4] and thus the diagram vanishes in dimensional regulatization. The zero here has to be read as a cancellation between an IR and a UV

[4]This is a consequence of the chosen gauge. In axial gauge for example the presence of n^2 and $p \cdot n$ makes the integral different from zero.

pole. Therefore we can write

$$\mathcal{D}_{(b)} = \mathcal{D}_{(c)} \propto \frac{1}{\varepsilon_{\rm UV}} - \frac{1}{\varepsilon_{\rm IR}} = 0 \,. \tag{2.22}$$

This can be easily seen setting $p^2 \neq 0$ in the calculation. This off-shellness ensures that no collinear divergence is present and the result is a pure UV pole.

The presence of UV divergent self-energy graphs reminds us that we need to add diagrams $\mathcal{D}_{(e)}$ and $\mathcal{D}_{(f)}$: these are counterterms for each quark line which follow from renormalizing the quark field ψ via a factor Z_ψ. Finally, one must include diagram $\mathcal{D}_{(d)}$, which is the counterterm for the electromagnetic vertex via the renormalization constant Z_1. As is well-known, gauge invariance implies that $Z_1 = Z_\psi$, such that the sum of all counterterms must vanish:

$$\mathcal{D}_{(d)} + \mathcal{D}_{(e)} + \mathcal{D}_{(f)} = 0 \,. \tag{2.23}$$

This is consistent with the fact that QCD corrections cannot renormalize a QED vertex, and thus the QED charge is conserved.

In conclusion, at one-loop the only diagram which requires an actual computation is the triangle diagram

$$\mathcal{D}_{(a)} = g^2 C_F \mu^{2\varepsilon} \int \frac{d^d k}{(2\pi)^d} \frac{\bar{v}(\bar{p})\gamma^\alpha(\not{\bar{p}} + \not{k})\gamma^\mu(\not{p} - \not{k})\gamma_\alpha u(p)}{(k^2 + i\eta)\left[(p-k)^2 + i\eta\right]^2 \left[(\bar{p}+k)^2 + i\eta\right]^2} \,. \tag{2.24}$$

This is a standard one-loop calculation and the result leads to the one-loop expression for the form factor:

$$\Gamma^{(1)}\left(\frac{\mu^2}{s}, \varepsilon\right) = \frac{\alpha_s}{4\pi} C_F \left(-\frac{4\pi\mu^2}{s}\right)^\varepsilon \frac{\Gamma^2(1-\varepsilon)\Gamma(1+\varepsilon)}{\Gamma(1-2\varepsilon)} \frac{2 - \varepsilon + 2\varepsilon^2}{\varepsilon^2(2\varepsilon - 1)} \tag{2.25}$$

$$= \frac{\alpha_s}{4\pi} C_F \left(-\frac{\bar{\mu}^2}{s}\right)^\varepsilon \left(-\frac{2}{\varepsilon^2} - \frac{3}{\varepsilon} + \frac{\pi^2}{6} - 8 + \varepsilon\left(-16 + \frac{\pi^2}{4} + \frac{14}{3}\zeta_3\right) \right.$$
$$\left. \varepsilon^2\left(-32 + \frac{2}{3}\pi^2 + 7\zeta_3 + \frac{47}{720}\pi^4\right) + \mathcal{O}(\varepsilon^3)\right) , \tag{2.26}$$

where we have introduced $\bar{\mu}^2 = 4\pi\mu^2 e^{-\gamma_E}$ (we have used $\overline{MS}$-scheme counterterms).

Now we want to apply the general techniques discussed in Section 2.1 and Section 2.2 at the *integrand level*, first at one-loop and then at all orders. We will focus on the triangle integral. After Feynman parametrization it reads

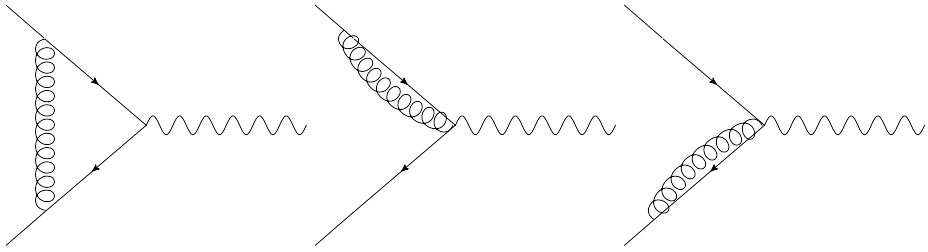

Figure 2.4: Reduced diagrams for the one loop quark form factor. Diagram (a) corresponds to the soft solution, while (b) and (c) to the collinear ones.

$$\mathcal{D}_{(a)} = 2\,g^2 C_F \mu^{2\varepsilon} \int \frac{d^d k}{(2\pi)^d} \int_0^1 dy_1 dy_2 dy_3\, \delta(1-y_1-y_2-y_3) \times \frac{\bar{v}(\bar{p})\gamma^\alpha(\bar{\not{p}}+\not{k})\gamma^\mu(\not{p}-\not{k})\gamma_\alpha u(p)}{\left[y_1 k^2 + y_2(p-k)^2 + y_3(\bar{p}+k)^2 + i\eta\right]^3}\,, \tag{2.27}$$

while the Landau equations read

$$\begin{cases} y_1 k^\mu - y_2(p-k)^\mu + y_3(\bar{p}+k)^\mu = 0 \\ y_1 = 0 \quad \text{or} \quad k^2 = 0 \\ y_2 = 0 \quad \text{or} \quad (p-k)^2 = 0 \\ y_3 = 0 \quad \text{or} \quad (\bar{p}+k)^2 = 0 \end{cases} . \tag{2.28}$$

There is one soft solution

$$k^\mu = 0\,, \qquad \frac{y_2}{y_1} = 0\,, \qquad \frac{y_3}{y_1} = 0\,, \tag{2.29}$$

and there are two collinear ones

$$\begin{cases} k^\mu = a\,p^\mu\,, & y_3 = 0\,, & y_1 = \frac{1-a}{a} y_2\,, \\ k^\mu = b\,\bar{p}^\mu\,, & y_2 = 0\,, & y_1 = \frac{-b-1}{b} y_3\,. \end{cases} \tag{2.30}$$

In order to prove that there is no other solution we can observe that there is no other possible reduced diagram. For example a diagram like the one shown in Fig. 2.5 does not have to be included.

Before moving to the power-counting, we need to identify the normal coordinates for each solution. For the soft pinch surface defined by $k^\mu = 0$ this is trivial, since all

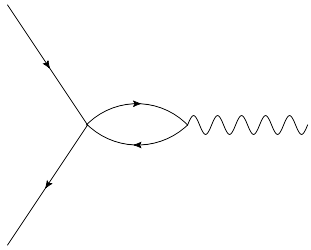

Figure 2.5: This reduce diagram is obtained by shrinking the gluon line in $\mathcal{D}_{(a)}$ into a point. It does not correspond to a solution to Landau equations since it does not describe a classical allowed configuration: two non-collinear particles cannot recombine after a free path.

the k^μ components are normal and there are no intrinsic coordinates. For the collinear singularity, instead, the parametrization of pinch surfaces requires the introduction of *light-cone coordinates*. We recall here some basic facts.

Light-cone variables mix the time and one spatial component of a standard Lorenz vector $(x^0, x^1, x^2, \dots, x^d)$ and are defined by

$$x^+ \equiv \frac{x^0 + x^3}{\sqrt{2}} \qquad x^- \equiv \frac{x^0 - x^3}{\sqrt{2}} \,. \tag{2.31}$$

Since the other $d-2$ coordinates do not change, they are collected as a single vectorial $x_\perp$ component. Thus light-cone components are indicated as $(x^+, x_\perp, x^-)$. The metric becomes

$$g_{\mu\nu} = \begin{pmatrix} 0 & 0 & 1 & 0 & \cdots \\ 0 & -1 & 0 & 0 & \cdots \\ 1 & 0 & 0 & 0 & \cdots \\ 0 & 0 & 0 & -1 & \\ \vdots & \vdots & \vdots & & \ddots \end{pmatrix} , \tag{2.32}$$

while the scalar product reads

$$x \cdot y = x_\mu y^\mu = x^- y^+ + x^+ y^- - x_\perp \cdot y_\perp \,, \tag{2.33}$$

where $x_\perp \cdot y_\perp$ is a standard Euclidean scalar product. The line and the volume element become

$$
\begin{aligned}
ds^2 &= 2dx^+dx^- - dx_\perp^2 \,, \\
d^dx &= dx^+dx^-d^{d-2}x_\perp = dx^+dx^-d|x_\perp||x_\perp|^{d-3}d\Omega_{d-2} \,,
\end{aligned}
\tag{2.34}
$$

where $d\Omega_{d-2} =$ is the differential solid angle in $d-2$ dimensions (which for $d=4$ reduces to a single azimuthal angle $d\phi$). Finally, we observe that for gamma matrices we have

$$
\left(\gamma^\pm\right)^2 = \frac{1}{2}\left\{\gamma^\pm,\gamma^\pm\right\} = g^{\pm\pm} = 0 \,,
\tag{2.35}
$$

while the Dirac equation $\not{p}\, u(p) = \bar{v}(\bar{p})\not{\bar{p}} = 0$, for $p = (p^+, 0_\perp, 0)$ and $\bar{p} = (0, 0_\perp, p^-)$, can be written simply as

$$
\gamma^- u(p) = \bar{v}(\bar{p})\gamma^+ = 0 \,.
\tag{2.36}
$$

We can now write the propagators of the triangle diagram in light-cone coordinates, after choosing the rest frame of the off-shell photon and setting $p = (p^+, 0_\perp, 0)$ and $\bar{p} = (0, 0_\perp, p^-)$:

$$
\begin{aligned}
k^2 &= 2k^+k^- - k_\perp^2 \,, \\
(p-k)^2 &= -2p^+k^- + 2k^+k^- - k_\perp^2 \,, \\
(\bar{p}+k)^2 &= 2\bar{p}^-k^+ + 2k^+k^- - k_\perp^2 \,.
\end{aligned}
\tag{2.37}
$$

Let us consider the collinear singularity $k \parallel p$ in which $(p-k)^2 \to 0$. The singularity is achieved when both k^- and $k_\perp$ become 0, thus both are normal coordinates. Then the remaining ones (the solid angle Ω and k^+) are intrinsic.

Soft power counting

The power counting for soft singularities is straightforward. Rescaling every momentum component as

$$
k^\mu \to \lambda^2 k^\mu \,,
\tag{2.38}
$$

which is equivalent in light-cone components to the scaling $(\lambda^2, \lambda^2, \lambda^2)$, all the parts we need in the integral scale as

$$
\begin{aligned}
&d^dk \sim \lambda^{2d} \,, \quad k^2 \sim \lambda^4 \,, \quad (p-k)^2 \sim \lambda^2 \,, \quad (\bar{p}+k) \sim \lambda^2 \,, \\
&\mathcal{N} \sim \; 2p\cdot\bar{p}\,\bar{v}\,(\bar{p})\gamma^\mu u(p) \;\sim\; \lambda^0 \,,
\end{aligned}
\tag{2.39}
$$

where in the numerator $\mathcal{N}$ we used the Dirac equation $\not{p}\, u(p) = 0$ and $\bar{v}(\bar{p})\,\not{\bar{p}} = 0$. Taking this limit in an amplitude goes under the name of *eikonal approximation*, where the

emitting fermion line propagator and the vertex can be combined into a single scalar effective Feynman rule. E.g. on the p line one has

$$\frac{(\not{p}-\not{k})\,\gamma^\mu\,u(p)}{k^2-2p\cdot k}\to-\frac{p^\mu}{p\cdot k}\,. \tag{2.40}$$

Hence the homogeneous integral is called eikonal integral $I^{\rm eik}$ and reads

$$I^{\rm eik}=-\lambda^{2d-8}\,g^2C_F\mu^{2\varepsilon}\,2p\cdot\bar p\,\bar v\,(\bar p)\gamma^\mu u(p)\int d^dk\frac{1}{(k^2+i\eta)(p\cdot k-i\eta)(\bar p\cdot k+i\eta)}\,, \tag{2.41}$$

while the degree of IR divergence is

$$n_{\mathcal S}=2d-8\,, \tag{2.42}$$

which corresponds to a logarithmic singularity in $d=4$. $I^{\rm eik}$ has a soft pinch surface at $k^\mu=0$ and collinear ones at $k^\pm=k_\perp=0$. This can be immediately seen writing the integral in light-cone components:

$$\begin{aligned}I^{\rm eik}=-\lambda^{2d-8}\,2\,g^2C_F\mu^{2\varepsilon}\,\bar v(\bar p)\gamma^\mu u(p)\int dk^+dk^-d|k_\perp|d\Omega_{d-2}\\ \times\frac{|k_\perp|^{d-3}}{(2k^+k^--k_\perp^2+i\eta)(k^++i\eta)(k^--i\eta)}\,.\end{aligned} \tag{2.43}$$

Both pinch surfaces are present also in the original integral, hence Eq. (2.43) gives the correct divergent behavior.

Collinear power counting

For the collinear case (say $k\parallel p$), demanding that the propagator in the second line of Eq. (2.37) must be kept on-shell, we can rescale the intrinsic coordinates as

$$k^-\to\lambda^2k^-\,,\qquad k_\perp^2\to\lambda^2k_\perp^2\,, \tag{2.44}$$

hence the light-cone components of a collinear vector will scale like $k_{{\rm coll}\,p}\sim(1,\lambda,\lambda^2)$. The various contributions scale as

$$\begin{aligned}&dk^-\sim\lambda^2\,,\quad d|k_\perp||k_\perp|^{d-3}\sim\lambda^{d-2}\,,\quad k^2\sim\lambda^2\,,\quad(p-k)^2\sim\lambda^2\,,\quad(\bar p+k)\sim\lambda^0\,,\\ &\mathcal{N}\;\sim\;\bar v(\bar p)\,\gamma^-(\not{\bar p}+\not{k})\gamma^\mu(\not{p}-\not{k})\gamma^+\,u(p)\;\sim\;\lambda^0\,,\end{aligned} \tag{2.45}$$

where in the numerator $\mathcal{N}$ we used again the Dirac equation. After some algebra, the homogeneous integral $I^{\rm coll}$ can be rewritten as

Singularity	Pinch surface	Normal coord.	Intrinsic coord.	$n_{\mathcal{S}}$
Soft	$k^\mu = 0; \frac{y_2}{y_1} = \frac{y_3}{y_1} = 0$	$\{k^\mu\}$	$\{0\}$	$2d-8$
Collinear p	$k^\mu = a\,p^\mu; y_3 = 0; y_1 = \frac{1-a}{a} y_2$	$\{k^-, k_\perp\}$	$\{k^+, \Omega_{d-2}\}$	$d-4$
Collinear $\bar{p}$	$k^\mu = b\,\bar{p}^\mu; y_2 = 0; y_1 = \frac{-b-1}{b} y_3$	$\{k^+, k_\perp\}$	$\{k^-, \Omega_{d-2}\}$	$d-4$

Table 2.1: Singularity structure for the triangle integral $\mathcal{D}_{(a)}$ that contributes to the one-loop quark form factor.

$$I_{\text{coll}} = \lambda^{d-4}\, g^2 C_F \mu^{2\varepsilon} \int dk^+ dk^- d|k_\perp| |k_\perp|^{d-3} d\Omega_{d-2} \times \frac{\bar{v}(\bar{p})\,\gamma^-(\not{\bar{p}} + \not{k})\gamma^\mu(\not{p} - \not{k})\gamma^+\, u(p)}{(2\bar{p}^- k^+ + i\eta)(2k^+k^- - k_\perp^2 + i\eta)(2k^+k^- - 2p^+k^- - k_\perp^2 + i\eta)} \,. \tag{2.46}$$

It is easy to see that the integral over the normal variables $\{k^-, |k_\perp|\}$ has a collinear pinch surface $k^- = |k_\perp| = 0$ and the trivial soft one $k^+ = k^- = |k_\perp| = 0$. Both are present also in the original integral, so that we conclude that superficial degree of divergence is

$$n_{\mathcal{S}} = d - 4 \,, \tag{2.47}$$

which is again a logarithmic singularity in $d = 4$.

Finally, we have seen that soft and collinear pinch surfaces intersect and give rise to a soft-collinear pinch surface

$$k^+ = k^- = |k_\perp| = 0 \,, \tag{2.48}$$

which corresponds to the collinear subsurface of the soft surface of Eq. (2.43). This is again a logarithmic divergence in $d = 4$, and it is responsible for the double pole of the form factor. The structure of all singularities for the one-loop triangle diagram is summarized in Table 2.1.

IR analysis at all orders

At higher orders the form factor involves loops made out of quarks and gluons, with 3- and 4-gluon vertices. It is here that the use of reduced diagrams becomes an especially powerful tool, allowing us to isolate the IR divergences without explicitly referring to the complicated structure of Landau equations. From an analysis of the possible reduced diagrams it follows that the structure of singularities found at one-loop persists at higher orders. Collinear and soft lines can be organized in jet and soft subdiagrams respectively. All these regions are in principle connected by gluons and fermions accordingly to the

loop order the diagram corresponds to. It is possible to show by power counting that many of these lines are suppressed and thus can be removed. The full derivation can be found in the original work of [66] or in the reviews in [51,58,60]. Here we limit ourselves to observe some key aspects of the procedure.

First of all, we can already conclude that lines between H and S are suppressed: given a diagram, adding a soft line joining H and S would add another shrunk off-shell line in H, which makes the diagram subleading. We can thus assume in the following that in leading diagram no lines connect H and S.

Then, we are left with lines connecting all others leading regions. In order to remove them, we need to determine the degree of divergence for the entire reduced diagram $\mathcal{S}$. This will be made of 2 jets and one soft subdiagram, and the superficial degree of divergence will be the sum of these regions

$$n_{\mathcal{S}} = n_{\text{Soft}} + \sum_{i=1}^{2} n_{J_i} \ . \tag{2.49}$$

In principle, one has to work out separately n_{Soft} and n_{J_i}. From the purely technical point of view, this computation is a simple algebraic computation, given by the topological properties of a generic diagram. However, this procedure is notoriously tedious, since one has to introduce a nomenclature for all the lines connecting various subdiagrams.

The soft power counting is relatively easy and one can determine precisely the value of n_{Soft}. On the other hand, collinear power counting is much more involved due to the non-trivial dependence of the numerator on normal variables. Specifically, after discriminating gluons with longitudinal and transverse polarization, it is possible to constrain n_{J_i} only with an inequality. Therefore, after combining soft and collinear power counting, the final result of this procedure is only a lower bound for the superficial degree of divergence. Recalling that the divergent behavior of the entire diagram is given by the sign of $n_{\mathcal{S}}$, we have to determine the minimum value of this lower bound. By looking at its explicit expression [58–60] this can be found demanding that:

- there is no line between H and S,
- J^i and H are connected only through 1 fermion line and longitudinal polarized gluons,
- J^i and S are connected only by longitudinal polarized gluons
- every vertex in the jet is a three- or four-gluon vertex (in principle shrinking lines in the reduced diagram may give rise to higher points vertices).

Imposing these constraints simplifies quite a lot both the diagrammatic structure of the full diagram in terms of leading regions and the lower bound for $n_{\mathcal{S}}$. However, we still cannot specify the sign of $n_{\mathcal{S}}$. This can be determined only after fixing the number of fermions and transverse polarized gluons connecting the hard and the jet subdiagrams. To go further we have to make now some important observations about the choice of gauge.

If we work in a physical gauge like the **axial gauge** where the gluon propagator is

$$G_{\mu\nu}(k) = \frac{1}{k^2 + i\eta}\left(-g_{\mu\nu} + \frac{n_\mu k_\nu + n_\nu k_\mu}{n\cdot k} - n^2\frac{k_\mu k_\nu}{(n\cdot k)^2}\right) , \tag{2.50}$$

then unphysical longitudinal polarizations are automatically suppressed since

$$k^\nu G_{\mu\nu}(k) = \frac{n_\mu}{n\cdot k} - n^2\frac{k_\mu}{(n\cdot k)^2} , \tag{2.51}$$

has no pole at $k^2 = 0$. Thus lines connecting H and J can be removed and

$$n_{\mathcal{S}} \geq 0 , \tag{2.52}$$

which yields at worst a logarithmic divergence for the original diagram.

Alternatively, we can choose a covariant gauge such as the **Feynman gauge**. Then longitudinally polarized gluons between H and J do propagate. Such a configuration, even if different from zero for a specified diagram, vanishes for a gauge invariant quantity after summing over all the diagrams, via Ward identities. This is the case for the form factor, as we saw at one-loop when we added self-energy and triangle diagrams (with their relative UV counterterms). Therefore also for the Feynman gauge the form factor has no line connecting J and H and $n_{\mathcal{S}} \geq 0$. However, on a diagram by diagram basis, this is not guaranteed as in the axial gauge.

We would like to have a factorization that is not gauge dependent. Thus we have still to deal with these longitudinal polarized gluons and eventually prove that they can be removed. This can be performed through some diagrammatic manipulation.

2.4 Diagrammatic analysis and Wilson lines

The results achieved in the previous sections are remarkable and would benefit from a brief summary before proceeding further. Starting from very general tools to isolate singularities at all orders, we considered the quark form factor, and we have shown that soft and collinear singularities can be represented in the most general reduced diagram through sub-diagrams collecting singular lines. Then we have derived constraints showing that most of the lines connecting these regions are actually suppressed by power

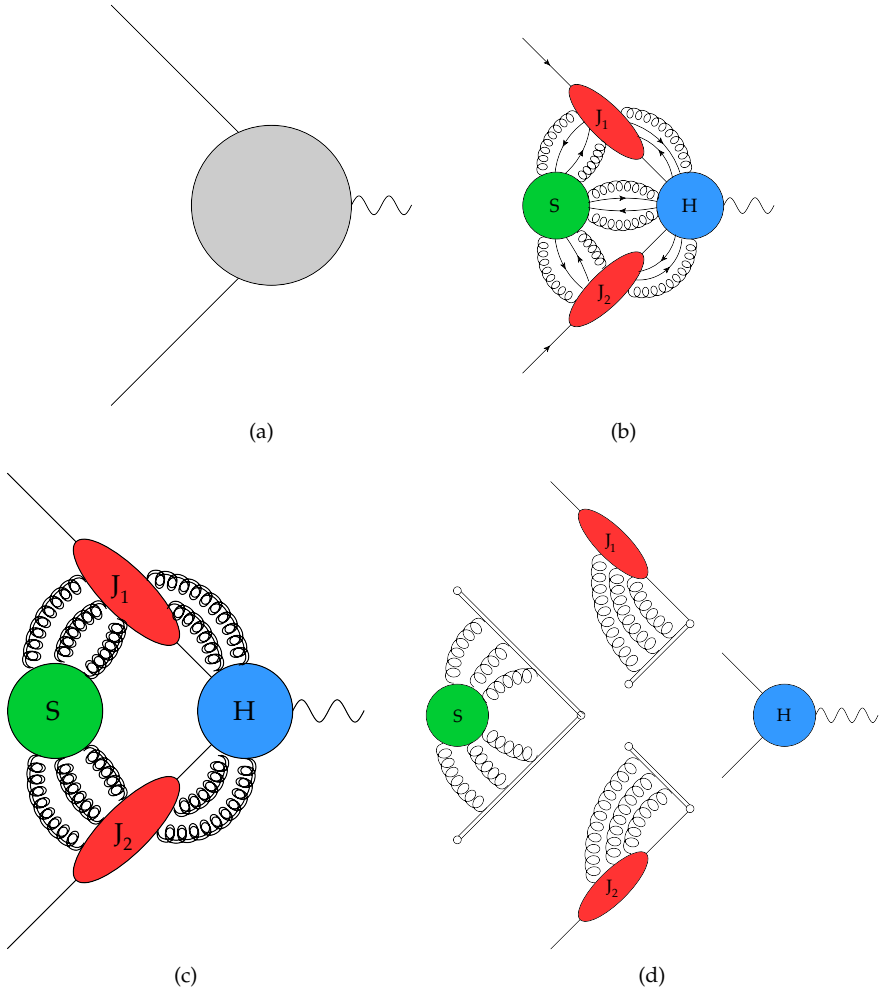

Figure 2.6: Diagrammatic representation of the factorization in covariant gauge for two massless partons. The form factor in (a) consists of an arbitrary order QCD correction to the electromagnetic vertex. Solving Landau equations we can represent the most general singular diagram in the Coleman Norton picture as in (b), where S is a subdiagram collecting on-shell soft lines, while J_1 and J_2 collect on-shell collinear lines; H is the hard vertex collecting off-shell lines that have been shrunk to a point. After power counting we select the actual singular contributions and we get diagram (c): no line connects H and S, and gluons are only longitudinally polarized (indicated by a double line). Finally, making use of Ward identities and some diagrammatic manipulation we can decouple the longitudinal gluons with Wilson lines, as shown in (d). Note that S, J_1 and J_2 in the last picture are merely subdiagrams and thus are somewhat different from the operator definition of soft and jet functions $\mathcal{S}$, $\mathcal{J}_1$ and $\mathcal{J}_2$ given in Eq. (2.63) and Eq. (2.64).

counting arguments. Some of the lines survive the procedure, but their nature is very particular: they are gluons with longitudinal polarizations, and therefore these physical configurations are suppressed through Ward identities.

In axial gauge the ultimate goal has been reached: H, S and J are disconnected regions and the form factor is factorized in terms of sub-diagrams that have a precise definition as functions whose loop momenta are restricted to the leading region of the sub-diagram they belong to. However, we would like to have a gauge-independent framework where factorization is preserved on a diagram by diagram basis also for covariant gauges. Moreover, we would like to have a generalization such that momenta in each leading region are not constrained to that region.

To solve the last problem, one might try to mimic what happens in the axial gauge, where the gauge vector n allows a separation of scales $p \cdot n$ and $k \cdot n$. In this regard this n does not only ensure gauge invariance, but also acts as a *factorization vector*, in the same spirit as the common renormalization or factorization scales μ_R or μ_F separate different scales of energy. The factorization we are trying to set up here involves an intricate Lorentz and spinor structure, thus it is not too surprising that for this purposes we need a vector instead of a simple energy scale.

The key ingredient for such a program is one of the few objects that is widely used both in perturbative and non-perturbative physics: the **Wilson line**. It is defined as[5]

$$\Phi_n(\lambda_2, \lambda_1) \equiv \mathcal{P} \exp\left(ig\mu^\varepsilon \int_{\lambda_1}^{\lambda_2} d\lambda \; n \cdot A(\lambda n) \right) \; , \tag{2.53}$$

where the symbol $\mathcal{P}$ is the path ordering, which takes into account the non-abelian nature of the gauge field A. Explaining the rich mathematics behind the Wilson line and its applications is beyond the scope of this thesis. Perhaps the simplest way to introduce it is thinking about it as a tool that makes combinations of operators like $\bar{\psi}(\lambda_2)\psi(\lambda_1)$ gauge invariant: the role of the Wilson line is to "transport" the field along a path parametrized by λ, from λ_1 to λ_2, keeping it parallel to the tangent of the line. When the path is closed, it is often called Wilson loop, and becomes itself a gauge invariant quantity.

In this section we will discuss how all this can be used for factorization. First we will show how soft and collinear interactions correspond to effective vertices whose Feynman rules are generated by Wilson lines. This can be easily seen at one-loop by looking at the triangle diagram of the one-loop form factor and can be generalized to all-orders by means of Ward identities. In the next section we will use this all-order statement to

[5]In this chapter we assume that the the group generator into the field A is different when coupling to particles or antiparticles respectively. Therefore, in the QED case, a different sign in the charge will not be encoded by the extrema λ_1 and λ_2. This convention will be revisited in Chapter 5.

re-define the subgraphs of a general reduced diagram as matrix elements of correlators of Wilson lines, which will give the final factorization formula for the quark form factor.

We start by discussing soft gluons. Specifically, we consider a soft emission of momentum k from an hard line of momentum $p+k$. We also restrict our analysis focusing on the abelian part and neglecting color generators. Then we have

$$\frac{(\not{p}-\not{k})\gamma^\mu u(p)}{(p-k)^2} = -\frac{p^\mu}{p\cdot k - i\eta} + \mathcal{O}(k^2)\,. \tag{2.54}$$

This can be easily generalized to higher orders since n ordered emissions lead to

$$\frac{p^{\mu_1}}{p\cdot k_1}\times\frac{p^{\mu_2}}{p\cdot(k_1+k_2)}\times\cdots\times\frac{p^{\mu_n}}{p\cdot(k_1+k_2+\cdots+k_n)} = \prod_{i=1}^{n}\frac{p^{\mu_i}}{p\cdot\left(\sum_{j=1}^{i}k_j\right)}\,. \tag{2.55}$$

Summing over all possible orderings we get the so-called *eikonal identity*, which will be discussed further in Chapter 3. It allows us to state that soft emissions can be expressed in terms of the (scalar) eikonal Feynman rule $p^\mu/p\cdot k$. It is easy to show that this type of interaction can be described by a Wilson line $\Phi_n(\infty,0)$, by considering its Fourier transform. One finds

$$\Phi_n(\infty,0) = \exp\left(ig\mu^\varepsilon\int_0^\infty d\lambda\, n\cdot A(\lambda n)\right) = \exp\left(g\mu^\varepsilon\int\frac{d^dk}{(2\pi)^d}\frac{n^\mu}{n\cdot k}\tilde{A}_\mu(k)\right)\,. \tag{2.56}$$

Expanding it in powers of g as

$$1 + g\int\frac{d^dk}{(2\pi)^d}\frac{n^\mu}{n\cdot k}\tilde{A}_\mu(k) + \frac{g^2}{2}\int\frac{d^dk_1}{(2\pi)^d}\frac{d^dk_2}{(2\pi)^d}\frac{n^\mu}{n\cdot k_1}\frac{n^\nu}{n\cdot k_2}\tilde{A}_\mu(k_1)\tilde{A}_\nu(k_2) + \dots\,, \tag{2.57}$$

we can read order by order in the Fourier modes the eikonal Feynman rule of soft gluon emissions from a hard line in the same direction as the Wilson line.

Now let us consider the triangle diagram of the one-loop form factor at the integrand level. In the limit in which the momentum k^μ of the virtual gluon becomes soft, both interactions with the hard legs become eikonal. Therefore, the soft limit is equivalent to replacing the two quarks with two Wilson lines, as shown in Fig. 2.7(a).

The analysis carried out for the soft case can be taken further for the collinear region. Let us consider once again the one-loop triangle diagram, in the limit $k^\mu \parallel p^\mu$. Then, omitting coupling constants, we have

$$\frac{\bar{v}(\bar{p})\,\gamma^-(\not{\bar{p}}+\not{k})\gamma^\mu(\not{p}-\not{k})\gamma^+\,u(p)}{k^2(p-k)^2(\bar{p}+k)^2}\,. \tag{2.58}$$

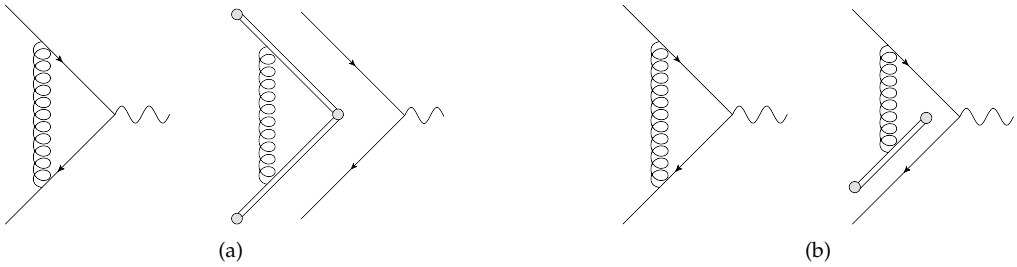

Figure 2.7: Decoupling of soft (a) and collinear (b) virtual corrections from the hard part of the one-loop quark form factor. In both cases the interaction is given by an eikonal vertex which is generated by a Wilson line (indicated by the double line).

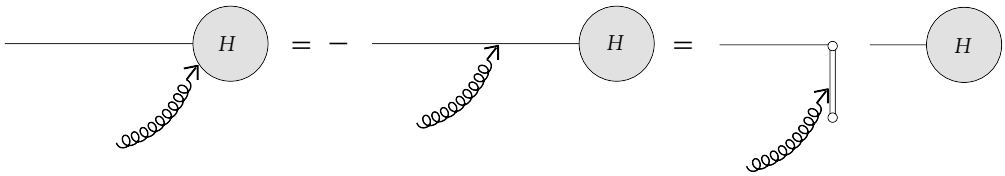

Figure 2.8: Ward identity for one (longitudinally polarized) gluon, by means of which it is possible to decouple J and H.

Taking the leading power in the normal variables, after some algebra, we get

$$\frac{\bar{v}(\bar{p})\gamma^{\mu}(\not{p}-\not{k})\gamma_{\nu}u(p)}{k^2(p-k)^2}\frac{\bar{p}^{\nu}}{\bar{p}\cdot k}\,, \tag{2.59}$$

where, as for the soft case, $\bar{p}=(0,0_{\perp},\bar{p}^{-})$. We see that the interaction of the gluon with the $\bar{p}$ line is eikonal, while the vertex on the p line is not. Therefore, the interaction of the collinear gluon can be described once again in term of a Wilson line whose direction is proportional to $\bar{p}$, as shown in Fig. 2.7(b). In order not to introduce spurious collinear singularities associated with this line, it is customary to choose the Wilson line in the generic direction n, demanding that $n^2\neq 0$.

In conclusion we have seen from an explicit one-loop diagrammatic analysis that soft and collinear interactions eikonalize and can be described in terms of a Wilson line. To generalize this procedure to all orders, it is convenient to use Ward identities. As is well-known, these relate different correlators summing over all possible momentum insertions. To see how this can be useful for factorization, let us consider the decoupling of the jet and the hard regions. If we consider only a single gluon, as shown in Fig. 2.8,

the number of possible momentum insertions is limited and we obtain that the first diagram is opposite to the second. In this way we can move the momentum insertion from the jet J to the hard line. This yields

$$H \; \frac{\not{p} - \not{k}}{(p-k)^2} \gamma^\alpha u(p) \epsilon_\alpha(k) \; . \tag{2.60}$$

Then from the analysis of the previous section we know that the soft gluon couples to a jet defined for the plus direction only through the minus component of both its momentum and polarization. Inserting this information in Eq. (2.60) we obtain

$$H \; \frac{\not{p} - \not{k}}{(p-k)^2} \gamma^+ u(p) \epsilon^-(k) \frac{k^- \beta_1^+}{k^- \beta_1^+} \; , \tag{2.61}$$

where β_1^μ is a light-like vector with only plus component. After some algebra this becomes

$$-H \; u(p) \, \frac{\beta_1 \cdot \epsilon(k)}{\beta_1 \cdot k} \; . \tag{2.62}$$

We see that the soft emission has decoupled from the jet. Obviously the same calculation can be applied to the other leg, choosing β_2 with only a minus component.

This analysis can now be generalized to higher orders. The number of possible insertions from the Ward identity increases. However making use of the eikonal identity it is possible to show that the result is equivalent to Eq. (2.62), and thus all the emissions can be expressed in term of the same eikonal Feynman rule.

2.5 A factorization formula

We have now all ingredients to write down a factorization formula for the quark form factor in covariant gauge, following the formalism originally developed by Collins [60]. By means of Wilson lines, it is possible to build composite operators whose perturbative expansion generate the leading singular regions of the form factor. However, the matrix elements of these composite operators generate more than required and this must be compensated in order to recover the contributions of the original singular regions.

Originally, in each leading region, momenta are restricted (e.g. in the jet subdiagram all the lines are collinear) and thus, for a one-to-one correspondence, the soft and jet functions should do the same. This seems to complicate the use of factorization severely and thus the formula we are looking for involves jet and soft functions without any restrictions on their internal momenta.

We start defining the soft function as

$$\mathcal{S}\left(\beta_1 \cdot \beta_2, \alpha_s(\mu^2), \varepsilon\right) = \langle 0 \, | \phi_{\beta_1}(\infty, 0) \phi_{\beta_2}(\infty, 0) | \, 0 \rangle \; , \tag{2.63}$$

where β_1 and β_2 are proportional to p_1 and p_2 and fix the directions of the Wilson lines. Secondly, in order to avoid a spurious collinear singularity in each jet function, it is enough to set the direction of the Wilson line to be $n^2 \neq 0$. The definition for each leg i will be then

$$J_i\left(\frac{(p_i\cdot n_i)^2}{n_i^2\mu^2},\alpha_s(\mu^2),\varepsilon\right)u(p) = \langle 0\,|\phi_{n_i}(\infty,0)\psi(0)|\,p_i\rangle\ . \tag{2.64}$$

The only missing step is avoiding double counting issues between the soft and the jet function: gluons which are both soft and collinear are contained in the operator definition of both $\mathcal{S}$ and J and we have to remove them by an extra division. The overlap factor can be seen either as the soft function whose gluons become collinear or as a jet function whose collinear gluons become soft. In both cases the object is again a correlator of light-like Wilson lines called **eikonal jet function** $\mathcal{J}$, which for every leg i reads

$$\mathcal{J}_i\left(\frac{(\beta_i\cdot n_i)^2}{n_i^2\mu^2},\alpha_s(\mu^2),\varepsilon\right) = \langle 0\,|\phi_{n_i}(\infty,0)\phi_{\beta_i}(\infty,0)|\,0\rangle\ . \tag{2.65}$$

We are now able to write the final formula for the factorized form factor which reads

$$\Gamma\left(\frac{\mu^2}{Q^2},\alpha_s(\mu),\varepsilon\right) = \mathcal{H}\left(\frac{\mu^2}{Q^2},\alpha_s(\mu^2)\right)\mathcal{S}\left(\beta_1\cdot\beta_2,\alpha_s(\mu^2),\varepsilon\right)\prod_{i=1}^{2}\frac{J_i\left(\frac{(p_i\cdot n_i)^2}{n_i^2\mu^2},\alpha_s(\mu^2),\varepsilon\right)}{\mathcal{J}_i\left(\frac{(\beta_i\cdot n_i)^2}{n_i^2\mu^2},\alpha_s(\mu^2),\varepsilon\right)}\ . \tag{2.66}$$

It is important to stress that this factorization for partonic amplitude is a multiplication of scalar functions. Note that soft and jet functions here are *universal* functions (they depend only on general properties of the external lines like spin and charge) and collect respectively soft and collinear singularities. The hard function instead is the process dependent part which might contain UV divergences but no IR ones. It is defined *by matching*, in particular demanding that the n-dependence of the finite part is zero, thus ensuring the gauge invariance of the amplitude.

The functional dependence of the functions in Eq. (2.66) (easily shown at one-loop and valid at all orders) is a consequence of the homogeneity with respect to the vector n^μ of eikonal Feynman rule $n^\mu/n\cdot k$ in the Wilson line of direction n, taking into account simple dimensional analysis involving $n^2 \neq 0$. The same cannot be said for β^μ since $\beta^2 = 0$ and thus the functions are not homogeneous in β^μ: this leads to the *cusp anomaly* [67] and is due to the presence of collinear singularities associated with the Wilson line in the β direction. As we already discussed, this is indicated by the presence of singularities which are both soft and collinear. However, in two combinations the anomaly cancels.

- For each jet i we can define

$$\overline{J_i}\left(\frac{Q^2}{\mu^2},\alpha_s(\mu^2),\varepsilon\right)\equiv\frac{J_i\left(\frac{(p_i\cdot n_i)^2}{n_i^2\mu^2},\alpha_s(\mu^2),\varepsilon\right)}{\mathcal{J}_i\left(\frac{(\beta_i\cdot n_i)^2}{n_i^2\mu^2},\alpha_s(\mu^2),\varepsilon\right)}\,, \tag{2.67}$$

  which collects collinear non-soft radiation. Now the soft function will contain the soft-collinear poles.

- Alternatively, the double counting can be removed from the soft function by defining $\overline{\mathcal{S}}$ which contains purely non-collinear radiation, while each jet function now contains also soft-collinear poles:

$$\overline{\mathcal{S}}\left(\rho_{12},\alpha_s(\mu^2),\varepsilon\right)=\frac{\mathcal{S}\left(\beta_1\cdot\beta_2,\alpha_s(\mu^2),\varepsilon\right)}{\mathcal{J}_1\left(\frac{(\beta_1\cdot n_1)^2}{n_1^2\mu^2},\alpha_s(\mu^2),\varepsilon\right)\mathcal{J}_2\left(\frac{(\beta_2\cdot n_2)^2}{n_2^2\mu^2},\alpha_s(\mu^2),\varepsilon\right)}\,, \tag{2.68}$$

  where

$$\rho_{12}\equiv\frac{(\beta_1\cdot\beta_2)^2\;n_1^2\;n_2^2}{(\beta_1\cdot n_1)^2\;(\beta_2\cdot n_2)^2}\,. \tag{2.69}$$

Another important remark about the factorization formula in Eq. (2.66) is that all correlators involved are matrix elements of composite operators, which generate new vertices and need a further UV renormalization. Even though introducing new singularities in building objects that factorize IR singularities might seem odd, it does not spoil the procedure. Indeed we have seen in the previous sections that the correct power counting for pinch surfaces, and thus the factorization of leading regions, is preserved as long as no new IR singularity is introduced in the process of expanding the integrands in the leading regions. Thus introducing UV counterterms is perfectly allowed.

Finally, we note that it might be convenient for calculational purposes to keep n on the light-cone, as will be further discussed in Chapter 5. As previously remarked, this will introduce spurious collinear singularities in the calculation and is the standard procedure followed for example in SCET. However, at least in this chapter, we will make use of the factorization formula for $n^2\neq 0$.

The factorization formula in Eq. (2.66) refers to the quark form factor. However, from our discussion in the previous sections, it should be clear that the same procedure applies to more generic amplitudes with generic number of external legs. The main complications arise because of the more intricate color dependence, which for more than two legs becomes non-trivial. However, this is only a technical problem. Much more problematic is the question related to Glauber gluons, which might spoil factorization

and are not easy to bring under control. Examples of factorization issues due to these effects exist in the literature and are a current topic of investigation [68–70].

However, if we ignore subtleties related to Glauber gluons, a factorized formula for multiparton processes exists and it is the direct generalization of Eq. (2.66). The main difference is that with a generic number m of partons, color flow becomes non-trivial and thus the amplitude is a vector $\mathcal{M}_{\{\alpha_k\}}$ in color space, where the color indices $\{\alpha_k\}$ depend on the representations of the gauge group and $k = 1, \ldots, m$. The amplitude can be decomposed after choosing a basis of independent color tensors $(c_a)_{\{\alpha_k\}}$, where a runs up to the number of irreducible representations of the gauge group which contribute to the process. Then the factorization formula is a matrix equation and reads [71]

$$\mathcal{M}_a\left(\frac{p_i}{\mu}, \alpha_s(\mu^2), \varepsilon\right) = \sum_b \overline{\mathcal{S}}_{ab}\left(\rho_{ij}, \alpha_s(\mu^2), \varepsilon\right) \mathcal{H}_b\left(\frac{p_i \cdot p_j}{\mu^2}, \frac{(p_i \cdot n_i)^2}{n_i^2 \mu^2}, \alpha_s(\mu^2), \varepsilon\right) \times \prod_{i=1}^{m} J_i\left(\frac{(p_i \cdot n_i)^2}{n_i^2 \mu^2}, \alpha_s(\mu^2), \varepsilon\right) , \quad (2.70)$$

where the indices a and b depend on the representation. The reduced soft matrix is the obvious generalization of the 2-leg case and reads

$$\overline{\mathcal{S}}_{ab}\left(\rho_{ij}, \alpha_s(\mu^2), \varepsilon\right) = \frac{\mathcal{S}_{ab}(\beta_i \cdot \beta_j, \alpha_s(\mu^2), \varepsilon)}{\prod_{i=1}^{n} \langle 0|\Phi_{n_i}(\infty, 0)\Phi_{\beta_i}(\infty, 0)|0\rangle} , \quad (2.71)$$

where ρ_{ij} is the generalization of Eq. (2.69) to two generic legs i and j. The definition of the soft matrix $\mathcal{S}$ instead is more subtle compared to the two-leg case, since soft gluon emissions from different Wilson lines mix the color component of the amplitude. One defines

$$(c_a)_{\{\alpha_k\}} \mathcal{S}_{ab}(\beta_i \cdot \beta_j, \alpha_s(\mu^2), \varepsilon) = \sum_{\{\eta_k\}} \langle 0| \prod_{i=1}^{m} \Phi_{\beta_i}(\infty, 0)_{\alpha_k, \eta_k} |0\rangle \, (c_b)_{\{\eta_k\}} . \quad (2.72)$$

We note that while the (reduced) soft function is a matrix in color space, jet functions are singlet, as can be proven by power counting [66]) and thus their definition is the same as for the quark form factor. It is evident that factorization with more than two legs has a richer structure and color plays a much more important role. Moreover, order by order in perturbation theory it is possible to derive some constraint on the functional dependence of the functions involved [71].

This concludes the section about the factorization of the quark form factor in terms of hard, soft and jet functions. Now we will explicitly examine it at one loop.

2.6 One-loop soft and jet functions

In this section we will explicitly compute the jet and soft functions at one loop, showing that they reproduce the pole structure of the one-loop form factor, as discussed in [72].

We start with the soft function. In the series expansion over the coupling constant $\alpha_s = g_s^2/4\pi$, we define each term of the series as a coefficient of $(\alpha_s C_F/4\pi)$ to some power, leading to

$$\mathcal{S}\left(\beta_1\cdot\beta_2, \alpha_s(\mu^2), \varepsilon\right) \equiv \sum_{i=0}^{\infty} \left(\frac{\alpha_s C_F}{4\pi}\right)^i \mathcal{S}^{(i)} \,. \tag{2.73}$$

From the definition in Eq. (2.63), at leading order the functional dependence is trivial, since each Wilson line equals 1, as shown in Fig. 2.9(a). Hence we have

$$\mathcal{S}^{(0)} = 1 \,. \tag{2.74}$$

At one-loop, it is easy to show that the result reproduces the one-loop eikonal integral of Eq. (2.41), introduced previously as the homogeneous integral of the form factor. Indeed

$$\begin{aligned}
\left(\frac{\alpha_s C_F}{4\pi}\right)\mathcal{S}^{(1)} &= -g_s^2\mu^{2\varepsilon}\,\beta_1^\nu\beta_2^\mu \int_0^{+\infty} d\zeta_1 \int_0^{+\infty} d\zeta_2 \;\langle 0|\, A_\nu(\zeta_1\beta_1)\; A_\mu(\zeta_2\beta_2)\,|0\rangle \\
&= -g_s^2\mu^{2\varepsilon}\,\beta_1^\nu\beta_2^\mu \int_0^{+\infty} d\zeta_1 \int_0^{+\infty} d\zeta_2 \int \frac{d^dk}{(2\pi)^d} e^{-ik\cdot(\zeta_2\beta_2-\zeta_1\beta_1)} \frac{ig^{\mu\nu}}{k^2+i\eta} \\
&= -ig_s^2\mu^{2\varepsilon}\,\beta_1\cdot\beta_2 \int \frac{d^dk}{(2\pi)^d} \frac{1}{(k^2+i\eta)(\beta_1\cdot k - i\eta)(\beta_2\cdot k + i\eta)} \,.
\end{aligned} \tag{2.75}$$

After Feynman parametrization and momentum integration this yields

$$\begin{aligned}
\left(\frac{\alpha_s C_F}{4\pi}\right)\mathcal{S}^{(1)} &= 2\,i\,g_s^2\mu^{2\varepsilon}\,4\beta_1\cdot\beta_2 \int_0^1 dx \int_0^1 \frac{dy\,y}{(1-y)^3} \\
&\qquad \int \frac{d^dk}{(2\pi)^d} \frac{1}{\left[k^2 + \frac{y}{1-y}(2x\beta_1\cdot k - (1-x)2\beta_2\cdot k)\right]^3} \\
&= -2\,g_s^2\mu^{2\varepsilon}\;\frac{(-2\beta_1\cdot\beta_2)^{\frac{d}{2}-2}\,\Gamma\left(3-\frac{d}{2}\right)}{(4\pi)^{\frac{d}{2}}} \\
&\qquad \int_0^1 dx\;[x(1-x)]^{\frac{d}{2}-3} \int_0^1 dy\, y^{d-5}(1-y)^{3-d} \,.
\end{aligned} \tag{2.76}$$

While the x integration gives simply the Euler beta function $B\left(\frac{d}{2}-2, \frac{d}{2}-2\right)$, the y integration is identically zero

$$I_y \equiv \int_0^1 dy\, y^{d-5}(1-y)^{3-d} = \frac{\Gamma(d-4)\Gamma(4-d)}{\Gamma(0)} \,. \tag{2.77}$$

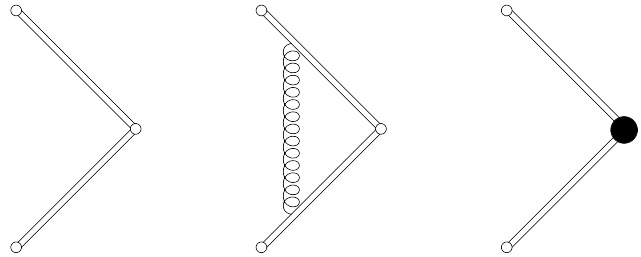

Figure 2.9: Diagrams contributing to the soft function at tree level (diagram (a)) and at one loop ((b) and (c)). The black solid circle represents the UV counterterm.

This could have been seen from the beginning of the calculation, since the integral is scaleless and thus vanishes in dimensional regularization. This remains valid at all orders and hence we conclude that, in a *bare* calculation, radiative corrections do not contribute and the soft function is equal to the identity

$$\begin{aligned} \mathcal{S}_{\text{bare}} &= \mathcal{S}^{(0)} = 1 \,, \\ \mathcal{S}^{(i)}_{\text{bare}} &= 0, \quad i > 0 \,. \end{aligned} \tag{2.78}$$

However, we know that composite operators need further UV renormalization. In this case, the UV divergence is due to the cusp formed by the two Wilson lines. Compared to the original integral with quadratic propagator, this UV divergence is a spurious one, due to the fact that we have linearized the propagator. In order to subtract it with a counterterm, we should isolate it in the integration. This can be done by observing that the vanishing of the scaleless integral in $d = 4$ is due to a cancellation of a IR and a UV pole. Indeed let us consider the y integration I_y and multiply it by $1 = (1 - y) + y$. Then it becomes

$$\begin{aligned} I_y &= \int_0^1 dy\, y^{d-4}(1-y)^{3-d} + \int_0^1 dy\, y^{d-5}(1-y)^{4-d} \\ &= \Gamma(d-3)\Gamma(4-d) + \Gamma(d-4)\Gamma(5-d) \,, \end{aligned} \tag{2.79}$$

which around $d = 4$ corresponds to a cancellation between two poles. Now, looking at first line in Eq. (2.76), by simple power counting, we see that the momentum integration has a different scaling for $y = 0, 1$:

$$y = 0 \quad \to \quad \mathcal{S}^{(1)} \sim \frac{d^d k}{k^6} \,, \tag{2.80}$$

$$y = 1 \quad \rightarrow \quad \mathcal{S}^{(1)} \sim \frac{d^d k}{k^3} \,. \tag{2.81}$$

We conclude that the UV pole is located at $y = 1$ and thus is opposite to the contribution multiplied by $(1 - y)$ which is $-\Gamma(d-4)\Gamma(5-d)$. The counterterm must cancel this and thus in the $\overline{MS}$ scheme it equals

$$I_y^{\text{CT}} = -\frac{1}{2\varepsilon} \,. \tag{2.82}$$

In conclusion at one loop the soft function is a pure counterterm which is equivalent to its IR pole (or equivalently minus the UV one). Inserting this into Eq. (2.76) we get

$$\mathcal{S}^{(1)} = 2 \left(-\frac{4\pi\mu^2}{2\beta_1 \cdot \beta_2} \right)^{2-\frac{d}{2}} \frac{\Gamma\left(3 - \frac{d}{2}\right) \Gamma^2\left(\frac{d}{2} - 2\right)}{\Gamma\left(d - 4\right)} \frac{1}{2\varepsilon} \,, \tag{2.83}$$

which expanded in ε gives

$$\mathcal{S}^{(1)} = -\left(\frac{2}{\varepsilon^2} + \frac{2}{\varepsilon} \log\left(-\frac{\overline{\mu}^2}{2\beta_1 \cdot \beta_2} \right) \right) + \mathcal{O}(\varepsilon^0) \,. \tag{2.84}$$

Now we move to the jet functions J and $\mathcal{J}$. In analogy with the soft function, we define their perturbative coefficients as

$$J\left(\beta_1 \cdot \beta_2, \alpha_s(\mu^2), \varepsilon\right) \equiv \sum_{i=0}^{\infty} \left(\frac{\alpha_s \, C_F}{4\pi} \right)^i J^{(i)} \,. \tag{2.85}$$

Starting from the definition in Eq. (2.64) we see that, as for the soft function, at leading order the jet function reduces to the identity

$$J^{(0)} u(p) = \langle 0 | \psi(0) | p \rangle = u(p) \,. \tag{2.86}$$

At one-loop there are two types of corrections: a self energy correction $J_p^{(1)}$ on the quark line and a gluon exchange between the quark and the Wilson line (vertex correction $J_V^{(1)}$). Let us start with the latter. From the definition we have to compute the following integral

$$J_V^{(1)} = 8\pi i \mu^{2\varepsilon} \int \frac{d^d k}{(2\pi)^d} \frac{(\not{p} - \not{k}) \not{n} \, u(p)}{(k^2 + i\eta)(k^2 - 2p \cdot k + i\eta)(2\, n \cdot k + i\eta)} \,, \tag{2.87}$$

whose result in the $\overline{MS}$ scheme reads

$$J_V^{(1)} = -\left\{ \left(\frac{n^2 \overline{\mu}^2}{(-2p \cdot n)^2} \right)^{\varepsilon} \left(\frac{1}{\varepsilon^2} + \frac{1}{\varepsilon} + 2 + \frac{5\pi^2}{12} \right) + \frac{2}{\varepsilon} - \frac{1}{\varepsilon_{\text{UV}}} \right\} \,. \tag{2.88}$$

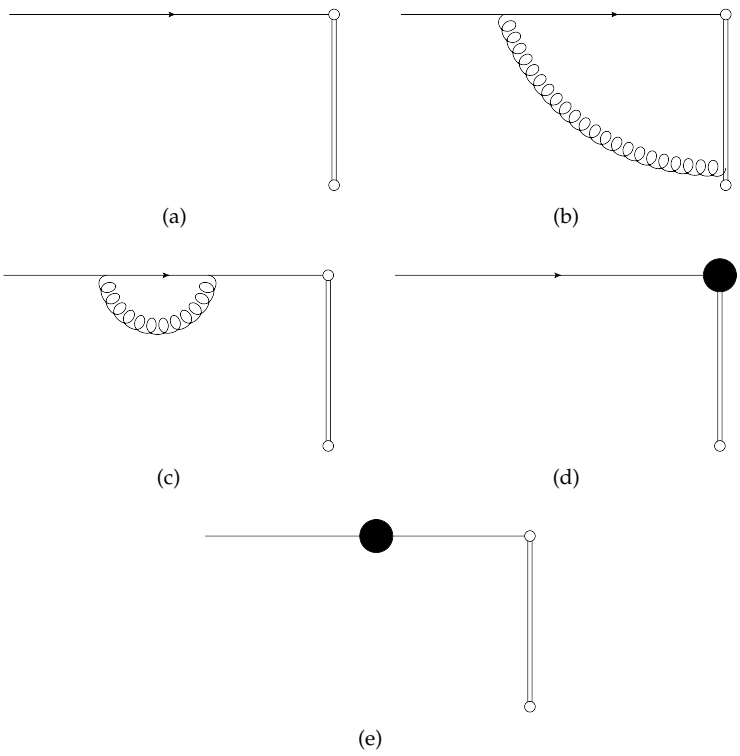

Figure 2.10: (a): Tree level jet function. (b)-(e): Diagrams contributing to the one-loop jet function. The black solid circles represent UV counterterms.

All the poles are of IR origin apart from $\varepsilon_{\rm UV}$. The UV counterterm for this vertex (which is not the usual vertex of QCD but it belongs specifically to the jet operator vertex where the quark and the Wilson line meet) is then

$$J^{(1)}_{V,CT} = -\frac{1}{\varepsilon_{\rm UV}} \,. \tag{2.89}$$

For the self energy diagram the story is the same as for the calculation of the form factor in Section 2.3, since the Wilson line is not involved here. The diagram vanishes in dimensional regularization, and one is left with the standard wave function renormalization counterterm

$$J^{(1)}_{p} = \frac{1}{\varepsilon} \,. \tag{2.90}$$

Finally, we turn to the last piece, which is the eikonal jet function. For this, the only

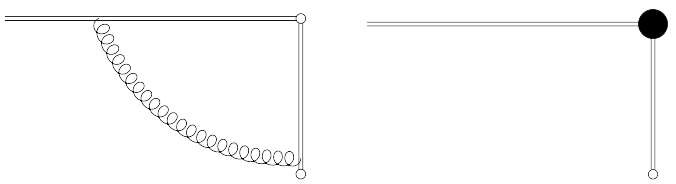

(a) (b)

Figure 2.11: Diagrams contributing to the one loop eikonal jet function. The black solid circle represents the UV counterterm.

non vanishing contribution comes from the vertex correction. The result is

$$\mathcal{J}_V^{(1)} = -\left\{\frac{1}{\varepsilon^2} + \frac{1}{\varepsilon}\log\left(\frac{n^2\overline{\mu}^2}{2(\beta\cdot n)^2}\right)\right\} . \tag{2.91}$$

Putting together all the contributions from soft and jet functions and considering only the pole part, we see that indeed we reproduce the pole part of the one-loop form factor

$$\begin{aligned} 2\,J^{(1)} - 2\,\mathcal{J}_V^{(1)} + \mathcal{S}^{(1)} &= 2\left(J_V^{(1)} + J_{V,CT}^{(1)} + J_p^{(1)} - \mathcal{J}_V^{(1)}\right) + \mathcal{S}^{(1)} \\ &= \left[-\frac{2}{\varepsilon^2} - \frac{2}{\varepsilon}\log\left(-\frac{\mu^2}{Q^2}\right) - \frac{3}{\varepsilon}\right] , \end{aligned} \tag{2.92}$$

which matches with the pole structure of Eq. (2.26).

In conclusion, we have seen that the singular part of the one-loop form factor is correctly reproduced by the universal functions which encode its soft and collinear behavior. The finite part, as already mentioned, can be reproduced by matching to the full QCD calculation, defining the hard function which depends on the particular structure of the electromagnetic vertex.

This concludes the chapter, where we have discussed soft-collinear factorization at leading power in the soft approximation. We have introduced three important concepts that will be used in the rest of the thesis: the use of diagrammatic techniques based on the eikonal approximation, the presence of leading singular regions, and the definition of the factorization formula in terms of soft and jet functions. The following three chapters will use in turn one of these three approaches to investigate the soft approximation at subleading power.

CHAPTER 3

A diagrammatic approach to next-to-soft corrections

In this chapter the main topic of this thesis is introduced, which is extending the soft approximation to subleading power. As such, many of the tools and the set up exposed here will be relevant also for next chapters. In particular, the Drell-Yan process as a case study is introduced here and will be used in the rest of the thesis as an application of the various techniques developed. Though largely an introductory chapter, new results are presented, namely the eikonal expansion of the quark form factor and the computation of the factorizable contributions to the Drell-Yan K-factor.

The approach followed in this chapter is a diagrammatic one, building on the work done in [73]. There it is shown that the use of effective vertices typical of the eikonal approximation (E) can be generalized to subleading level, known as *next-to-eikonal* (NE). Already here we can state that we do not expect this approach to be a complete picture. Indeed it is well-known since the time of Low [74] that at subleading power in the soft expansion there are terms that break the naive factorization framework and cannot be caught by this effective Feynman rules approach. This issue will be thoroughly discussed in next chapters, and is related to the main results discussed in this thesis. However, in order to better clarify the structure of soft-collinear factorization at subleading power and in order to introduce the main differences with the standard eikonal approximation, it is interesting to show what can be reproduced with the use of these simple expanded vertices, as these computations are not explicitly available in the literature. Moreover, it is interesting to see the differences between threshold and soft expansion, and how this naive factorization works at the amplitude and cross-section level.

The structure of the chapter is as follows. After introducing the reasons for going beyond the soft approximation we explain how the next-to-eikonal effective rules can

be constructed. Then, we implement them in the computation of the one-loop quark form factor, showing how this can be decomposed in the various terms of the eikonal expansion. Finally, we move from amplitude to cross section level and consider the Drell-Yan K-factor. After presenting the results from a traditional full QCD computation, we compute it in this effective framework, showing which parts of it are reproduced.

3.1 Beyond the soft approximation

It is well-known that IR singularities cancel for suitably defined inclusive cross sections, after real and virtual diagrams are added. However, after this cancellation, potentially large residual contributions can persist to all orders in the form of logarithms. Being so numerically large, they might spoil the predictivity of perturbation theory and therefore need to be resummed. Generally, the arguments of these logarithms might involve different scales depending on the masses and kinematical invariants of the process. Here, the class of logarithms we will discuss are called *threshold* logarithms.

The argument of these logarithms involves a dimensionless variable ξ, called *threshold* variable, that is differently defined according to the specific process one is looking at. Various examples include: Deep Inelastic Scattering (DIS), where $\xi = 1 - x$ with x equal to the Bjorken variable; electroweak annihilation processes where $\xi = 1 - z$ (such as Higgs production via gluon fusion where $z = M_H^2/s$ and M_H is the Higgs mass or Drell-Yan production where $z = Q^2/s$ and Q^2 is the invariant mass of the lepton pair); $t\bar{t}$ production where $\xi = 1 - z = 1 - 4m_t^2/s$ and m_t is the top mass. In all these cases s represents the squared partonic center-of-mass energy. When $\xi \to 0$, expressions for these cross sections follow the pattern

$$\frac{d\sigma}{d\xi} = \sum_{n=0}^{\infty} \alpha_s^n \sum_{m=0}^{2n-1} \left[a_{nm} \left(\frac{\log^m(\xi)}{\xi} \right)_+ + b_{nm}\delta(\xi) + c_{nm} \log^m(\xi) + \mathcal{O}(\xi) \right] , \tag{3.1}$$

where the subscript $+$ denotes the plus distribution, which arises by expanding in ε as

$$\xi^{-1+n\varepsilon} = \frac{1}{n\,\varepsilon}\,\delta(\xi) + \sum_{i=0}^{m} \frac{(n\,\varepsilon)^i}{i!} \left(\frac{\log^i(\xi)}{\xi} \right)_+ + \mathcal{O}(\varepsilon^{m+1}) . \tag{3.2}$$

Much is known about the coefficients a_{nm} and b_{nm}, which belong to leading power (LP) threshold logarithms and originate from pure soft and collinear gluon emissions. The literature about the resummation of these terms is vast [53, 75–80], and largely relies on the eikonal approximation. The knowledge of the coefficients c_{nm} of the subleading terms, known as *next-to-leading power* (NLP) threshold logarithms, requires the extension of the standard techniques in soft gluon resummation at a subleading level, also known

as *next-to-eikonal* level. For completeness, we recall that in Mellin space LP and NLP logarithms correspond to $\log^i N$ and $(1/N)\log^i N$ respectively, whereas the threshold limit is achieved for large-N. As several studies have shown [81–84], the inclusion of these terms might be important for phenomenological applications. Preliminary studies have been performed [73, 85–91], but a systematic framework that allows a full resummation is still lacking.

Recently, this topic received also much attention in a more formal context. Studying the symmetry of the quantum gravity S-matrix and certain particular transformations acting on past and future null infinity, it has been conjectured that at tree-level the Weinberg soft theorem [92] can be generalized with a universal next-to-soft factor [93]. This has led to a number of further studies both in gauge and gravity theories that have investigated the breakdown of next-to-soft theorems at loop level [94–103]. This topic has been investigated also with the use of effective field theories in [104]. There, besides discussing next-to-soft theorems, a systematic approach to next-to-soft corrections is presented in terms of effective operators at next-to-leading power.

In the next section we discuss the simplest approach to extend the soft approximation to subleading power, through the use of diagrammatic techniques.

3.2 Diagrammatics

In the previous section we have motivated the investigation of the soft expansion at subleading power, recalling that this is relevant both for phenomenology and for more formal contexts. Now we shall explicitly construct a framework that is able to deal with such subleading corrections.

As one might imagine, the simplest way to set this up is to perform the soft expansion after the full QCD amplitudes have been constructed. In [73, 86] it was proven that carrying these expansions is equivalent to the definition of effective Feynman rules for eikonal (E) and next-to-eikonal (NE) emissions. The goal of this section is not to review this proof, which is based on the exponentiation of these vertices, but rather to give the reader an intuitive understanding of how these effective rules emerge, by considering the case of a two gluon emission. For simplicity, we will present the calculation for the abelian part of the amplitude, ignoring color generators. The result for full QCD can be found in [73]. Even though the argumentation we present pertains to a gauge theory, it is worthwhile to note that these techniques have been generalized to perturbative gravity [94, 100].

We now consider the emission of two soft gluons of momenta k and q from a hard fermion line of momentum p, and then sum over all possible insertions of them. The

amplitude for such a process reads

$$\mathcal{M}_0(p)\,\left(\frac{\not p-\not q-\not k}{(p-q-k)^2}\,\gamma^\nu\frac{\not p-\not q}{(p-q)^2}\,\gamma^\mu+\frac{\not p-\not q-\not k}{(p-q-k)^2}\,\gamma^\mu\frac{\not p-\not k}{(p-k)^2}\,\gamma^\nu\right)u(p)\,, \tag{3.3}$$

where $\mathcal{M}_0(p)$ collects the rest of the amplitude and we have omitted the polarization vectors of the gluons. We wish to expand this to NE level. Corrections to the denominators are straightforward and give rise to four different NE combinations:

$$\begin{aligned}&\frac{q^2}{2p\cdot(k+q)(2p\cdot q)^2}\,, &&\frac{(k+q)^2}{2p\cdot q(2p\cdot(k+q))^2}\,,\\ &\frac{k^2}{2p\cdot(k+q)(2p\cdot k)^2}\,, &&\frac{(k+q)^2}{2p\cdot k(2p\cdot(k+q))^2}\,.\end{aligned} \tag{3.4}$$

Numerators are slightly more tedious. In the eikonal limit, after using the Dirac equation, they are trivial ($2p^\mu$ or $2p^\nu$) since all soft momenta in the numerator can safely be put to zero. At NE level we have to consider the four possible combinations in which one emission maintains all momenta. We get for each NE combination:

$$\not p\gamma^\nu(\not p-\not q)\gamma^\mu\;u(p)=(-2p^\nu\not q\gamma^\mu+2p\cdot q\gamma^\nu\gamma^\mu-2p^\mu\gamma^\nu\not q)u(p)\,, \tag{3.5}$$

$$(\not p-\not q-\not k)\gamma^\nu\not p\gamma^\mu\;u(p)=-2p^\mu(\not q+\not k)\gamma^\nu u(p)\,, \tag{3.6}$$

$$\not p\gamma^\mu(\not p-\not k)\gamma^\nu\;u(p)=(-2p^\mu\not k\gamma^\nu+2p\cdot k\gamma^\mu\gamma^\nu-2p^\nu\gamma^\mu\not k)u(p)\,, \tag{3.7}$$

$$(\not p-\not q-\not k)\gamma^\mu\not p\gamma^\nu\;u(p)=-2p^\nu(\not q+\not k)\gamma^\mu u(p)\,. \tag{3.8}$$

We must now combine everything to the correct order in the soft expansion. Combining numerators and denominators at E level we find the well-known eikonal identity, represented in Fig. 3.1,

$$\frac{1}{(p\cdot(k+q))(p\cdot k)}+\frac{1}{(p\cdot(k+q))(p\cdot q)}=\frac{1}{p\cdot k}\frac{1}{p\cdot q}\,, \tag{3.9}$$

which tells us that, at leading order in the softness, soft emissions factorize and can be expressed in terms of independent emissions whose vertices are given by the effective eikonal rule

$$V_E^\mu(p,k)=-\frac{p^\mu}{p\cdot k-i\eta}\,. \tag{3.10}$$

We see that this vertex is a scalar, due to the well-known fact that eikonal emissions are insensitive to the spin of the emitting particle.

Extending this analysis to NE order, we compute separately corrections to numerators and denominators. The latter are obtained after combining the sum of the four terms in Eq. (3.4) with $4p^\mu p^\nu$. After some algebra this yields

$$\frac{-p^\mu p^\nu q^2}{2(p\cdot q)^2p\cdot k}+\frac{-p^\mu p^\nu k^2}{2(p\cdot q)^2p\cdot k}+\frac{-p^\mu p^\nu(k\cdot q)}{2(p\cdot(k+q))p\cdot qp\cdot k}\,. \tag{3.11}$$

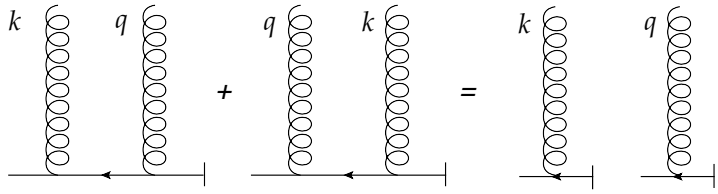

Figure 3.1: Eikonal identity for two gluons. Vertices are assumed to be eikonal on both sides of the equation.

For numerator corrections, we have to combine the sum of Eq. (3.5) and Eq. (3.6) with $(4p\cdot(k+q)p\cdot q)^{-1}$, and the sum of Eq. (3.7) and Eq. (3.8)) with $(4p\cdot(k+q)p\cdot k)^{-1}$. The total contribution now reads

$$\frac{\not{q}\gamma^\mu p^\nu}{2p\cdot kp\cdot q}+\frac{\not{k}\gamma^\nu p^\mu}{2p\cdot kp\cdot q}-\frac{g^{\mu\nu}}{p\cdot(k+q)}+\frac{q^\nu p^\mu p\cdot k+k^\mu p^\nu p\cdot q}{(p\cdot(k+q))(p\cdot q)(p\cdot q)}\,. \tag{3.12}$$

The first two terms in Eq. (3.11) with the first two in Eq. (3.12) form a combination of two independent E and NE emissions, from which we can define a single-vertex NE Feynman rule

$$\begin{aligned}V^\mu_{NE}(p,k) =& =\frac{\not{k}\gamma^\mu}{2p\cdot k}-\frac{p^\mu k^2}{(p\cdot k)^2}\\ &=-\frac{p^\mu k^2}{(p\cdot k)^2}+\frac{k^\mu}{2p\cdot k}-\frac{\mathrm{i}\,k_\alpha\Sigma^{\alpha\mu}}{p\cdot k}\,.\end{aligned} \tag{3.13}$$

where we introduced the Lorentz generator

$$\Sigma^{\alpha\nu}\;=\;\frac{\mathrm{i}}{4}\Big[\gamma^\alpha,\gamma^\nu\Big]\,, \tag{3.14}$$

to isolate the spin dependent part of the NE emission. Notice that it takes the form of a magnetic moment coupling to the fermion leg. The generalization to emitters with different spin amounts to choosing the proper form of the Lorentz generator. Therefore, at NE level soft emissions *are* sensitive to the spin of the emitting particles. Note also that for *real* radiation, in Eq. (3.13) only the $\Sigma^{\alpha\nu}$ term is relevant: the first term is zero by the on-shell condition $k^2=0$ while the second one vanishes after contraction with a physical polarization tensor obeying $k^\mu\epsilon_\mu(k)=0$. Finally, we remind that we are considering only abelian-like emissions and that the QED charge (equals to -1 and $+1$ for incoming particles and incoming antiparticles respectively) has been already included in the effective E and NE vertices.

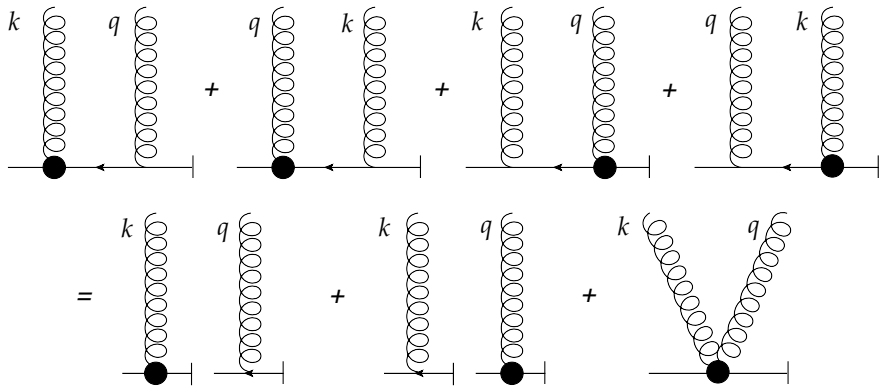

Figure 3.2: Next-to-Eikonal Identity for two gluons. Black solid circles represent a next-to-eikonal emission while other vertices are eikonal. We note the presence of a 2-gluon vertex in the right hand side of the equation.

The residual terms from Eq. (3.11) and Eq. (3.12) form a tensor $R^{\mu\nu}$ that represents a two-gluon ("seagull") vertex:

$$R^{\mu\nu}(p,q,k) = \frac{p^\nu k^\mu (p\cdot q) + p^\mu q^\nu (p\cdot k) - (p\cdot k)(p\cdot q) g^{\mu\nu} - p^\mu p^\nu (q\cdot k)}{p\cdot(q+k)\, p\cdot k\, p\cdot q} \,. \tag{3.15}$$

The derivation is represented graphically in Fig. 3.2.

The argument presented here for two gluons can be generalized to n gluons, including also color generators. The structure remains the same, as the emissions can be rearranged in terms of single-gluon and seagull-type vertices, where the last ones represent a sum over all possible correlations between pairs of gluons. A pattern emerges and shows that these vertices exponentiate and therefore can be regarded in every respect as effective Feynman rules [73]. An alternative and somewhat more elegant proof of this exponentiation has been given in [86] with path integral techniques. There, next-to-soft emissions are regarded as fluctuations along the classical trajectory defined by the external hard line. The exponentiation then follows from standard quantum field theories properties of connected diagrams.

In any case, the fact that the structure of these effective vertices persists at all orders is a first hint that, at least for the contributions that can be described by such vertices, a factorization picture at next-to-soft level can be constructed. However, even in this simple analysis it is already evident that building up a factorization for NE corrections is much tougher than the pure eikonal ones, as can be seen by the presence of a seagull vertex that makes the soft emissions dependent on each other.

Having reviewed how next-to-eikonal Feynman rules emerge, we can now implement them at amplitude level in the one-loop quark form factor.

3.3 Eikonal expansion of the form factor

The eikonal Feynman rules constructed in the previous section are the simplest and more intuitive way in which subleading corrections in the soft expansion can be made systematic. However, at this point we have to make an important distinction when applying these rules. When dealing with *real* gluons, it is clear why one should use effective (next-to-)soft vertices to describe soft gluon emissions, since for on-shell particles the softness of their momentum corresponds to the vanishing of their energy. As we will see for the Drell-Yan process in the next sections, this implies that the soft (or eikonal) and the threshold expansion coincide. However, next-to-soft effective rules can also be applied to *virtual* gluons. In this case it is less intuitive how to handle these soft vertices, as the off-shell momentum of the virtual gluon can be also hard.

However, there are cases where one is allowed to use them, such as in the computation of the soft function [72]. As we described in the introduction, the soft function governs the soft behavior of the amplitudes at all orders and it is defined in terms of correlators of Wilson lines. Order by order in perturbation theory this corresponds to the inclusion of gluon exchanges between the Wilson lines, whose interactions are described by the eikonal effective vertex. Moreover, the argument that enters in the exponent of the soft function is made by a subset of diagrams: in the abelian case this is the set of all *connected* diagrams [105], while in the non-abelian case is the set of the so-called *webs* [106–109]. It has been shown in [108] that the use of webs can be generalized to next-to-eikonal level, and requires the use of NE effective vertices. Motivated by this, and by the general goal of shedding light on the structure of next-to-eikonal corrections at all-orders, we are now going to investigate the effects of NE vertices for virtual gluons.

The amplitude we consider is the one-loop quark form factor Γ we introduced in the previous chapter and whose integral representation is repeated here

$$\Gamma = g^2 C_F \mu^{2\varepsilon} \int \frac{d^d k}{(2\pi)^d} \frac{\bar{v}(\bar{p})\gamma^\alpha(-\bar{\not{p}} - \not{k})\gamma^\mu(\not{p} - \not{k})\gamma_\alpha u(p)}{k^2(p-k)^2(\bar{p}+k)^2} \,. \tag{3.16}$$

If we rescale the virtual gluon momentum $k^\mu \to \lambda k^\mu$, this implies the following expansion for the form factor

$$\Gamma = \sum_{n=1}^{\infty} \Gamma_i \lambda^i \,, \tag{3.17}$$

where every term Γ_i in the series corresponds to an expansion of the *integrand* in powers of λ. A we saw in the previous section, this is equivalent at E and NE level to the use of effective Feynman rules. Therefore we define the leading and subleading order contributions respectively as the *eikonal* and *next-to-eikonal form factor* Γ_E and Γ_{NE}. From its definition, it is clear that Γ_E should be equal to the soft function already defined in the first chapter. We recall here some basic facts about it. At one-loop the computation involves the basic scalar integral I, which reads

$$I = \int \frac{d^d k}{(2\pi)^d} \frac{1}{(k^2 + i\eta)(2\, p \cdot k - i\eta)(2\, \bar{p} \cdot k + i\eta)} \,. \tag{3.18}$$

Upon Feynman parametrizing it and performing the momentum integration we get

$$I = \frac{i}{(4\pi)^2} \left(-\frac{4\pi}{s}\right)^{\varepsilon} \frac{1}{s} \Gamma(1+\varepsilon) B(-\varepsilon, -\varepsilon) \int_0^1 dy\, y^{-1+2\varepsilon} (1-y)^{-1-2\varepsilon} \,. \tag{3.19}$$

The integration over y vanishes because of a cancellation between a UV and a IR pole, and it is a consequence of the fact that the eikonal approximation linearizes propagators and therefore introduces spurious UV divergences in $d = 4 - 2\varepsilon$. Those need to be subtracted by a counterterm and thus evaluating the (renormalized) integral amounts to extracting its UV part, as we discussed in the first chapter. The final expression for the eikonal form factor, after restoring prefactors, reads

$$\Gamma_E = \frac{\alpha_s C_F}{4\pi} \left(-\frac{4\pi\mu^2}{s}\right)^{\varepsilon} \frac{\Gamma(1+\varepsilon) B(-\varepsilon, -\varepsilon)}{\varepsilon} \,. \tag{3.20}$$

We stress that this expression holds to all orders in ε.

We can now move to subleading corrections in the eikonal expansion. As discussed in detail in the previous subsections, two kinds of corrections are possible, due to either numerator or denominator. In the case of the one-loop form factor, in the former there are only E, NE and NNE terms, while in the latter all terms in the series are present. We start analyzing NE corrections to the numerator, which involves the basic vector integral I^μ, defined as

$$I^\mu = \int \frac{d^d k}{(2\pi)^d} \frac{k^\mu}{(k^2 + i\eta)(2\, p \cdot k - i\eta)(2\, \bar{p} \cdot k + i\eta)} \,. \tag{3.21}$$

After using standard techniques we get

$$I^\mu = \frac{-i}{(4\pi)^2} \left(-\frac{4\pi}{s}\right)^{\varepsilon} \frac{1}{s} \Gamma(1+\varepsilon) B(1-\varepsilon, -\varepsilon) (p^\mu - \bar{p}^\mu) \int_0^1 dy\, (1-y)^{-2\varepsilon} y^{-2+2\varepsilon} \,. \tag{3.22}$$

As in the eikonal case, we are left with a y-integral that vanishes. However, the situation here is more subtle, as this does not correspond to a cancellation of UV and IR poles

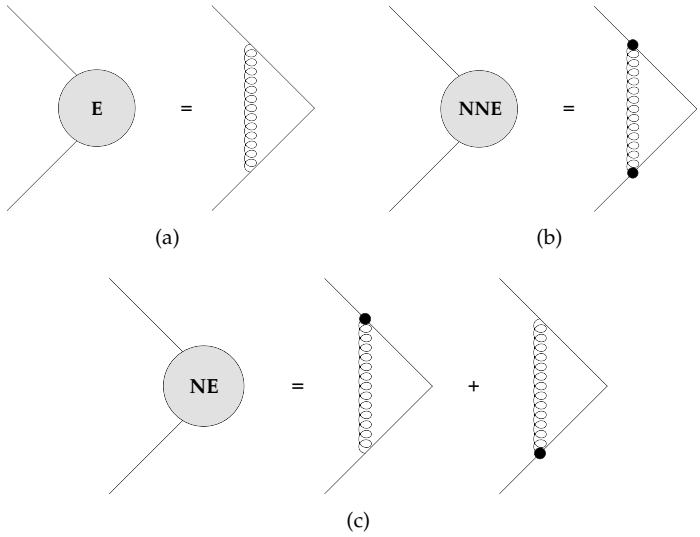

Figure 3.3: Depiction of the eikonal, next-to-eikonal and next-tonext-to eikonal form factors in terms of the effective Feynman rules.

in $d = 4$. Nonetheless, if we analytically continue our function from $d = 4$ to $d = 3$, we see that the situation is similar to the eikonal case, as there is a UV pole given by $1/(d-3) = 1/(1-2\varepsilon)$. More generally, whenever we find an integral $G(d, n)$ defined as

$$G(d,n) = \int_0^1 y^{n-1-d}(1-y)^{d-n-1} \,, \tag{3.23}$$

since this integral vanishes because of a cancellation between IR and UV poles around $d = n$, we can define a procedure to evaluate the renormalized integral in dimensional regularization, replacing it by its UV counterterm in $d = n$:

$$G(d,n) \to \frac{1}{d-n} = \frac{1}{4-2\varepsilon-n} \,. \tag{3.24}$$

In doing so, the basic NE vector integral reads

$$I^\mu = \frac{-i}{(4\pi)^2}\left(-\frac{4\pi}{s}\right)^\varepsilon \frac{1}{s}\frac{\Gamma(1+\varepsilon)\Gamma(1-\varepsilon)\Gamma(-\varepsilon)}{\Gamma(2-2\varepsilon)}(p^\mu - \bar{p}^\mu) \,. \tag{3.25}$$

Before presenting the result for the NE form factor, we consider the second basic integral we need, defined as

$$I^{\mu\nu} = \int \frac{d^dk}{(2\pi)^d}\frac{k^\mu k^\nu}{(k^2+i\eta)(2\,p\cdot k - i\eta)(2\,\bar{p}\cdot k + i\eta)} . \tag{3.26}$$

After using standard techniques and Eq. (3.24) for $n = 2$, it becomes

$$I^{\mu\nu} = \frac{1}{(4\pi)^2}\left(-\frac{4\pi}{s}\right)^{\varepsilon}\frac{1}{s}\frac{1}{2-2\varepsilon}B(1-\varepsilon,1-\varepsilon) \times\left[\frac{s}{2}g^{\mu\nu}\Gamma(\varepsilon)-\left(p^{\mu}\bar{p}^{\nu}+p^{\nu}\bar{p}^{\mu}+\frac{1-\varepsilon}{\varepsilon}(p^{\mu}p^{\nu}+\bar{p}^{\mu}\bar{p}^{\nu})\right)\Gamma(1-\varepsilon)\right]. \quad (3.27)$$

Note that in the above expression special care must be taken for the case $\mu = \nu$. Indeed in that particular case the integral has no UV pole for $d = 2$, and thus the application of the rule of Eq. (3.24) makes no sense anymore. From a straightforward evaluation of Eq. (3.27) one get a factor $2 - 2\varepsilon$ which cancels the same factor in the denominator (which represents the UV pole around $d = 2$). So in this case the integral must be set to zero. It can be verified that the same behavior appears with higher powers of k^2, and therefore all denominators corrections, which involve only powers of k^2, vanish in this setting.

We conclude that at NE level only the basic integral I^{μ} is needed. Inserting it in the full spin-dependent numerator yields

$$\Gamma_{NE} = \frac{\alpha_s C_F}{4\pi}\left(-\frac{4\pi\mu^2}{s}\right)^{\varepsilon}\frac{4\,\Gamma(1+\varepsilon)\Gamma(1-\varepsilon)\Gamma(-\varepsilon)}{\Gamma(2-2\varepsilon)}\,. \quad (3.28)$$

Now, looking at the full form factor, we can define a remainder term that collects all corrections which are subleading with respect to the NE form factor (i.e. NNE, NNNE, etc.). However, we note that the only non-vanishing contribution is order NNE, because all other subleading terms in the eikonal expansion are due to denominator corrections. Thus, using Eq. (3.27) we get the (remainder) NNE form factor:

$$\Gamma_{NNE} = \frac{\alpha_s C_F}{4\pi}\left(-\frac{4\pi\mu^2}{s}\right)^{\varepsilon}(1-2\varepsilon)\Gamma(\varepsilon)B(1-\varepsilon,1-\varepsilon)\,. \quad (3.29)$$

Adding Eq. (3.20), Eq. (3.28) and Eq. (3.29), and comparing with Eq. (2.26), we see that

$$\Gamma = \Gamma_E + \Gamma_{NE} + \Gamma_{NNE}\,, \quad (3.30)$$

at *every* order in ε. This verifies the eikonal expansion set up so far and forms a non-trivial check of the diagrammatic approach based on effective rules.

However, to get full sense of the strength and the weakness of this approach, we have to refer to an example of phenomenological interest, such as the Drell-Yan process.

3.4 The Drell-Yan K-factor in full QCD

Until now we have been working at amplitude level, considering generic gluon emissions at leading and subleading power in the soft expansion. However, to see how this

approach can be useful for phenomenology applications, we have to move from the amplitude to the cross-section level. In particular, referring to Eq. (3.1), we would like to understand how LP and NLP terms in the threshold expansion are related to the use of E and NE effective rules.

As announced, we consider the Drell-Yan process, i.e. the inclusive production of an off-shell vector boson of invariant mass Q^2

$$q(p) + \bar{q}(\bar{p}) \;\to\; V^*(Q)\,, \tag{3.31}$$

where the vector boson V could be a photon, a Z or a $W^\pm$ boson. There is more than one reason for choosing such a process. The first is phenomenological, as this is an important process to test the electroweak sector of the Standard Model. Moreover it forms the prototype for other processes at hadron colliders, such as the Higgs boson production through gluon fusion. A final important motivation is that kinematical constraints in the case of the Drell-Yan process force threshold radiation to be soft, and therefore *every* logarithm enhancement corresponds to the vanishing of the energy of at least one *real* gluon. However, as we shall discuss in the following chapters, this does not imply that these logarithms are insensitive to *virtual* gluons. In particular, we will see that part of the NLP logarithms are sensitive to a virtual gluon when its momentum becomes collinear to one of the incoming quarks.

The object we investigate is not the cross-section, but rather the K-factor defined as

$$K^{(n)}(z) \;=\; \frac{1}{\sigma^{(0)}}\,\frac{d\sigma^{(n)}(z)}{dz}\,, \tag{3.32}$$

where $\sigma^{(0)}$ is the Born cross section and n is the order of expansion in α_s. One of the advantages of working with this quantity is that in the computation of the diagrams, order by order in perturbation theory, overall factors shared with $\sigma^{(0)}$ such as the electroweak coupling or the color average drop out.

For simplicity, we will consider in this thesis not the entire K-factor, but only the terms proportional to the color prefactor C_F^2. These terms are the same as those that would appear in an abelian theory, and therefore can be obtained neglecting diagrams involving three- or four-gluon couplings. This is sufficient to illustrate the key points of the different approaches outlined in this thesis reducing technical complications.

To further restrict our analysis, we will investigate the two-loop K-factor $K^{(2)}$, for the following reasons. At two loops, we can distinguish three different sets of contributions to the K-factor: the double-real (RR), the real-virtual interference (RV) and the double virtual (VV). In the VV contributions no other final state is produced other than the electroweak boson. Therefore its invariant mass squared Q^2 will be equal to the incoming energy squared s, which implies that all contributions will be proportional to $\delta(1-z)$.

This set of LP terms is under control [110] and is not further investigated in this thesis. Instead, RR and RV contributions will have a non-trivial dependence on z, as final state gluons will take part of the available incoming energy. The functional dependence will be quite complicated, and in general the description will require harmonic polylogarithms [41, 111]. However, as we said, in the threshold limit $z \to 1$, the functional dependence is reduced to LP and NLP logarithms, which follows in the generic pattern of Eq. (3.1). Our goal will be to reproduce with three different approaches the result obtained from the threshold limit of the full QCD calculation. In Section 3.5 we will implement the approach based on diagrammatic techniques, while the other two will be discussed in Chapter 4 and Chapter 5 respectively.

We can now make a further distinction beween RR and RV diagrams. In the former all gluons are real, therefore the soft limit on both emissions corresponds in the limit in which the total energy flows into the vector boson propagator: soft and threshold expansion coincide. Hence we expect that for this class of diagrams the use of effective rules is sufficient to reproduce the full result. This has been verified in [73] and the conclusion is that both LP and NLP are reproduced with the next-to-eikonal Feynman rules.

The story for the RV case is clearly different. Taking the soft limit in both gluons will still imply that the incoming energy tends to entirely flow in the vector boson. However, configurations where the real gluon is soft but the virtual is not, are not taken into account in this setting and will still contribute to the threshold limit. Therefore, to disentangle IR singularities and to test various approaches towards this issue, we focus on the RV diagrams. Before discussing this in the effective approach, let us review the result in the full QCD calculation.

The relevant Feynman diagrams are shown in Fig. 3.4, leading to the following contributions to the squared diagrams (suppressing overall coupling, colour factors and integration measures)

$$
\begin{aligned}
(a): &\quad \frac{\mathrm{Tr}\left[\bar{\not{p}}\gamma^\mu(k_1\!-\!\bar{\not{p}})\gamma^\alpha(\not{p}\!+\!\not{k}_1\!-\!\not{k}_2)\gamma^\nu(\not{p}\!+\!\not{k}_1)\gamma_\mu\,\not{p}\gamma_\alpha(-\bar{\not{p}}\!+\!\not{k}_2)\gamma_\nu\right]}{k_1^2(k_1-\bar{p})^2(p+k_1-k_2)^2(p+k_1)^2(\bar{p}-k_2)^2}\,,\\
(b): &\quad \frac{\mathrm{Tr}\left[\bar{\not{p}}\gamma^\mu(k_1\!-\!\bar{\not{p}})\gamma^\alpha(\not{p}\!+\!\not{k}_1\!-\!\not{k}_2)\gamma^\nu(\not{p}\!+\!\not{k}_1)\gamma_\mu\,\not{p}\gamma_\nu(\not{p}\!-\!\not{k}_2)\gamma_\alpha\right]}{k_1^2(k_1-\bar{p})^2(p+k_1-k_2)^2(p+k_1)^2(p-k_2)^2}\,,\\
(c): &\quad \frac{\mathrm{Tr}\left[\bar{\not{p}}\gamma^\mu(k_1\!-\!\bar{\not{p}})\gamma^\alpha(\not{p}\!+\!\not{k}_1\!-\!\not{k}_2)\gamma_\mu(\not{p}\!-\!\not{k}_2)\gamma^\nu\,\not{p}\gamma_\alpha(-\bar{\not{p}}\!+\!\not{k}_2)\gamma_\nu\right]}{k_1^2(k_1-\bar{p})^2(p+k_1-k_2)^2(p-k_2)^2(k_2-\bar{p})^2}\,,\\
(d): &\quad \frac{\mathrm{Tr}\left[\bar{\not{p}}\gamma^\mu(k_1\!-\!\bar{\not{p}})\gamma^\alpha(\not{p}\!+\!\not{k}_1\!-\!\not{k}_2)\gamma_\mu(\not{p}\!-\!\not{k}_2)\gamma^\nu\,\not{p}\gamma_\nu(\not{p}\!-\!\not{k}_2)\gamma_\alpha\right]}{k_1^2(k_1-\bar{p})^2(p+k_1-k_2)^2(p-k_2)^2(p-k_2)^2}\,,\\
(e): &\quad \frac{\mathrm{Tr}\left[\bar{\not{p}}\gamma^\alpha(\not{p}\!-\!\not{k}_2)\gamma^\mu(\not{p}\!+\!\not{k}_1\!-\!\not{k}_2)\gamma^\nu(\not{p}\!+\!\not{k}_1)\gamma_\mu\,\not{p}\gamma_\nu(\not{p}\!-\!\not{k}_2)\gamma_\alpha\right]}{k_1^2(p-k_2)^2(p+k_1-k_2)^2(p+k_1)^2(p-k_2)^2}\,,
\end{aligned}
$$

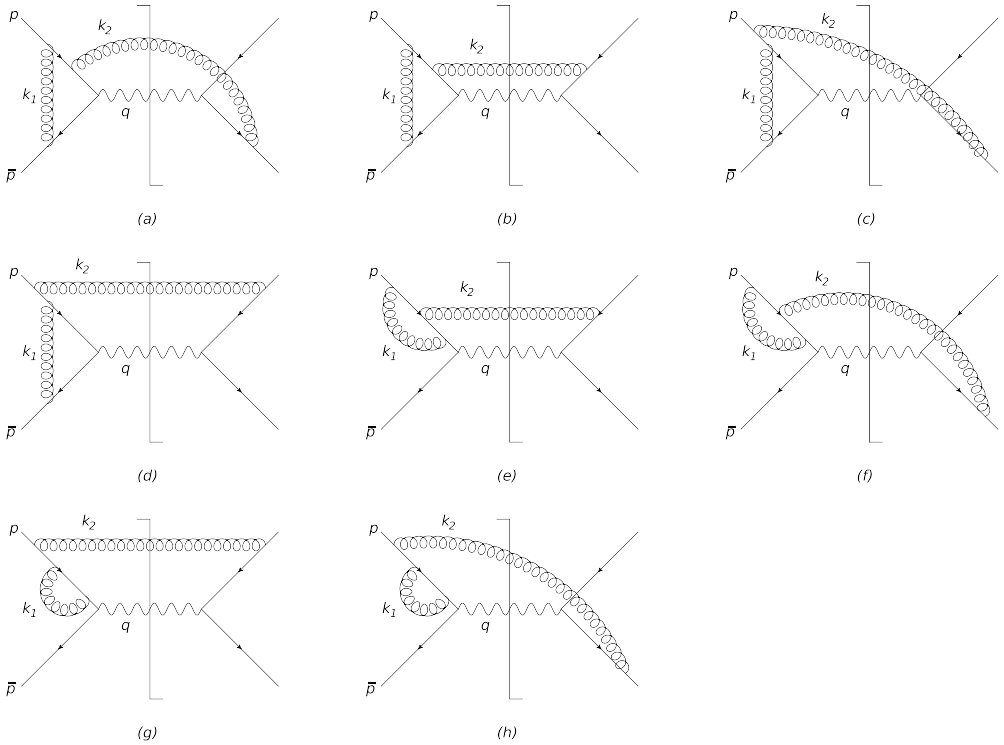

Figure 3.4: Squared diagrams contributing to DY production at NNLO, involving one real and one virtual emission. Diagrams obtained by interchanging $p \leftrightarrow \bar{p}$ and/or complex conjugation are not shown.

$$
\begin{aligned}
(f): &\quad \frac{\mathrm{Tr}\left[\bar{\not{p}}\gamma^\alpha(\not{p}-\not{k}_2)\gamma^\mu(\not{p}+\not{k}_1-\not{k}_2)\gamma^\nu(\not{p}+\not{k}_1)\gamma_\mu\ \not{p}\gamma_\alpha(-\bar{\not{p}}+\not{k}_2)\gamma_\nu\right]}{k_1^2(p-k_2)^2(p+k_1-k_2)^2(p+k_1)^2(k_2-\bar{p})^2}\,, \\
(g): &\quad \frac{\mathrm{Tr}\left[\bar{\not{p}}\gamma^\alpha(\not{p}-\not{k}_2)\gamma^\mu(\not{p}+\not{k}_1-\not{k}_2)\gamma_\mu(\not{p}-\not{k}_2)\gamma^\nu\ \not{p}\gamma_\nu(\not{p}-\not{k}_2)\gamma_\alpha\right]}{k_1^2(p-k_2)^2(p+k_1-k_2)^2(p-k_2)^2(p-k_2)^2}\,, \\
(h): &\quad \frac{\mathrm{Tr}\left[\bar{\not{p}}\gamma^\alpha(\not{p}-\not{k}_2)\gamma^\mu(\not{p}+\not{k}_1-\not{k}_2)\gamma_\mu(\not{p}-\not{k}_2)\gamma^\nu\ \not{p}\gamma_\alpha(-\bar{\not{p}}+\not{k}_2)\gamma_\nu\right]}{k_1^2(p-k_2)^2(p+k_1-k_2)^2(p-k_2)^2(k_2-\bar{p})^2}.
\end{aligned}
\tag{3.33}
$$

After carrying out the Dirac trace and performing virtual integration over the loop momentum k_1, one may expand the squared amplitude as a Laurent series in $(1-z)$, where the NE order corresponds to the first subleading corrections. Then the integration over the two-particle phase space follows straightforwardly. It is useful to present results for each individual Feynman diagram. In so doing, we will neglect all transcendental constants for brevity, as these do not bring any relevant information and can be easily

reconstructed from overall pre-factors. One finds:

$$
\begin{aligned}
(a): \quad & \left(\frac{\alpha_s}{4\pi}C_F\right)^2 \left[\frac{-24+24\mathcal{D}_0(z)}{\varepsilon^3} + \frac{-88+24\mathcal{D}_0(z)-72\mathcal{D}_1(z)+88L(z)}{\varepsilon^2}\right. \\
& + \frac{-104+48\mathcal{D}_0(z)-72\mathcal{D}_1(z)+108\mathcal{D}_2(z)+272L(z)-148L^2(z)}{\varepsilon} \\
& - 208+96\mathcal{D}_0(z)-144\mathcal{D}_1(z)+108\mathcal{D}_2(z)-108\mathcal{D}_3(z) \\
& \left. + 352L(z)-416L^2(z)+\frac{476}{3}L^3(z)\right], \\
(b): \quad & \left(\frac{\alpha_s}{4\pi}C_F\right)^2 \left[\frac{8}{\varepsilon^2}+\frac{8-8L(z)}{\varepsilon}+32-4L^2(z)\right], \\
(c): \quad & \left(\frac{\alpha_s}{4\pi}C_F\right)^2 \left[\frac{-8+8\mathcal{D}_0(z)}{\varepsilon^3} + \frac{-8+24\mathcal{D}_0(z)+8\mathcal{D}_1(z)-24L(z)}{\varepsilon^2}\right. \\
& + \frac{-80+80\mathcal{D}_0(z)-24\mathcal{D}_1(z)-44\mathcal{D}_2(z)-80L(z)+84L^2(z)}{\varepsilon} \\
& - 192+160\mathcal{D}_0(z)-112\mathcal{D}_1(z)-12\mathcal{D}_2(z) \\
& \left. + \frac{196}{3}\mathcal{D}_3(z)+224L^2(z)-116L^3(z)\right], \\
(d): \quad & 0; \\
(e): \quad & \left(\frac{\alpha_s}{4\pi}C_F\right)^2 \left[\frac{4}{\varepsilon^2}+\frac{4-12L(z)}{\varepsilon}+8-12L(z)+18L^2(z)\right], \\
(f): \quad & \left(\frac{\alpha_s}{4\pi}C_F\right)^2 \left[-\frac{12\mathcal{D}_0(z)}{\varepsilon^2}+\frac{12-12\mathcal{D}_0(z)+36\mathcal{D}_1(z)}{\varepsilon}\right. \\
& \left. - 24\mathcal{D}_0(z)+36\mathcal{D}_1(z)-54\mathcal{D}_2(z)-36L(z)\right], \\
(g): \quad & 0; \\
(h): \quad & \left(\frac{\alpha_s}{4\pi}C_F\right)^2 \left[\frac{-12+12\mathcal{D}_0(z)}{\varepsilon^2} + \frac{-36+12\mathcal{D}_0(z)-36\mathcal{D}_1(z)+36L(z)}{\varepsilon}\right. \\
& - 48+24\mathcal{D}_0(z)-36\mathcal{D}_1(z)+54\mathcal{D}_2(z) \\
& \left. + 108L(z)-54L^2(z)\right].
\end{aligned}
\tag{3.34}
$$

Each expression has been multiplied by 4 to take account of complex conjugate diagrams and those obtained from Fig. 3.4 by $p \leftrightarrow \bar{p}$. We have also introduced the short-hand

notation

$$\mathcal{D}_i(z) = \left(\frac{\log^i(1-z)}{1-z}\right)_+ \quad \text{and} \quad L^i(z) = \log^i(1-z)\,. \tag{3.35}$$

It is interesting to note here that there are eikonal terms in graphs (e)–(h) that cancel when all such contributions are added together. As noted in ref. [45], the fact that such terms appear in individual diagrams is an artifact of our (Feynman) gauge choice. Summing all diagrams together, one obtains

$$\begin{aligned} K^{(2)}(z) = \left(\frac{\alpha_s}{4\pi}C_F\right)^2 \Bigg[& \frac{32\mathcal{D}_0(z) - 32}{\varepsilon^3} + \frac{-64\mathcal{D}_1(z) + 48\mathcal{D}_0(z) + 64L(z) - 96}{\varepsilon^2} \\ & + \frac{64\mathcal{D}_2(z) - 96\mathcal{D}_1(z) + 128\mathcal{D}_0(z) - 64L^2(z) + 208L(z) - 196}{\varepsilon} \\ & - \frac{128\mathcal{D}_3(z)}{3} + 96\mathcal{D}_2(z) - 256\mathcal{D}_1(z) + 256\mathcal{D}_0(z) \\ & + \frac{128}{3}L^3(z) - 232L^2(z) + 412L(z) - 408 \;\; + \mathcal{O}(1-z) \Bigg] \quad , \end{aligned} \tag{3.36}$$

which is in agreement with the result found in the literature [40, 41].

This is the result we are going to use as a theoretical laboratory to test different methods discussed here and in the next two chapters of this thesis. The first one is the effective Feynman rule approach described above and will be illustrated in the next section.

3.5 The Drell-Yan K-factor with effective rules

The simplest way to set up the calculation with the effective Feynman rules vertices is to refer to the diagrammatic depiction of the NE identity shown in Fig. 3.2. To show explicitly how this works, we can consider two (next-to)soft-gluon attachment on the quark p-line, as schematically shown in Fig. 3.5. Rearranging the terms in this way, we see that the contributions can be written in terms of a two-gluon vertex and the E and NE form factors calculated in Section 3.3. We will now calculate these contributions separately.

We start with the diagrams with a two-gluon vertex. These are shown in the first and second line of Fig. 3.6. The amplitude on the left hand side of the cut is proportional to

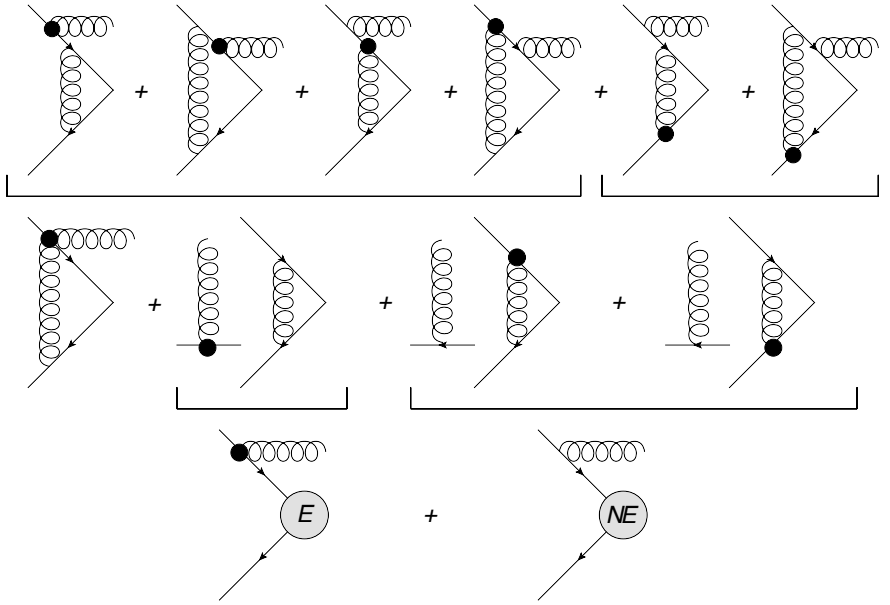

Figure 3.5: The application of the E and NE identities with one real and one virtual gluon. In the upper line, the first four diagrams are rearranged via the NE identity (yielding the first three terms in second line) while the last two with the E identity (yielding last term in second line). On the third line, the E and NE form factors are completely factorized from E and NE emissions. Therefore, the sum of the contributions from the first line is rearranged in a two-gluon vertex and form factors contributions.

$$R^{\mu\nu}(k_1,k_2)\bar{p}_\nu \;\propto\; (p\cdot k_2)(k_1\cdot\bar{p})p^\mu \;+\; (p\cdot k_1)(p\cdot\bar{p})k_2^\mu \\ -\,(p\cdot k_1)(p\cdot k_2)\bar{p}^\mu \;-(k_1\cdot k_2)(p\cdot\bar{p})p^\mu. \tag{3.37}$$

Contracting with eikonal Feynman rules for the right hand side of the cut, the upper and lower two-gluon vertex graphs of Fig. 3.6 are proportional to $p_\mu R^{\mu\nu}\bar{p}_\nu$ and $\bar{p}_\mu R^{\mu\nu}p_\nu$ respectively. We may simplify these combinations as follows. From Eq. (3.37) one finds

$$p_\mu R^{\mu\nu}\bar{p}_\nu = 0\,, \tag{3.38}$$

where $p^2 = 0$ has been used. Next, one has

$$\bar{p}_\mu R^{\mu\nu}\bar{p}_\nu \;\propto\; -(p\cdot\bar{p})^2 k_1^\mu k_2^\nu\left[\eta_{\mu\nu} - \frac{p_{(\mu}\bar{p}_{\nu)}}{p\cdot\bar{p}}\right]\,, \tag{3.39}$$

where we introduced the shorthand notation $a_{(\mu}b_{\nu)} = a_\mu b_\nu + a_\nu b_\mu$. The bracketed term in eq. (3.39) acts on an arbitrary 4-vector to project out the part that is orthogonal to both p^μ and $\bar{p}^\mu$. The cross-section integrated over the virtual momentum k_1^μ will then be

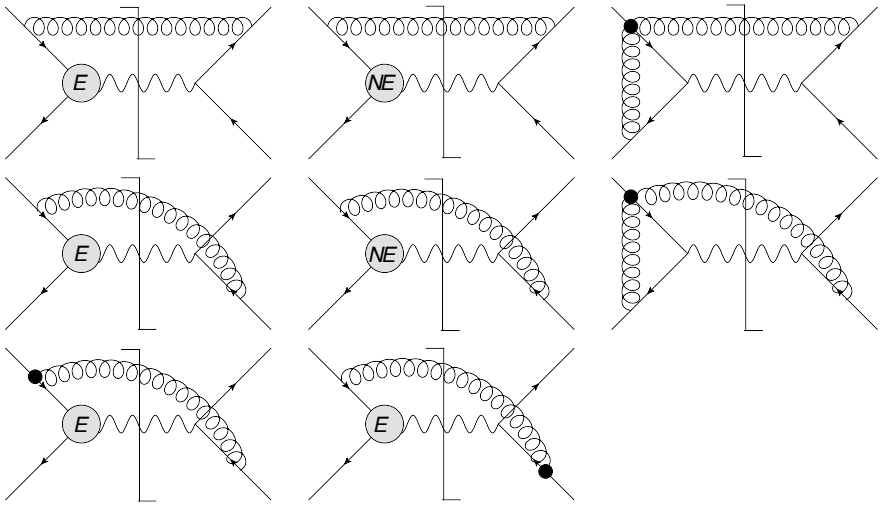

Figure 3.6: The sum of the diagrams in fully factorized form. The vertices shown here are the local ones of the effective theory (E and NE). As such, the emissions are completely factorized from form factors, whose incoming momenta are not shifted by the real gluon momentum. Hence, these form factors are only scalar functions multiplying the diagrams. As before, diagrams resulting from $p \leftrightarrow \bar{p}$ exchange and complex conjugation are not shown.

proportional to

$$\begin{aligned}
&\left[\eta_{\mu\nu} - \frac{p_{(\mu}\bar{p}_{\nu)}}{p\cdot\bar{p}}\right]\int d^dk_1 \frac{k_1^\mu}{k_1^2\, p\cdot k_1\, \bar{p}\cdot k_1\, p\cdot(k_1+k_2)} \\
&= \left[\eta_{\mu\nu} - \frac{p_{(\mu}\bar{p}_{\nu)}}{p\cdot\bar{p}}\right][A(p\cdot k_2, p\cdot\bar{p})p^\mu + B(p\cdot k_2, p\cdot\bar{p})\bar{p}^\mu] \\
&= 0\,,
\end{aligned} \tag{3.40}$$

where the absence of term proportional to k_2^μ in the decomposition in the second line follows from the absence of $k_1 \cdot k_2$ in the denominator of the integral. Hence, we see that this contribution vanishes due to the action of the projector. Arguments similar to the above may be used to show that the diagrams in which the two-gluon vertex attaches to the antiquark leg also vanish. Therefore, the contribution to the K-factor from the two-gluon vertex is zero.

It is interesting to note that the two-gluon vertex was also found to give no contribution to the RR part of the NNLO Drell-Yan K-factor [73]. It presumably will contribute, however, in more complicated amplitudes. For example, Eq. (3.40) will not vanish if contracted with a leg whose momentum is neither p nor $\bar{p}$. This indicates that the two-gluon vertex will contribute in amplitudes with more external partons.

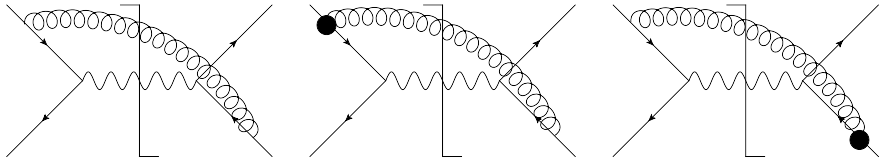

Figure 3.7: Tree-level building blocks.

As a result of our operations we are left with expressions that have the structure of tree level diagrams multiplied by E or NE form factors that factorize from the tree level diagrams. The task of evaluating the diagrams of Fig. 3.4 to E and NE order is now simplified: one need only evaluate the tree-level building blocks of Fig. 3.7, combine them with scalar form factors and phase space measure. In this procedure terms of order $(1-z)^1$ will be dropped.

Before presenting the results, it is important to make the following remark. The eikonal approximation in phase space, form factor and tree level building blocks will result in LP terms while NE corrections in either the phase space or the building block yields simple logarithms (NLP). NE corrections to the form factor instead, being a function of ε and not of $(1-z)$ or k_2, will be not subleading in the threshold expansion and will produce LP logarithms. Applying this procedure to the diagrams of Fig. 3.6, we get the following contribution:

$$\begin{aligned} K_{E+NE} = \left(\frac{\alpha_s}{4\pi}C_F\right)^2 \Bigg[& \frac{32\mathcal{D}_0 - 32}{\varepsilon^3} + \frac{64\mathcal{D}_0 - 64\mathcal{D}_1 + 64L_1 - 32}{\varepsilon^2} \\ & \frac{128\mathcal{D}_0 - 128\mathcal{D}_1 + 64\mathcal{D}_2 + 64L_1 - 64L_2 - 64}{\varepsilon} \\ & 256\mathcal{D}_0 - 256\mathcal{D}_1 + 128\mathcal{D}_2 - \frac{128}{3}\mathcal{D}_3 + 128L_1 - 64L_2 + \frac{128}{3}L_3 - 128 \Bigg] . \end{aligned} \tag{3.41}$$

We have thus worked out an expression which is the contribution to the K-factor due to the sum of E and NE rules combined with an expansion at NLP power. Comparing this result with the result from the full QCD calculation of Eq. (3.36), we see that there is no full agreement. Specifically, the only agreement is found for LP terms with highest power (e.g. $\mathcal{D}_3$ in the finite part).

The fact that both LP and NLP terms are missing is not surprising, since we considered an expanded form factor rather than the full one. Indeed, one may improve upon the previous approximation in a somewhat heuristic way and collect the entire factorizable contribution to the Drell-Yan K-factor. The effective Feynman rule is then applied only to the real gluon, assuming that this completely factorizes from the virtual gluon. With

this choice, virtual corrections are not written anymore with effective rules and form the *full* one-loop form factor. Clearly the eikonal expansion of the form factor is then not needed. However, we can still make use of that expansion by noting that in this way the only missing factorizable contribution comes from the NNE form factor.

Therefore, combining phase space, tree level building blocks and *full* form factor, and then expanding the final result at NLP, we get

$$\begin{aligned} K_\Gamma = \left(\frac{\alpha_s}{4\pi}C_F\right)^2 \Bigg[& \frac{32\mathcal{D}_0 - 32}{\varepsilon^3} + \frac{48\mathcal{D}_0 - 64\mathcal{D}_1 + 64L_1 - 80}{\varepsilon^2} \\ & \frac{128\mathcal{D}_0 - 96\mathcal{D}_1 + 64\mathcal{D}_2 + 160L_1 - 64L_2 - 176}{\varepsilon} \\ & 256\mathcal{D}_0 - 256\mathcal{D}_1 + 96\mathcal{D}_2 - \frac{128}{3}\mathcal{D}_3 + 352L_1 - 160L_2 + \frac{128}{3}L_3 - 384 \Bigg] . \end{aligned} \tag{3.42}$$

Comparing this result with the full one in Eq. (3.36), we see that all LP and the leading NLP terms are correctly reproduced, confirming that this naive factorization works at eikonal level. Parts of the NLP logarithms however are still missing.

3.6 Conclusions

In this chapter we analyzed next-to-soft corrections by means of effective Feynman rules and diagrammatic techniques, building upon the work of [73]. First we showed how this can be applied at amplitude level in order to decompose the quark form factor. This is equivalent to calculations required for next-to-eikonal webs. Then we moved to the cross-section level and we introduced the logarithmic structure of the Drell-Yan K-factor, which will be used also in next chapters. The application of the effective rules to both real and virtual gluons allowed us to identify the logarithms that naturally exponentiate, thanks to a naive factorization of both emissions. Then we applied this effective rule only to the real gluon, assuming a factorization of the full form factor. In this way all LP and the leading NLP logarithms are fully reproduced.

Part of the missing NLP terms are easy to trace, thanks to the work of Low, Burnett and Kroll [74, 112]. Indeed, even though for these terms virtual and real emissions do not factorize, following gauge symmetry arguments it is possible to relate the amplitude with a real emission to the non radiative amplitude. Even after this correction, there are further missing NLP logarithms that are of collinear nature, as first observed by Del Duca [113].

The precise calculation of these missing logarithms and the exposition of their universal nature, which is the key in the path towards a resummation formalism, will be investigated in the two following chapters.

CHAPTER 4

Drell-Yan with the method of regions

Feynman integrals depend on various kinematical invariants formed from the momenta of the external legs and the masses of the particles involved. From these quantities it is possible to build dimensionless ratios, whose values may take small or large values for particular kinematical configurations. In the limit in which one of these ratios is small, one may think that, upon expanding the integrand, the original integral is converted into a series of simpler terms. This is the general idea behind the strategy followed by Beneke and Smirnov in [114] and is called *expansion by regions* (also known in the literature as *strategy of regions* or *method of regions*).

For a general review we refer the reader to [115, 116], where also the mathematical foundations of the expansion are investigated. Here we are not going to present the method in full generality, since we are only interested in exploiting it in the computation of NNLO Drell-Yan K-factor that we introduced in Chapter 3. Specifically, we will see that all leading power (LP) and next-to-leading power (NLP) threshold logarithms will be reproduced.

The structure of the chapter is the following. After reviewing the basic features of the method, we set up the formalism of the expansion for the specific case of Drell-Yan in the threshold limit. Then we will show how the expansion can be performed considering a representative case of the calculation. Finally we will present the result of each region for the K-factor. The result for each individual diagram is discussed in an appendix at the end of this chapter.

4.1 The expansion by regions approach

The method of regions consists in the application of the following prescriptions for computing loop integrals. First, one has to consider a specified asymptotic limit, given in

the simplest case by a large hierarchy between two scales. Then, in this limit, one has to divide the space of loop momenta into different regions, according to the singular behavior of the integrand. Finally, one can expand the integrand in each region and perform the integration over the *whole* integration domain. Adding the contributions from all regions, one can reconstruct the original integral.

When the asymptotic limit involves only masses and time-like off-shell momenta squared, the expansion can be defined in Euclidian space. In this case it is also called "expansion by subgraphs" in the literature, and some arguments have been provided towards its mathematical consistency [115, 117]. For general cases, a formal proof is still lacking but at present there are no known cases where this procedure breaks down. Moreover, it has passed several highly non-trivial checks, such as a $\mathrm{N^3LO}$ computation in Higgs production with more than 30 powers of the expansion [118, 119].

In order to show the basic features of the method, before moving to the actual implementation in NNLO Drell-Yan production, we would like to see how this machinery works in a simple toy example, along the lines of the discussion in [57]. Let us consider the following Feynman integral

$$\begin{aligned} I &= \int d^d k \, \frac{1}{(k^2 - m^2)(k^2 - M^2)} \\ &= i \, \pi^{d/2} \, \Gamma\left(1 - \frac{d}{2}\right) \frac{m^2 \, M^d - M^2 \, m^d}{m^2 \, M^2 \, (m^2 - M^2)} \, , \end{aligned} \tag{4.1}$$

where the second line is obtained with standard techniques. Now we consider the case in which $M \gg m$, and observe that the result can be written as an asymptotic series in m^2/M^2. Taking only the leading contribution, it yields

$$I = -i \, \pi^{d/2} \, \Gamma\left(1 - \frac{d}{2}\right) \frac{M^{d-2} - m^{d-2}}{M^2} + \mathcal{O}\left(\frac{m^2}{M^2}\right) \, . \tag{4.2}$$

In this limit, we expect the contribution to the integral to come from two different regions: one where the momentum $k^2 \sim m^2$ and another where $k^2 \sim M^2$. We call the two regions respectively *soft* and *hard*. Therefore, we recompute the integral in Eq. (4.1), first expanding the integrand in these regions. In the soft region we can expand in powers of k^2/M^2, as

$$\begin{aligned} I_{\text{soft}} &= \int d^d k \, \frac{-1}{(k^2 - m^2) M^2} \left(1 + \frac{k^2}{M^2} + \frac{k^4}{M^4} + \cdots\right) \\ &= i \, \pi^{d/2} \, \Gamma\left(1 - \frac{d}{2}\right) \frac{m^{d-2}}{M^2} + \mathcal{O}\left(\frac{m^2}{M^2}\right) \, , \end{aligned} \tag{4.3}$$

where only the first term of the expansion has been integrated. In the hard region instead the expansion is in powers of m^2/k^2, which gives

$$\begin{aligned} I_{\text{hard}} &= \int d^d k \, \frac{1}{k^2(k^2 - M^2)} \left(1 + \frac{m^2}{k^2} + \frac{m^4}{k^4} \cdots \right) \\ &= -i \, \pi^{d/2} \, \Gamma\left(1 - \frac{d}{2}\right) \frac{M^{d-2}}{M^2} + \mathcal{O}\left(\frac{m^2}{M^2}\right) , \end{aligned} \tag{4.4}$$

where once again we have integrated only the first term of the expansion. Adding Eq. (4.3) and Eq. (4.4) we recover the result for the original integral in Eq. (4.2).

This toy example shows the basic features of the expansion by regions. A key point is that the soft and the hard regions have a different scaling, m^{d-2} and M^{d-2} respectively. This guarantees that, even if the integration has been performed on the whole integration domain, no double counting is introduced. The matching between the sum over the regions and the original integral has been verified at leading order in m^2/M^2. Actually, in this simple example it is possible to make a further check, verifying that this holds at all orders in the expansion. However, it is clear that when this method is applied to more complicated cases, this is not feasible anymore.

In this chapter we will apply these techniques to the Drell-Yan process in the threshold limit $z \to 1$. Therefore, the role of the expansion parameter m^2/M^2 will be played by the threshold variable $(1 - z)$. Being interested in reproducing NLP logarithms, the expansion in each region must be performed at second non-trivial order in the expansion parameter. The formalism we will use will be slightly different than the one used in this example. Indeed, since collinear divergences will be present, the classification of the different momentum regions will be defined in light-cone coordinates. Moreover, since $p^2 = \bar{p}^2 = 0$, we will introduce an auxiliary vector n to rescale the collinear directions.

As a final remark, we observe that in the way the method of regions has been introduced in this section, it might seem merely a tool to perform integrations. However, it is noteworthy that the expansion by regions approach is much more powerful: it is possible to define an effective field theory whose degrees of freedom reproduce the result in different momentum regions. For massless theories where soft and collinear are the typical regions required, one may define Soft-Collinear Effective Theories (SCET). However, in the following we will not set up any Lagrangian and we simply use the method to disentangle the NNLO Drell-Yan K-factor in different regions, and to understand which of them contribute at NLP. Moreover, this will serve as a non-trivial check of the method itself at subleading power.

4.2 The regions for Drell-Yan production

In this section we set up the formalism for the specific case of the Drell-Yan production. The K-factor for this process has already been introduced in the previous chapter, where a calculation in full QCD and in an effective approach has been presented. Here we wish to repeat the calculation with the method of regions.

In the following we will consider again only the set of the (abelian-like) real-virtual interference diagrams of the NNLO cross-section. We recall that our main motivation here is to analyze the entangled effect of soft and collinear radiation. For what concerns the definitions of the different regions, we note that for this class of diagrams, where we have one real and one virtual gluon, the softness of the momentum k_2 of the real gluon defines the asymptotic limit (which coincides with the threshold limit $z \to 1$) while the loop integral over the momentum k_1 can be decomposed in different regions.

We introduce a set of auxiliary vectors n_i collinear to each hard line i. For Drell-Yan production we define n_+ and n_- collinear respectively to p and $\bar{p}$ such that $n_+^2 = n_-^2 = 0$ and $n_- \cdot n_+ = 2$. With this definition, and introducing the short-hand notation $n_\pm \ell = n_\pm \cdot l$, each vector l^μ can be decomposed as

$$\ell^\mu = (n_- \ell)\frac{n^{\mu +}}{2} + (n_+ \ell)\frac{n_-^\mu}{2} + \ell_\perp^\mu \,, \tag{4.5}$$

or equivalently

$$\ell = (n_- \ell, \ell_\perp, n_+ \ell) \,. \tag{4.6}$$

Now we can distinguish the different regions for the loop momentum k_1 according to the different scaling of its components. Introducing a book-keeping parameter $\lambda \sim \sqrt{1-z}$ which defines the soft limit $z \to 1$, the relevant regions are defined by the following scaling of the loop momentum:

$$\begin{aligned} &\text{hard}: \; k_1 \sim (1,1,1) && \text{collinear}: \; k_1 \sim (1,\lambda,\lambda^2) \\ &\text{soft}: \; k_1 \sim (\lambda^2,\lambda^2,\lambda^2) && \text{anticollinear}: \; k_1 \sim (\lambda^2,\lambda,1) \quad . \end{aligned} \tag{4.7}$$

By definition, the momentum k_2 of the real gluon is soft and therefore, before phase space integration, its scaling is fixed on

$$k_2 \sim (\lambda^2, \lambda^2, \lambda^2) \,. \tag{4.8}$$

One might ask why we considered only these regions. Indeed, a priori we might have included regions that scale as $(\lambda, \lambda, \lambda)$ or more generally $(\lambda^n, \lambda^n, \lambda^n)$. However, the set of diagrams that involve gluon exchanges between two hard massless legs is a well-studied

case in the literature (see for instance [120]) and we know that for this case it is sufficient to consider the regions of Eq. (4.7). Other scalings would produce only scaleless integrals, as it could be explicitly proven [121], and therefore can be ignored. More generally, finding the set of all non-vanishing regions contributing to an integral is a non-trivial task and requires the use of automated implementations like `asy.m` [122, 123].

The task of computing Feynman diagrams at leading and subleading order in the threshold expansion now turns into an evaluation of simpler loop integrals, obtained after performing an expansion in powers of λ at the proper order. Different contributions to the Drell-Yan K-factor will come from different regions of the loop momentum k_1. To set the correct accuracy in λ before any integration, one should also include the expansion of the loop and phase space measures, which can be combined as

$$\int [dk_1][dk_2](2\pi)\delta(k_2^2)\theta(k_2^0)\delta\left(\frac{\sqrt{s}(1-z)}{2}-k_2^0\right) , \tag{4.9}$$

where the integration measure $[dk_i]$ is defined as

$$\int [dk_i] \equiv \frac{e^{\varepsilon\gamma_E}}{(4\pi)^\varepsilon}\bar{\mu}^{2\varepsilon}\int \frac{d^dk_i}{(2\pi)^d} , \tag{4.10}$$

with $\bar{\mu} = \mu e^{-\gamma_E/2}(4\pi)^{1/2}$. Observing that

$$\int \frac{d^dk}{(2\pi)^d} = \frac{1}{2}\int_{-\infty}^{+\infty}\frac{dn_+k}{2\pi}\int_{-\infty}^{+\infty}\frac{dn_-k}{2\pi}\int\frac{d^{d-2}k_\perp}{(2\pi)^{d-2}} , \tag{4.11}$$

we can see that, around $d = 4$, the scaling of $[dk_1]$ will be 1 for the hard region, λ^4 for the (anti)-collinear region and λ^8 for the soft region.

Before presenting results for the DY amplitudes in different regions, it is instructive to show the expansion procedure in a representative example from the full calculation.

4.3 Structure of the calculation

After the review of the general set-up for an expansion in regions, the procedure to follow is now clear: in every region we have a well defined scaling of k_1 and k_2 which determines an expansion both of the integration measure and the amplitude. However, the order in λ to reach at the amplitude level is different for various components, since the integration measure has a different scaling in every region. Therefore, the simplest way to illustrate the structure of the calculation is to show explicitly the expansion of a single propagator. In particular, we consider the most complicated propagator involved in the calculation, which is

$$\frac{\not{p}+\not{k}_1-\not{k}_2}{(p+k_1-k_2)^2} . \tag{4.12}$$

We will expand this to second non-trivial order in λ in every region.

In the hard and soft regions all components have the same scaling, which considerably simplifies the algebra. Moreover, in both these cases the expansion is in powers of λ^2. Specifically, the expansion of the hard region starts at $\mathcal{O}(\lambda^0)$ and yields

$$\begin{aligned}\text{Hard}: \quad & \frac{\sqrt{\hat{s}}\,\frac{\not{n}_+}{2}+\not{k}_1}{k_1^2+(n_+k_1)\sqrt{\hat{s}}}+\left[-\frac{\not{k}_2}{k_1^2+(n_+k_1)\sqrt{\hat{s}}}\right.\\ & \left.+\frac{\Big((n_+k_2)\sqrt{\hat{s}}+2(k_1k_2)\Big)\Big(\sqrt{\hat{s}}\,\frac{\not{n}_+}{2}+\not{k}_1\Big)}{(k_1^2+(n_+k_1)\sqrt{\hat{s}})^2}\right]+\mathcal{O}(\lambda^4)\,. \end{aligned} \tag{4.13}$$

The soft region instead starts at order $\mathcal{O}(\lambda^{-2})$ and reads

$$\begin{aligned}\text{Soft}: \quad & \frac{1}{(n_+k_1)-(n_+k_2)}\,\frac{\not{n}_+}{2}+\left[\frac{1}{(n_+k_1)-(n_+k_2)}\,\frac{\not{k}_1-\not{k}_2}{\sqrt{\hat{s}}}\right.\\ & \left.-\frac{1}{\big((n_+k_1)-(n_+k_2)\big)^2}\,\frac{(k_1-k_2)^2}{\sqrt{\hat{s}}}\,\frac{\not{n}_+}{2}\right]+\mathcal{O}(\lambda^2)\,. \end{aligned} \tag{4.14}$$

Collinear and anticollinear regions require more algebraic manipulation, since the different scaling of each component produces more terms. In both regions the expansion is in powers of λ. Specifically, the anticollinear region starts at order $\mathcal{O}(\lambda^0)$ and reads

$$\begin{aligned}\text{Anticollinear}: \quad & \frac{1}{\sqrt{\hat{s}}}\frac{\not{n}_-}{2}+\frac{1}{(n_+k_1)}\frac{\not{n}_+}{2}+\left[\frac{1}{(n_+k_1)}\frac{\not{k}_{1\perp}}{\sqrt{\hat{s}}}\right.\\ & \left.+\left(-\frac{k_{1\perp}^2}{(n_+k_1)^2\sqrt{\hat{s}}}+\frac{(n_+k_2)}{(n_+k_1)^2}+\frac{(n_-k_2)}{(n_+k_1)\sqrt{\hat{s}}}\right)\frac{\not{n}_+}{2}\right]\\ & +\left[\left(-\frac{k_1^2}{(n_+k_1)\,\hat{s}}+\frac{(n_+k_2)}{(n_+k_1)\sqrt{\hat{s}}}+\frac{(n_-k_2)}{\hat{s}}\right)\frac{\not{n}_-}{2}\right.\\ & \left.-\frac{\not{k}_2}{(n_+k_1)\sqrt{\hat{s}}}\right]+\mathcal{O}(\lambda^3)\,. \end{aligned} \tag{4.15}$$

The collinear region is the most involved calculation and starts at $\mathcal{O}(\lambda^{-2})$. One finds

$$\begin{aligned}\text{Collinear}: \quad & \frac{\Big(\sqrt{\hat{s}}+(n_-k_1)\Big)\,\frac{\not{n}_+}{2}}{k_1^2+(n_+k_1)\sqrt{\hat{s}}-(n_+k_2)\Big(\sqrt{\hat{s}}+(n_-k_1)\Big)}\\ & +\left[\frac{\not{k}_{1\perp}}{k_1^2+(n_+k_1)\sqrt{\hat{s}}-(n_+k_2)\Big(\sqrt{\hat{s}}+(n_-k_1)\Big)}\right.\end{aligned}$$

$$
\begin{aligned}
&+\frac{2\left(k_{1\perp}k_{2\perp}\right)\left(\sqrt{\hat{s}}+\left(n_{-}k_1\right)\right)\frac{\not{n}_{+}}{2}}{\left(k_1^2+\left(n_{+}k_1\right)\sqrt{\hat{s}}-\left(n_{+}k_2\right)\left(\sqrt{\hat{s}}+\left(n_{-}k_1\right)\right)\right)^2}\Bigg] \\
&+\Bigg[\frac{\left(n_{+}k_1\right)\frac{n_{-}}{2}-\not{k}_2}{k_1^2+\left(n_{+}k_1\right)\sqrt{\hat{s}}-\left(n_{+}k_2\right)\left(\sqrt{\hat{s}}+\left(n_{-}k_1\right)\right)} \\
&\quad+\frac{2\left(k_{1\perp}k_{2\perp}\right)\not{k}_{1\perp}+\left(\left(n_{+}k_1\right)\left(n_{-}k_2\right)-k_2^2\right)\left(\sqrt{\hat{s}}+\left(n_{-}k_1\right)\right)\frac{\not{n}_{+}}{2}}{\left(k_1^2+\left(n_{+}k_1\right)\sqrt{\hat{s}}-\left(n_{+}k_2\right)\left(\sqrt{\hat{s}}+\left(n_{-}k_1\right)\right)\right)^2} \\
&\quad+\frac{4\left(k_{1\perp}k_{2\perp}\right)^2\left(\sqrt{\hat{s}}+\left(n_{-}k_1\right)\right)\frac{\not{n}_{+}}{2}}{\left(k_1^2+\left(n_{+}k_1\right)\sqrt{\hat{s}}-\left(n_{+}k_2\right)\left(\sqrt{\hat{s}}+\left(n_{-}k_1\right)\right)\right)^3}\Bigg]+\mathcal{O}(\lambda)\,.
\end{aligned}
\tag{4.16}
$$

In the above results, different powers of λ are enclosed in each squared brackets. As we can see, the subleading order in λ to be included for this propagator is different for every region, and could even correspond to $\mathcal{O}(\lambda^3)$.

The same procedure applies to other propagators. However, it should be pointed out that not all other propagators are independent from one another. For example the collinear regions on one leg can be obtained from the anticollinear region of the other leg from exchanging $p \leftrightarrow \bar{p}$.

This example shows in the Drell-Yan case how the expansion by regions works in practice, before performing any integration. Even if many terms are produced and the expressions look lengthy, the method is systematic and will produce simpler integrals. In the next section we will present results in different regions after loop and phase space integrals have been performed.

4.4 Results for each region

The procedure sketched in the previous section can be applied to all amplitudes shown in Fig. 3.4. Expanding to subleading order in λ both amplitudes and integration measure will produce a result that extends to subleading power in the threshold expansion, leading to both LP and NLP threshold logarithms.

The results for individual diagrams in all regions are presented at the end of this chapter in Section 4.A. Here we will discuss the total result for each region, stressing in a subscript to K the distinction between contributions that, after loop integration but before phase space integration, are respectively leading (E) and subleading (NE) in λ.

The terminology here clearly refers to the eikonal expansion, forming a natural bridge to the diagrammatic approach described in Chapter 3.

Soft region

In this region all integrals are scaleless, and therefore vanish in dimensional regularization. As we observed in Chapter 2, this is due to a cancellation of IR and UV poles. Since we are performing a bare calculation, UV poles are not separated from the IR ones, and one is left with a vanishing integral. This may seems counterintuitive since it is known that a subset of logarithms in the K-factor comes from the softness of the virtual gluon, and we have just concluded that this momentum region is zero. However, this contribution has migrated into the hard region, as can be seen applying the scaling of 4.7. This is consistent with the fact that dimensional regularization can shift singularities from the IR to the UV.

Hard region

The hard region of diagrams (e)-(h) vanishes after integrating over the loop momentum k_1, so that the contribution to the hard region arises exclusively from diagrams (a)-(d). It reads

$$\begin{aligned} K^{(2)}_{\mathrm{E,\,h}}(z) = \left(\frac{\alpha_s}{4\pi}C_F\right)^2 \Bigg[& \frac{32\mathcal{D}_0(z)}{\varepsilon^3} + \frac{-64 + 48\mathcal{D}_0(z) - 64\mathcal{D}_1(z)}{\varepsilon^2} \\ & + \frac{-96 + 128\mathcal{D}_0(z) - 96\mathcal{D}_1(z) + 64\mathcal{D}_2(z) + 128L(z)}{\varepsilon} \\ & + 256\mathcal{D}_0(z) - 256\mathcal{D}_1(z) + 96\mathcal{D}_2(z) - \frac{128\mathcal{D}_3(z)}{3} \\ & + 192L(z) - 128L^2(z) - 256 \Bigg] , \end{aligned} \tag{4.17}$$

$$\begin{aligned} K^{(2)}_{\mathrm{NE,\,h}}(z) = \left(\frac{\alpha_s}{4\pi}C_F\right)^2 \Bigg[& -\frac{32}{\varepsilon^3} + \frac{16 + 64L(z)}{\varepsilon^2} + \frac{-80 + 32L(z) - 64L^2(z)}{\varepsilon} \\ & + 160L(z) - 32L^2(z) + \frac{128}{3}L^3(z) - 128 \Bigg] , \end{aligned} \tag{4.18}$$

As we did in Chapter 3, we have omitted terms involving transcendental functions, and we have set $\mu^2_{\overline{MS}} = Q^2$. Already at this point we observe that all LP logarithms of the exact NNLO Drell-Yan calculation are reproduced by $K^{(2)}_{\mathrm{E,\,h}}(z)$. Therefore, we expect other contributions to contribute only at NLP.

Collinear and anticollinear region

Even though the expressions in Eq. (4.15) and Eq. (4.16) are not identical, after summing all diagrams (including those related by $p \leftrightarrow \bar{p}$ symmetry and complex conjugation) collinear and anticollinear regions give the same contributions. This could have been guessed from the symmetry of the diagrams. Therefore we present result with the subscript $c + \bar{c}$. The total contribution reads

$$K^{(2),\,(\mathrm{a})-(\mathrm{d})}_{\mathrm{NE},\,\mathrm{c}+\bar{\mathrm{c}}}(z) \;=\; \left(\frac{\alpha_s}{4\pi}C_F\right)^2 \left[-\frac{8}{\varepsilon^2}+\frac{24\,L(z)}{\varepsilon}-36\,L^2(z)+16\right], \tag{4.19}$$

$$K^{(2),\,(\mathrm{e})-(\mathrm{h})}_{\mathrm{NE},\,\mathrm{c}+\bar{\mathrm{c}}}(z) \;=\; \left(\frac{\alpha_s}{4\pi}C_F\right)^2 \left[-\frac{8}{\varepsilon^2}+\frac{-20+24L(z)}{\varepsilon}+60L(z)-36L^2(z)-40\right]. \tag{4.20}$$

As expected, the collinear regions contribute only at NLP and thus do not spoil the LP logarithmic structure already reproduced with the hard region. However, on a diagram by diagram basis, the collinear region does contain LP terms, which fortunately cancel between diagrams where the attachment of the real and virtual gluon to the p leg is swapped. The intermediate appearance of LP terms is a consequence of having used a non-physical gauge i.e. the Feynman gauge, since non-physical polarization contributions for individual diagrams may reduce the order in the threshold expansion.

4.5 Total contribution

We can now combine the results from the soft, hard and collinear regions, to arrive at an expression for the total abelian-like K-factor for real-virtual interference diagrams from the method of regions. One finds

$$\begin{aligned} K^{(2)}(z) = \left(\frac{\alpha_s}{4\pi}C_F\right)^2 \Bigg[&\frac{32\mathcal{D}_0(z)-32}{\varepsilon^3}+\frac{-64\mathcal{D}_1(z)+48\mathcal{D}_0(z)+64L(z)-96}{\varepsilon^2} \\ &+\frac{64\mathcal{D}_2(z)-96\mathcal{D}_1(z)+128\mathcal{D}_0(z)-64L^2(z)+208L(z)-196}{\varepsilon} \\ &-\frac{128\mathcal{D}_3(z)}{3}+96\mathcal{D}_2(z)-256\mathcal{D}_1(z)+256\mathcal{D}_0(z) \\ &+\frac{128}{3}L^3(z)-232L^2(z)+412L(z)-408 \;+\; \mathcal{O}(1-z)\Bigg] \quad . \end{aligned} \tag{4.21}$$

This is in perfect agreement with the result of Eq. (3.36), which was obtained from expanding to subleading order in $(1-z)$ the result from the full calculation (both LP and NLP, including constant terms, which are not logarithmic enhanced). This confirms the

conjecture that one can carry out these calculations as a threshold expansion in $(1-z)$, not only at leading order in this parameter, but also including subleading contributions.

We can now compare the result presented in each region with the diagrammatic approach developed in Chapter 3. In particular, the comparison can be performed not only for the total result, but also on a diagram by diagram basis, using the results shown in Section 4.A. This is indeed possible since in both calculations no UV renormalization has been carried out and the same (Feynman) gauge has been adopted.

We start by analyzing diagrams with vertex corrections, i.e. diagrams (a)-(d) of Fig. 3.4. In particular, we consider separately the sums $(a)+(c)$ and $(b)+(d)$. Each of these two combinations represents a sum of two diagrams where the attachment of the real and virtual gluons on the p-leg is swapped. In the spirit of the eikonal identity of Eq. (3.9), we know that in a factorization picture the summing over these permutations yields a factorized external emission that multiplies a one-loop form factor.

We focus first on the sum $(a)+(c)$, observing that eikonal collinear regions cancel out. As we already pointed out, the presence of these terms in each diagram is due to the choice an unphysical gauge. We are then left with the hard region (both E and NE) and the collinear region (only NE). From direct comparison, the E and NE hard regions correspond to the result given in a diagrammatic approach, where the loop form factor is factored out from the E and NE real emission diagram. From this analysis we see that the collinear region has been completely left out in the diagrammatic approach. We also note that this effect is only NE, and therefore does not affect LP logarithms.

We now move to the sum $(b)+(d)$. In the diagrammatic approach this contribution vanishes. This is easy to understand: assuming that the form factor is external to the amplitude, we are left with a non-crossed diagram where the gluon connects two p-leg lines. This contribution is zero both at E and NE level. Therefore, in this case both the hard and the collinear regions are left out from the diagrammatic approach. Again the effect is only NE.

Finally, we consider diagrams (e)-(h), where one-loop virtual corrections involve only one leg. Similar conclusions can be reached: the collinear region is completely left out by the diagrammatic approach, and this effect is again only NE. Moreover, this is the only non-vanishing region for this class of diagrams. In the diagrammatic approach all these diagrams vanish: assuming that the one-loop correction can be factored out from the external leg, we are left with a self energy correction only. This yields a scaleless integral and therefore vanishes in dimensional regularization.

In conclusion, in a naive factorization picture such as the diagrammatic approach described in Chapter 3, the hard region of diagram (b) and the entire collinear region of all diagrams are completely left out. Both effect are of NE order. On the contrary,

the hard region is partially reproduced (entirely at E level and partially at NE level) by the diagrammatic approach and therefore the use of E and NE Feynman rules catches only this region. As explained in the previous section, the fact that this (next-to-)soft contribution manifests itself in the hard region (and not in the soft one) is due to the standard transformation of IR poles into UV ones.

4.6 Loop effects on the soft expansion

The results presented in the previous section can be examined in the light of recently proposed next-to-soft theorems [93,96,98,100]. All these studies deal with a generalization at next-to-soft level of Weinberg theorem [92], originally proposed for soft gravitons. We will discuss these issues more quantitatively in Section 5.4. Here, it suffices to say that these theorems have been proposed at tree-level, and there has been interest in understanding how loop corrections affect them. In particular, the discussion under investigation [95,97] was whether the order in which the dimensional regularization and soft expansions are carried out is relevant, and which one has to be chosen.

The computation of the Drell-Yan K-factor with the method of regions presented in this chapter can shed light on this matter. For this purpose, we have to look at the scaling of the diagrams in the real gluon momentum k_2. Clearly, the results presented in each region do not depend on neither the real nor the virtual gluon momenta, as those are integrated out. Therefore, we look at each region before integrating over the phase space. In particular, after integrating over the loop momentum k_1, we find the following scaling for the hard and the collinear regions:

$$\text{Hard} \sim \frac{(2p\cdot\bar{p})^{-\varepsilon}}{\varepsilon^2}\,[\text{E}+\text{NE}+\dots]+\mathcal{O}(\varepsilon^{-1}) \tag{4.22}$$

$$\text{Collinear} \sim \frac{(-2p\cdot k_2)^{-\varepsilon}}{\varepsilon}\,[\text{NE}+\dots]+\mathcal{O}(\varepsilon^{0}) \tag{4.23}$$

$$\text{Anticollinear} \sim \frac{(-2\bar{p}\cdot k_2)^{-\varepsilon}}{\varepsilon}\,[\text{NE}+\dots]+\mathcal{O}(\varepsilon^{0}) \tag{4.24}$$

where E and NE denote respectively terms of order $\mathcal{O}(k_2^{-1})$ and $\mathcal{O}(k_2^0)$, while the ellipsis represent further subleading corrections in the soft expansion. These scalings can be understood following the standard soft-collinear factorization formula derived in Chapter 2. Indeed, in that formula, soft and collinear virtual radiation is captured by hard, soft and jet functions. No extra soft real gluon is present and therefore it cannot depend on k_2. We know that eikonal terms can be explained as single emissions factorized from the form factor and therefore that formula can handle them. Hence, they must be contained in the hard function, whose scaling does not contain k_2. The collinear and anticollinear

regions, on the other hand, do depend on k_2. They both can be converted into a $(1-z)$ scaling with

$$(-2p\cdot k_2)^{-\varepsilon} \sim (1-z)^{-\varepsilon}(-2\bar{p}\cdot k_2)^{-\varepsilon} \sim (1-z)^{-\varepsilon}\,. \tag{4.25}$$

This has to be integrated over the phase space, which contributes with an overall power of $[(1-z)z]^{1-2\varepsilon}$ [73]. Moreover this integration yields an additional single pole ε^{-1}. The resulting total scaling is then

$$\frac{(1-z)^{-3\varepsilon}}{\varepsilon^2} = \frac{1}{\varepsilon^2} - 3\frac{\log(1-z)}{\varepsilon} + \frac{9}{2}\log^2(1-z)\,, \tag{4.26}$$

which is precisely the same pattern of Eq. (4.19) and Eq. (4.20) after restoring the proper normalization.

These considerations resolve the issue of the soft expansion in the context of dimensional regularization. The factor $(p\cdot k_2)$ would be absent if the soft expansion was performed *before* the expansion in ε, as this would imply that the soft expansion had been performed before the integration over the loop momentum k_1. This can be further clarified looking at a particular example. Considering diagram (a), performing the soft expansion before loop integration is equivalent to make the replacement

$$\frac{1}{p-k_1-k_2} \to \frac{1}{p-k_1}\,. \tag{4.27}$$

It is clear that with this replacement no logarithm of $(p\cdot k_2)$ can appear in the final result, and this would result in a wrong evaluation of the total Drell-Yan K-factor. Neglecting terms proportional to k_2 in the numerator would not spoil the result, as these terms do not contribute to the singularity of the Feynman integral, as discussed in Chapter 2. This fixes the order in which the soft and the dimensional regularization expansions must be carried out: the soft expansion has to be performed *after* virtual integration, otherwise contributions that scale with powers of $(p\cdot k_2)$ or $(\bar{p}\cdot k_2)$, that govern the (anti)collinear region, cannot be detected. Collinear effects are responsible for the breakdown of the Low-Burnett-Kroll theorem at next-to-soft level, as first noted by Del Duca in [113]. This will be the subject of Chapter 5.

4.7 Conclusions

In this chapter we have used the method of regions to compute the Drell-Yan K-factor. After the full QCD calculation and the diagrammatic approach presented in Chapter 3, this is the third calculation for this object presented so far in this thesis. We have seen that the result fully agrees with the full QCD calculation, and therefore can be used to

investigate the missing terms from the diagrammatic approach. In particular, comparing it with the diagrammatic approach, we have identified the regions that explicitly break a naive factorization approach, namely the entire collinear region and part of the hard region. As expected both regions affect only NLP logarithms.

On a more general grounds, the method has been useful in clarifying the source of breakdown at loop-level of the recently proposed next-to-soft theorems. By explicit calculation, we have shown that at loop level the collinear region plays a key role and fixes unambiguously the order of soft and dimensional regularization expansion.

Despite these strengths, and the fact that we have been able to address a specific singular region (hard, soft or collinear) to every threshold logarithm, the method however does not give any further insight into higher orders and has no predictive power towards contributions from higher orders as such. Therefore, on the road towards a resummation formalism for NLP threshold logarithms, we need to move to a factorization approach, which will be discussed in the next chapter.

4.A Results for each diagram

We present here the regions for the diagrams of Fig. 3.4. As we did for the total result, we distinguish between eikonal (E) and next-to-eikonal (NE) contributions, which correspond respectively to the leading and next-to-leading term in the λ expansion before phase space integration. Results for the hard regions are indicated with the subscript h, while $c+\bar{c}$ indicates the sum of the collinear and anti-collinear regions.

Diagrams (a)-(d) involve one-loop vertex corrections while diagrams (e)-(h) include self energy corrections. For all diagrams we include the contribution from complex conjugated diagrams or from the diagrams with emission from the lower leg.

Diagram (a)

$$\begin{aligned} K^{(2)}_{\rm NE}(z)|_{\rm (a),\,h} &= \left(\frac{\alpha_s}{4\pi}\right)^2 \left(C_F^2 - \frac{C_A C_F}{2}\right) \left[\frac{16}{\varepsilon^3} + \frac{8 - 32\log(1-z)}{\varepsilon^2}\right. \\ &\quad + \frac{32\log^2(1-z) - 16\log(1-z) + 40}{\varepsilon} \\ &\quad - \frac{64}{3}\log^3(1-z) + 16\log^2(1-z) - 80\log(1-z) + 64 \\ &\quad + \varepsilon\left(\frac{32}{3}\log^4(1-z) - \frac{32}{3}\log^3(1-z) + 80\log^2(1-z)\right. \\ &\quad \left.\left. -128\log(1-z) + 128\right)\right], \end{aligned} \tag{4.28}$$

$$\begin{aligned} K^{(2)}_{\rm E}(z)|_{\rm (a),\,c+\bar{c}} &= \left(\frac{\alpha_s}{4\pi}\right)^2 \left(C_F^2 - \frac{C_A C_F}{2}\right) \left[\frac{24\mathcal{D}_0(z)}{\varepsilon^3} + \frac{-72\mathcal{D}_1(z) + 24\mathcal{D}_0(z) - 48}{\varepsilon^2}\right. \\ &\quad + \frac{108\mathcal{D}_2(z) - 72\mathcal{D}_1(z) + 48\mathcal{D}_0(z) + 144\log(1-z) - 48}{\varepsilon} \\ &\quad - 108\mathcal{D}_3(z) + 108\mathcal{D}_2(z) - 144\mathcal{D}_1(z) + 96\mathcal{D}_0(z) \\ &\quad - 216\log^2(1-z) + 144\log(1-z) - 96 \\ &\quad + \varepsilon\big(81\mathcal{D}_4(z) - 108\mathcal{D}_3(z) + 216\mathcal{D}_2(z) \\ &\quad\quad - 288\mathcal{D}_1(z) + 192\mathcal{D}_0(z) + 216\log^3(1-z) \\ &\quad\quad \left. - 216\log^2(1-z) + 288\log(1-z) - 192\big)\right], \end{aligned} \tag{4.29}$$

$$\begin{aligned} K^{(2)}_{\rm NE}(z)|_{\rm (a),\,c+\bar{c}} &= \left(\frac{\alpha_s}{4\pi}\right)^2 \left(C_F^2 - \frac{C_A C_F}{2}\right) \left[-\frac{40}{\varepsilon^3} + \frac{-48 + 120\log(1-z)}{\varepsilon^2}\right. \\ &\quad + \frac{-180\log^2(1-z) + 144\log(1-z) - 96}{\varepsilon} \end{aligned}$$

$$
\begin{aligned}
&+180\log^3(1-z)-216\log^2(1-z)+288\log(1-z)-176\\
&+\varepsilon\Big(-135\log^4(1-z)+216\log^3(1-z)-432\log^2(1-z)\\
&\qquad+528\log(1-z)-336\Big)\Bigg].
\end{aligned}
\tag{4.30}
$$

Diagram (b)

$$
\begin{aligned}
K^{(2)}_{\rm NE}(z)|_{\rm (b),\,h} \;=\; &\left(\frac{\alpha_s}{4\pi}\right)^2\left(C_F^2-\frac{C_AC_F}{2}\right)\left[\frac{16}{\varepsilon^2}+\frac{24-32\log(1-z)}{\varepsilon}\right.\\
&+\;32\log^2(1-z)-48\log(1-z)+64\\
&+\;\varepsilon\Bigg(-\frac{64}{3}\log^3(1-z)+48\log^2(1-z)\\
&\qquad-128\log(1-z)+128\Bigg)\Bigg],
\end{aligned}
\tag{4.31}
$$

$$
\begin{aligned}
K^{(2)}_{\rm NE}(z)|_{\rm (b),\,c+\bar{c}} \;=\; &\left(\frac{\alpha_s}{4\pi}\right)^2\left(C_F^2-\frac{C_AC_F}{2}\right)\left[-\frac{8}{\varepsilon^2}+\frac{-16+24\log(1-z)}{\varepsilon}\right.\\
&-36\log^2(1-z)+48\log(1-z)-32\\
&+\varepsilon\big(36\log^3(1-z)-72\log^2(1-z)+96\log(1-z)-64\big)\Bigg].
\end{aligned}
\tag{4.32}
$$

Diagram (c)

$$
\begin{aligned}
K^{(2)}_{\rm E}(z)|_{\rm (c),\,h} \;=\; &\left(\frac{\alpha_s}{4\pi}\right)^2 C_F^2\left[\frac{32\mathcal{D}_0(z)}{\varepsilon^3}+\frac{-64\mathcal{D}_1(z)+48\mathcal{D}_0(z)-64}{\varepsilon^2}\right.\\
&+\frac{64\mathcal{D}_2(z)-96\mathcal{D}_1(z)+128\mathcal{D}_0(z)+128\log(1-z)-96}{\varepsilon}\\
&-\frac{128}{3}\mathcal{D}_3(z)+96\mathcal{D}_2(z)-256\mathcal{D}_1(z)+256\mathcal{D}_0(z)\\
&-128\log^2(1-z)+192\log(1-z)-256\\
&+\varepsilon\Bigg(\frac{64}{3}\mathcal{D}_4(z)-64\mathcal{D}_3(z)+256\mathcal{D}_2(z)\\
&\qquad-512\mathcal{D}_1(z)+512\mathcal{D}_0(z)+\frac{256}{3}\log^3(1-z)\\
&\qquad-192\log^2(1-z)+512\log(1-z)-512\Bigg)\Bigg],
\end{aligned}
\tag{4.33}
$$

$$
K^{(2)}_{\rm NE}(z)|_{\rm (c),\,h} \;=\; \left(\frac{\alpha_s}{4\pi}\right)^2 C_F^2\left[-\frac{48}{\varepsilon^3}+\frac{-40+96\log(1-z)}{\varepsilon^2}\right.
$$

$$
\begin{aligned}
&+\frac{-96\log^2(1-z)+80\log(1-z)-144}{\varepsilon}\\
&+64\log^3(1-z)-80\log^2(1-z)+288\log(1-z)-256\\
&+\varepsilon\Bigg(-32\log^4(1-z)+\frac{160}{3}\log^3(1-z)-288\log^2(1-z)\\
&\qquad+512\log(1-z)-512\Bigg)\Bigg],
\end{aligned}
\tag{4.34}
$$

$$
\begin{aligned}
K_{\rm E}^{(2)}(z)|_{\rm (c),\,c+\bar{c}} \;=\; &\left(\frac{\alpha_s}{4\pi}\right)^2 C_F^2\Bigg[-\frac{24\mathcal{D}_0(z)}{\varepsilon^3}+\frac{72\mathcal{D}_1(z)-24\mathcal{D}_0(z)+48}{\varepsilon^2}\\
&+\frac{-108\mathcal{D}_2(z)+72\mathcal{D}_1(z)-48\mathcal{D}_0(z)-144\log(1-z)+48}{\varepsilon}\\
&+108\mathcal{D}_3(z)-108\mathcal{D}_2(z)+144\mathcal{D}_1(z)-96\mathcal{D}_0(z)\\
&+216\log^2(1-z)-144\log(1-z)+96\\
&+\varepsilon\big(-81\mathcal{D}_4(z)+108\mathcal{D}_3(z)-216\mathcal{D}_2(z)\\
&\qquad+288\mathcal{D}_1(z)-192\mathcal{D}_0(z)-216\log^3(1-z)\\
&\qquad+216\log^2(1-z)-288\log(1-z)+192\big)\Bigg],
\end{aligned}
\tag{4.35}
$$

$$
\begin{aligned}
K_{\rm NE}^{(2)}(z)|_{\rm (c),\,c+\bar{c}} \;=\; &\left(\frac{\alpha_s}{4\pi}\right)^2 C_F^2\Bigg[\frac{40}{\varepsilon^3}+\frac{48-120\log(1-z)}{\varepsilon^2}\\
&+\frac{180\log^2(1-z)-144\log(1-z)+112}{\varepsilon}\\
&+180\log^3(1-z)+216\log^2(1-z)-336\log(1-z)+224\\
&+\varepsilon\big(135\log^4(1-z)-216\log^3(1-z)+504\log^2(1-z)\\
&\qquad-672\log(1-z)+448\big)\Bigg].
\end{aligned}
\tag{4.36}
$$

Diagram (d)

The contribution from this diagram is zero.

Diagram (e)

$$
\begin{aligned}
K_{\rm NE}^{(2)}(z)|_{\rm (e),\,c+\bar{c}} \;=\; &\left(\frac{\alpha_s}{4\pi}\right)^2\left(C_F^2-\frac{C_AC_F}{2}\right)\Bigg[\frac{4}{\varepsilon^2}+\frac{4-12\log(1-z)}{\varepsilon}+18\log^2(1-z)\\
&-12\log(1-z)+8+\varepsilon\big(-18\log^3(1-z)\\
&\qquad+18\log^2(1-z)-24\log(1-z)+16\big)\Bigg].
\end{aligned}
\tag{4.37}
$$

Diagram (f)

$$K_{\rm E}^{(2)}(z)|_{\rm (f),\,c+\bar{c}} = \left(\frac{\alpha_s}{4\pi}\right)^2 \left(C_F^2 - \frac{C_A C_F}{2}\right) \Bigg[\frac{-12\mathcal{D}_0(z)}{\varepsilon^2} + \frac{36\mathcal{D}_1(z) - 12\mathcal{D}_0(z) + 24}{\varepsilon} - 54\mathcal{D}_2(z) + 36\mathcal{D}_1(z) - 24\mathcal{D}_0(z) - 72\log(1-z) + 24 + \varepsilon\big(54\mathcal{D}_3(z) - 54\mathcal{D}_2(z) + 72\mathcal{D}_1(z) - 48\mathcal{D}_0(z) + 108\log^2(1-z) - 72\log(1-z) + 48\big)\Bigg], \quad (4.38)$$

$$K_{\rm NE}^{(2)}(z)|_{\rm (f),\,c+\bar{c}} = \left(\frac{\alpha_s}{4\pi}\right)^2 \left(C_F^2 - \frac{C_A C_F}{2}\right) \Bigg[-\frac{12}{\varepsilon} + 36\log(1-z) - 24 + \varepsilon\big(-54\log^2(1-z) + 72\log(1-z) - 48\big)\Bigg], \quad (4.39)$$

Diagram (g)

The contribution from this diagram is zero.

Diagram (h)

$$K_{\rm E}^{(2)}(z)|_{\rm (h),\,c+\bar{c}} = \left(\frac{\alpha_s}{4\pi}\right)^2 C_F^2 \Bigg[\frac{12\mathcal{D}_0(z)}{\varepsilon^2} + \frac{-36\mathcal{D}_1(z) + 12\mathcal{D}_0(z) - 24}{\varepsilon} + 54\mathcal{D}_2(z) - 36\mathcal{D}_1(z) + 24\mathcal{D}_0(z) + 72\log(1-z) - 24 + \varepsilon\big(-54\mathcal{D}_3(z) + 54\mathcal{D}_2(z) - 72\mathcal{D}_1(z) + 48\mathcal{D}_0(z) - 108\log^2(1-z) + 72\log(1-z) - 48\big)\Bigg], \quad (4.40)$$

$$K_{\rm NE}^{(2)}(z)|_{\rm (h),\,c+\bar{c}} = \left(\frac{\alpha_s}{4\pi}\right)^2 C_F^2 \Bigg[-\frac{12}{\varepsilon^2} + \frac{-12 + 36\log(1-z)}{\varepsilon} - 54\log^2(1-z) + 36\log(1-z) - 24 + \varepsilon\big(54\log^3(1-z) - 54\log^2(1-z) + 72\log(1-z) - 48\big)\Bigg]. \quad (4.41)$$

CHAPTER 5

A next-to-soft factorization theorem

In this chapter we investigate next-to-soft corrections with a factorization approach. Specifically, building upon the work of Low [74], Burnett and Kroll [112] and more recent modifications by Del Duca [113], we derive a factorization theorem valid up to next-to-soft level, by means of which it is possible to have full control of the NLP threshold logarithms to NNLO. In so doing, we will use the soft-collinear factorization formalism derived in Chapter 2, putting the auxiliary vector n on the light-cone. In particular, by presenting the theorem in different forms, we will discuss also a one-loop expanded version that will turn out to be useful to clarify the recently proposed next-to-soft theorems.

The structure of the chapter is as follows. In Section 5.1 we recall the formalism of soft-collinear factorization, stressing the difference between choosing $n^2 = 0$ and $n^2 \neq 0$. Using this language, in Section 5.2 we will derive the so-called LBKD theorem, without any assumption on n. Then, in the subsequent sections we will simplify the factorization formula of the theorem, first setting $n^2 = 0$, and then expanding it to one-loop. Finally, in Section 5.5, we will implement the one-loop formula in the NNLO Drell-Yan K-factor, showing that *all* NLP threshold logarithms (and even the constant terms) are reproduced.

5.1 Factorization on and off the light-cone

The starting point is the soft-collinear factorization formula for a partonic non-radiative amplitude with two external hard lines, which reads

$$\mathcal{A}\left(\frac{Q^2}{\mu^2}, \alpha_s(\mu^2), \varepsilon\right) = \mathcal{H}\Big(\{p_i\}, \{n_i\}, \alpha_s(\mu^2), \varepsilon\Big) \times \mathcal{S}\Big(\{\beta_i\}, \alpha_s(\mu^2), \varepsilon\Big) \times \prod_{i=1}^{2} \left[\frac{J_i\left(p_i, n_i, \alpha_s(\mu^2), \varepsilon\right)}{\mathcal{J}_i\left(\beta_i, n_i, \alpha_s(\mu^2), \varepsilon\right)}\right], \tag{5.1}$$

where Q is the scale associated with the hard interaction, p_i and β_i are respectively the momentum and velocity of the i-th hard external leg and n_i are the auxiliary four-vectors that separate collinear and hard modes. The derivation of this formula has been already discussed in Chapter 2. However, the formalism that will be used in this chapter is slightly different, since we are going to put the n_i vectors on the light-cone, i.e. $n_i^2 = 0$. This choice will slightly complicate the structure of singularities but it will be useful from the computational point of view in the rest of this chapter. Before discussing this, it is useful to recall for sake of completeness the main ingredients of this formula, without any assumption on n_i.

Soft and collinear singularities are captured respectively by the soft function $\mathcal{S}$ and the jet functions J_i, defined as

$$J_i\Big(p_i, n_i, \alpha_s(\mu^2), \varepsilon\Big) u(p_i) \;\equiv\; \langle 0\,|\Phi_{n_i}(\infty, 0)\psi(0)|\,p_i\rangle \;, \tag{5.2}$$

$$\mathcal{S}\left(\beta_1 \cdot \beta_2, \alpha_s(\mu^2), \varepsilon\right) \;\equiv\; \langle 0\,|\Phi_{\beta_2}(\infty, 0)\Phi_{\beta_1}(0, -\infty)|\,0\rangle \;. \tag{5.3}$$

Both definitions require the introduction of the Wilson line Φ, which ensures gauge invariance in the factorization of soft and collinear divergences. The convention used in this chapter is that a Wilson line Φ in the direction v is defined as

$$\Phi_v(\lambda_2, \lambda_1) \;\equiv\; \mathcal{P} \exp\left[ig_s\mu^\varepsilon \int_{\lambda_1}^{\lambda_2} d\lambda\, v \cdot A(\lambda v)\right] \;, \tag{5.4}$$

where the group generator contained in A is defined to be the same for coupling with particles and antiparticles. Divergences due to radiation which is at the same time soft and collinear to the i-th external line, which show up as double poles in $1/\varepsilon$ at one-loop, are included both in the soft $\mathcal{S}$ and in the jet function J_i. To remove this double counting, each jet line must be divided by an eikonal jet function, defined as

$$\mathcal{J}_i\Big(\beta_i, n_i, \alpha_s(\mu^2), \varepsilon\Big) \;\equiv\; \langle 0\,|\Phi_{n_i}(\infty, 0)\Phi_{\beta_i}(0, -\infty)|\,0\rangle \;. \tag{5.5}$$

The ratio $J_i/\mathcal{J}_i$ constructed in this way has no soft divergence but only collinear ones, while the soft function $\mathcal{S}$ gathers soft radiation which could be also collinear. Alternatively, one could perform the eikonal subtraction[1] directly in the soft function rather than in the set of jet functions. Hence, one can introduce a function called *reduced* soft function $\overline{\mathcal{S}}$ which collects only soft wide-angle radiation, defined as

$$\overline{\mathcal{S}}\left(\{\beta_i\}, \{n_i\}, \alpha_s(\mu^2), \varepsilon\right) \;\equiv\; \frac{\mathcal{S}(\beta_1 \cdot \beta_2, \alpha_s(\mu^2), \varepsilon)}{\prod_i \mathcal{J}_i(\beta_i, n_i, \alpha_s(\mu^2), \varepsilon)} \,. \tag{5.6}$$

[1] Even though strictly speaking it is a division, it becomes a subtraction order by order in perturbation theory.

Soft-collinear poles are in this way contained in jet functions.

Traditionally, to explore factorization issues by means of formula Eq. (5.1), it is common to set $n_i^2 \neq 0$. This has the advantage of not introducing any spurious collinear singularity in the jet functions. Moreover, nice functional properties of the factorization formula emerge: the dependence of the jet function on p_i and n_i will be through the combination $(p \cdot n)^2/n^2$, while the eikonal jet will be a function of $(\beta \cdot n)^2/n^2$. Hence, with this choice, both the jet and the eikonal jet functions are invariant under rescaling $n_i \to \kappa_i n_i$. Moreover, the reduced soft function $\overline{\mathcal{S}}$ defined in Eq. (5.6) will depend on the kinematical invariants only through the combination

$$\rho_{12} \equiv \frac{(\beta_1 \cdot \beta_2)^2 n_1^2 n_2^2}{(\beta_1 \cdot n_1)^2 (\beta_2 \cdot n_2)^2} \,, \tag{5.7}$$

which is manifestly invariant rescaling of both β_i and n_i.

However, moving from the analysis of formal factorization properties to actual calculations with jet and soft functions, one soon realizes that the functional dependence, and therefore the computation itself, is greatly simplified setting $n_i^2 = 0$. This is also the standard choice adopted in effective field theory calculations. The price to pay, of course, is that some of the above properties are spoiled since spurious collinear singularities are now produced in the jet functions. In particular, jet and eikonal jet will be functions respectively of $p_i \cdot n_i$ and $\beta_i \cdot n_i$, while the reduced soft function will depend on $\frac{(\beta_1 \cdot \beta_2)^2}{(\beta_1 \cdot n_1)^2 (\beta_2 \cdot n_2)^2}$. The spurious singularities will however cancel when combined in Eq. (5.1).

In the following section, we will generalize this formalism to the next-to-soft level by means of the LBKD theorem. To make the derivation as general as possible, no assumption will be made on n^μ; the simplification of setting it on the light-cone will be presented in a subsequent section. Moreover, when we will move to the actual implementation in the the Drell-Yan cross-section, we will make a further restriction, rescaling $n_i \to n_i Q/2$ and setting $n_1 = \bar{p}$ and $n_2 = p$.

Finally, in order to have expressions that are easier to be handled, it is convenient to define a function H that combines the hard function $\mathcal{H}$ and the reduced soft function $\overline{\mathcal{S}}$. Suppressing the functional dependence for simplicity, this means

$$H \equiv \mathcal{H} \times \overline{\mathcal{S}} \,. \tag{5.8}$$

With this definition, H collects everything that is not collinear. The factorization formula 5.1 can now be written simply as

$$\mathcal{A} = H \times \prod_{i=1}^{2} J_i \,. \tag{5.9}$$

We now discuss the LBKD theorem with this formalism.

5.2 The LBKD theorem

The question of the factorization of hard and soft modes has a long history, and dates back to the time of Low [74]. In his seminal work, Low considered the emission of soft photons from hard scalar particles. The result he achieved, known as Low's theorem, is that the radiative amplitude can be fully expressed in terms of the non-radiative one, which includes its derivative. This was later extended to the case of fermionic hard emitters by Burnett and Kroll [112], and the subsequent generalization is then referred to as the Low-Burnett-Kroll theorem.

An underlying assumption in these theorems is that the mass m of the emitting particle is non-vanishing, such that the limit $E/m \to 0$ is well defined, where E is the energy of the soft emitted particle. However, in order to eventually apply this machinery to QCD, a generalization of this procedure to the case of massless emitters is needed. This program was carried out by Del Duca in the early 90s [113], who extended the analysis of soft photons in the region $m^2/Q \leq E < m$, where Q is the energy scale of the hard emitter. In this region one can safely take the limit $m \to 0$ and collinear divergences are properly taken into account.

In this section we will revisit, in more modern language, this body of work, collectively referred to as Low-Burnett-Kroll-Del Duca (LBKD) theorem, in the light of the soft-collinear factorization formula described in the previous section, which was formalized in subsequent years [72]. In particular, we will reformulate it taking special care of the notion of eikonal jet functions, and keeping track of the auxiliary gauge vector n_i.

To construct a factorization formalism that is valid up to next-to-soft level and that takes into account virtual and real emissions, we have to generalize the soft-collinear factorization formula of Eq. (5.1) for the non-radiative amplitude $\mathcal{A}$ to the radiative case $\mathcal{A}^\mu$, when an extra (next-to-)soft gluon is emitted. To achieve this, we will build upon the work of [113]. Using Eq. (5.9) and including polarization tensors, this radiative amplitude may be decomposed into three terms, where the soft gluon attaches respectively to the H function or one of the J functions. One can write

$$\mathcal{A}_\mu \, \epsilon^\mu(k) \;=\; \mathcal{A}^{J_1}_\mu \, \epsilon^\mu(k) + \mathcal{A}^{J_2}_\mu \, \epsilon^\mu(k) + \mathcal{A}^{H}_\mu \, \epsilon^\mu(k) \,. \tag{5.10}$$

All these amplitudes must be properly defined in terms of correlators. The procedure we follow is to define first $\mathcal{A}^{J_i}_\mu$, the amplitude for the emission of a gluon from the i-th jet,

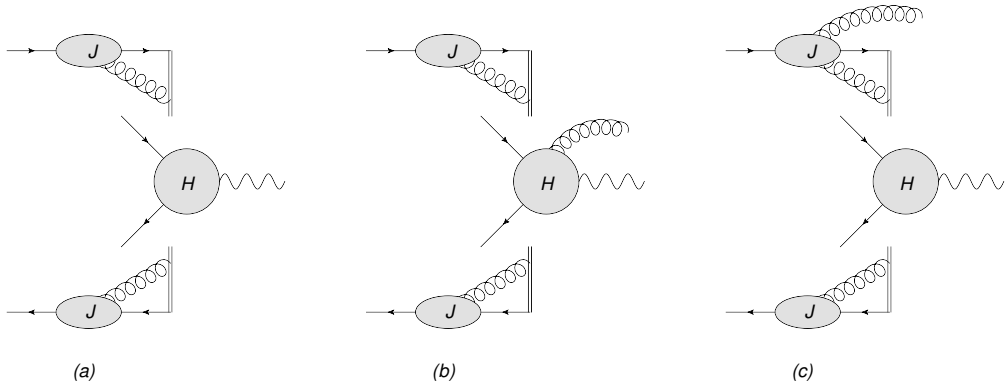

Figure 5.1: In (a) the non-radiative amplitude is factorized into a non-collinear function $H = \overline{\mathcal{S}} \times \mathcal{H}$ and collinear jet functions J. In (b) and (c) it is shown how the factorization in (a) implies a factorization also for the radiative amplitude, where the emitted gluon can be attached either to the H or J.

and then reconstruct $\mathcal{A}_\mu^H$ from it. To define $\mathcal{A}_\mu^{J_i}$, we need to introduce a new object called *radiative jet function* J^μ (also called jet emission function), defined as

$$J^\mu\left(p, n, k, \alpha_s(\mu^2), \varepsilon\right) u(p) \equiv \int d^d y \; \mathrm{e}^{-\mathrm{i}(p-k)\cdot y} \; \langle 0 \,|\, \Phi_n(y, \infty)\, \psi(y)\, j^\mu(0) \,|\, p \rangle \; . \tag{5.11}$$

This definition is very similar to the standard non-radiative jet function J in Eq. (5.2), the only difference being the presence of the current $j^\mu(0)$, which is defined in this QED-like case as

$$j_a^\mu(x) \; = \; \overline{\psi}(x)\, \gamma^\mu\, T_a\, \psi(x)\,, \tag{5.12}$$

where coupling constants and color factors have been suppressed. This current is valid also in QCD as long as one does not consider gluon jets and only fermion emitting lines. As we will see at the end of this chapter, this restriction will be enough to implement these techniques in the real-virtual interference diagrams of the Drell-Yan cross-section. To stress further the difference between the radiative and non-radiative jet function, we see that in the latter the initial state $|p\rangle$ is annihilated by the field ψ at position 0. Here, a Wilson line is created and generates all the interactions with the initial quark line. For the radiative jet function instead, following the definition Eq. (5.11), before the creation of a Wilson line at the generic point y, the quark field has lost part of its momentum at point 0 through the emission of a gluon.

Clearly, even if the emitted gluon attaches to the jet, also the hard and soft functions (captured by H) are affected by this emission: the momentum of the external leg i where

the emitted gluon is attached and that enters the hard and soft functions becomes $p_i - k$. The other leg is instead unaffected. The expression for $\mathcal{A}_\mu^{J_i}$ in Eq. (5.10) is then

$$\mathcal{A}_\mu^{J_i} \equiv \mathcal{A}_\mu^J(p_i;k) \equiv H(p_i-k;p_j,n_j)\, J_\mu(p_i,k,n_i) \prod_{j\neq i} J(p_j,n_j)\,. \tag{5.13}$$

To elaborate upon Eq. (5.10) and Eq. (5.13), we need to discuss further the radiative jet function J^μ. At this point we do not need an expression for it, and therefore an explicit one-loop calculation is postponed to Section 5.4. For the purposes of deriving the LBKD theorem, it is sufficient to explore general all-order properties of the radiative jet and the factorized radiative amplitude as a whole. In particular, we note that the radiative jet function obeys the Ward identity [113]

$$k^\mu\, J_\mu\left(p,n,k,\alpha_s(\mu^2),\varepsilon\right) = q\, J\left(p,n,\alpha_s(\mu^2),\varepsilon\right)\,, \tag{5.14}$$

where q, which represent the electric charge in the QED case, can be -1 or $+1$ according to whether the momentum p is incoming or outgoing respectively. For the QCD case, one has to replace q with the generator T_a. However, since eventually we are interested in applying this formalism to the threshold logarithms proportional to C_F^2, we can continue to use q in the rest of the chapter. Therefore, upon contracting with k^μ, each radiative jet is converted in a non-radiative jet function. Using Eq. (5.14) and Eq. (5.13) we can state that

$$k^\mu \sum_{i=1}^{2} \mathcal{A}_\mu^J(p_i,k) = \sum_{i=1}^{2} q_i\, H(p_i-k;p_j,n_j) \prod_{j=1}^{2} J(p_j,n_j)\,. \tag{5.15}$$

Until now we did not make any assumption on the momentum k of the emitted gluon. Now we impose the condition that this gluon is next-to-soft. Then, we can expand $H(p_i-k;p_j,n_j)$ to next-to-leading order in k and neglect terms of order $\mathcal{O}(k^2)$. We find

$$\begin{aligned}
k^\mu \sum_{i=1}^{2} \mathcal{A}_\mu^J(p_i,k) &= \sum_{i=1}^{2} q_i \left[H(p_i;p_j,n_j) + k^\mu \left(\frac{\partial}{\partial k^\mu} H(p_i-k;p_j,n_j) \right)_{k\to 0} \right] \prod_j J(p_j,n_j) \\
&= \sum_{i=1}^{2} q_i \left[H(p_i;p_j,n_j) - k^\mu \frac{\partial}{\partial p_i^\mu}\, H(p_i;p_j,n_j) \right] \prod_j J(p_j,n_j) \\
&= -\sum_{i=1}^{2} q_i \left(k^\mu \frac{\partial}{\partial p_i^\mu}\, H(p_i;p_j,n_j) \right) \prod_j J(p_j,n_j)\,,
\end{aligned} \tag{5.16}$$

where we exploited the functional dependence of H to turn a derivative with respect to k^μ into a derivative with respect to p^μ, and we used charge conservation leading to the vanishing of the zeroth order term.

Now we consider the Ward identity for the entire amplitude

$$k^\mu \mathcal{A}_\mu = 0 \,, \tag{5.17}$$

which implies

$$k^\mu \, \mathcal{A}_\mu^H \;=\; - \, k^\mu \, \left(\mathcal{A}_\mu^{J_1} + \mathcal{A}_\mu^{J_2} \right) \,. \tag{5.18}$$

Therefore, the information on the radiative jets can be transferred to the emission from the H function. In particular, if we assume that in $\mathcal{A}_\mu^H$ there are no contributions proportional to k^μ, we have

$$\mathcal{A}_\mu^H(p_i, k) \;=\; \sum_{i=1}^{2} q_i \left(\frac{\partial}{\partial p_i^\mu} H(p_i; p_j, n_j) \right) \prod_{j=1}^{2} J(p_j, n_j) \,. \tag{5.19}$$

In principle $\mathcal{A}_\mu^H$ could also contain transverse contributions like $k^\mu/(n_i \cdot k)$. However, these terms must cancel in the full amplitude, which is gauge invariant, as is argued in [74, 101, 102]. Therefore we neglect them in the derivation below.

Now we return to amplitude $\mathcal{A}_\mu^J$ that describes the emission from the jet. For reasons that will become clear later, following [113, 124], it is convenient to decompose $\mathcal{A}_\mu^J$ in two pieces, each of which get contracted with a particular projection of the metric tensor $\eta_{\mu\nu}$. Specifically, for each hard line of momentum p_i, we define

$$\eta^{\mu\nu} \;\equiv\; G_i^{\mu\nu} + K_i^{\mu\nu} \,, \qquad K^{\mu\nu}(p_i; k) \;\equiv K_i^{\mu\nu} \;\equiv\; \frac{(2p_i - k)^\nu}{2p_i \cdot k - k^2} \, k^\mu \,. \tag{5.20}$$

We note that $G_i^{\mu\nu}$ satisfies

$$(p_i)_\mu G_i^{\mu\nu} \;=\; \mathcal{O}(k) \,, \qquad G_i^{\mu\nu} k_\nu \;=\; 0 \,, \tag{5.21}$$

while the K tensor may be expanded as

$$K^{\mu\nu}(p; k) = k^\mu \left(\frac{p^\nu}{p \cdot k} - \frac{k^\nu}{2p \cdot k} + \frac{p^\nu \, k^2}{2(p \cdot k)^2} + \mathcal{O}(k^2) \right) \,. \tag{5.22}$$

In the brackets we recognize the expression of the effective vertices described in Section 3.2 for a soft emission of momentum k from an hard line of momentum p. More precisely, looking at the ν component of Eq. (5.22) and comparing with Eq. (3.10) and Eq. (3.13) (after adjusting the sign of k that here is assumed to be outgoing), we recognize the sum of an eikonal vertex of and the scalar part of a next-to-eikonal vertex. We will come back to this point in Section 5.4. In the rest of the derivation we will continue using the more compact notation of Eq. (5.20) for the K-tensor. Finally, we observe that, in

the calculation we discuss here, the emitted gluon will be assumed to be on-shell. The generalization to the off-shell case is straightforward.

With these definitions, we can decompose accordingly the sum over polarizations of the emitted gluon from the jet function. In particular we will talk about G-gluon and a K-gluon respectively for contractions of a radiative amplitude with $G_{\mu\nu}$ and $K_{\mu\nu}$. We start examining a K-gluon emission from the i-th jet. Combining Eq. (5.13) and Eq. (5.14), it reads

$$\begin{aligned}\mathcal{A}_\nu^{J_i}\, K^{\nu\mu}(p_i;k) &= q_i\, \frac{(2p_i-k)^\mu}{2p_i\cdot k-k^2}\, H(p_i-k;p_j,n_j)\prod_{j=1}^{2} J(p_j,n_j) \\ &= q_i\left[\frac{(2p_i-k)^\mu}{2p_i\cdot k-k^2}\,\mathcal{A}-\left(K_i^{\nu\mu}\frac{\partial}{\partial p_i^\nu}\,H(p_i;p_j,n_j)\right)\prod_{j=1}^{2} J(p_j,n_j)\right], \quad (5.23)\end{aligned}$$

where we expanded up to $\mathcal{O}(k^2)$ and we isolated the total non-radiative amplitude $\mathcal{A}$. Here we see the simplification given by the K tensor: its contraction with the amplitude generated $k^\mu J_\mu$, which, by means of the Ward identity, turns the radiative jet function into the non-radiative one.

Now we can combine this result with the emission from the hard function, given in Eq. (5.19). One finds

$$\mathcal{A}^{H,\mu}+\sum_{i=1}^{2}\mathcal{A}_\nu^{J_i}K_i^{\nu\mu} \;=\; \sum_{i=1}^{2} q_i\left[\frac{(2p_i-k)^\mu}{2p_i\cdot k-k^2}\,\mathcal{A}+\left(G_i^{\nu\mu}\frac{\partial}{\partial p_i^\nu}\,H(p_i;p_j,n_j)\right)\prod_j J(p_j,n_j)\right]. \quad (5.24)$$

Using the factorization of the non-radiative amplitude of Eq. (5.9), we can rewrite this in a more useful form as

$$\begin{aligned}\mathcal{A}^{H,\mu}+\sum_{i=1}^{2}\mathcal{A}_\nu^{J_i}K_i^{\nu\mu} = \sum_{i=1}^{2} q_i\Bigg[&\left(\frac{(2p_i-k)^\mu}{2p_i\cdot k-k^2}+G_i^{\nu\mu}\,\frac{\partial}{\partial p_i^\nu}\right)\mathcal{A} \\ &-\; H(p_i;p_j,n_j)\,G_i^{\nu\mu}\,\frac{\partial}{\partial p_i^\nu}\prod_{j=1}^{2} J(p_j,n_j)\Bigg], \quad (5.25)\end{aligned}$$

so that derivatives with respect to hard momenta act on the full non-radiative amplitude and on the process-independent jet functions.

The last missing piece is the G-gluon emission from the jet function, which reads

$$\sum_{i=1}^{2}\mathcal{A}_\nu^{J_i}\,G_i^{\nu\mu} \;=\; \sum_{i=1}^{2} G_i^{\nu\mu}\,H(p_i-k;p_j,n_j)\,J_\nu(p_i,k,n_i)\prod_{j\neq i} J(p_j,n_j)\,. \quad (5.26)$$

Again we can expand $H(p_i-k;p_j,n_j)$ up to order $\mathcal{O}(k^2)$. However, this time the presence of the G-tensor in place of the K-tensor does not allow us to fully convert, by means

of the Ward identity, the radiative jet function into the non-radiative one. Therefore, for this contribution, we are forced to deal with this new object. After this algebraic manipulation, combining Eq. (5.26) and Eq. (5.25) and restoring the notation with $\mathcal{H}$ and $\overline{\mathcal{S}}$ via Eq. (5.8), we find

$$\mathcal{A}^{\mu}(p_j,k) = \sum_{i=1}^{2}\Bigg[q_i \left(\frac{(2p_i-k)^{\mu}}{2p_i\cdot k - k^2} + G_i^{\nu\mu}\,\frac{\partial}{\partial p_i^{\nu}} \right) \mathcal{A}(p_i;p_j) \tag{5.27}$$
$$+\ \mathcal{H}(p_j,n_j)\,\overline{\mathcal{S}}(\beta_j,n_j)\,G_i^{\nu\mu}\left(J_{\nu}(p_i,k,n_i) - q_i\,\frac{\partial}{\partial p_i^{\nu}} J(p_i,n_i) \right) \prod_{j\neq i} J(p_j,n_j) \Bigg].$$

This is the result of the LBKD theorem, re-derived within the modern language of the soft-collinear factorization formalism. It relates the amplitude of an emission of a next-to-soft (abelian-like) gluon to the non-radiative one. Looking at Eq. (5.27), both terms in the first line and the second term in the second line were already present in the analysis of Low, Burnett and Kroll (though in a different formalism). They are related to the pure soft regime, and persist also in the case of a massive emitter. The first term on the second line instead contains the radiative jet function first introduced by Del Duca, and encodes the presence of collinear effects.

Upon contracting Eq. (5.27) with the polarization vector $\epsilon_{\mu}(k)$, we get a factorization theorem at amplitude level that is the next-to-soft generalization of the leading power factorization formula of Eq. (5.1). Moreover, we expect that, when Eq. (5.27) is contracted with a soft real emission diagram to construct a NNLO annihilation cross-section, all NLP threshold logarithms are reproduced. We will verify this in Section 5.5.

It is noteworthy that no assumption on n_i has been made so far. Therefore the formula is valid also in the case $n_i^2 \neq 0$. However, as we discussed, setting $n_i^2 = 0$ many simplifications can be performed. This is the subject of the following section.

5.3 The theorem for light-like n

As we discussed in Section 5.1, in the literature about factorization it is common to work with an auxiliary gauge vector n^{μ} that is off the light-cone. Therefore, in this case, explicit expressions for jet and soft functions are already available and can be found e.g. in [53, 72].

In order to investigate how Eq. (5.27) can be simplified setting $n^2 = 0$, we need to recompute those functions with this particular choice. The function to start with can be chosen by generic arguments. For instance, $\mathcal{A}$ and $\mathcal{H}$ are process dependent while $\mathcal{S}$ does not depend on n^{μ}. Therefore, for the moment we focus on the jet function J, since this is not process-dependent and contains a dependence on n^{μ}. A priori, one has to perform a

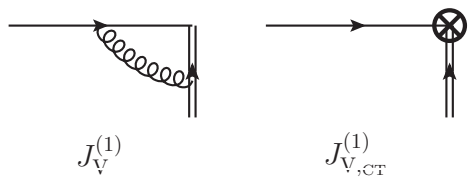

Figure 5.2: Diagrams contributing to the vertex correction to the one-loop jet function. Here $J^{(1)}_{V,CT}$ denotes the counterterm associated with the vertex graph $J^{(1)}_{V}$.

renormalized calculation up to a given order in perturbation theory. We can consider for instance the vertex correction to the one-loop jet function depicted in Fig. 5.2, which includes a counterterm. However, as we shall see at the end of this section, a shortcut can be used.

We can anticipate that the function will depend on $p \cdot n$. Indeed for $n^2 = p^2 = 0$ this is the only invariant which is possible to form. As we discussed in Section 5.1, this choice explicitly breaks the rescaling invariance $n^\mu \to \kappa n^\mu$. This might seems contradictory, as we know that gluon corrections originating from the Wilson line are described by an eikonal Feynman rule, which is manifestly invariant under such a rescaling. The solution to this puzzle is that all integrals are scaleless and can be set to zero in dimensional regularization. This remains true at all orders in perturbation theory. However, with $n^2 = 0$, UV counterterms will bring a dependence on $p \cdot n$, since the Wilson line carries a spurious collinear divergence. This explain why the renormalized light-like jet function will depend on $p \cdot n$. Let us clarify this issue by looking at a specific one-loop example.

We consider the first diagram in Fig. 5.2, which represents a one-loop vertex correction and is denoted by $J_V^{(1)}$. It reads

$$\begin{aligned} J_{\rm V}^{(1)}(p,n;\varepsilon) &= 2{\rm i}\mu^{2\varepsilon} g_s^2 \int \frac{d^dk}{(2\pi)^d} \frac{(\not p - \not k)\ \not n}{k^2\, 2n\cdot k\,(p-k)^2} \\ &= 2{\rm i}\mu^{2\varepsilon} g_s^2 \int \frac{d^dk}{(2\pi)^d} \int_0^1 dx \int_0^1 dy \frac{2y\,(\not p - \not k)\ \not n}{\big[yk^2 - 2xyk\cdot p + 2(1-y)n\cdot k\big]^3} \\ &= \frac{\alpha_s}{2\pi}\left(4\pi\mu^2\right)^\varepsilon (-2p\cdot n)^{-\varepsilon}\, \frac{\Gamma(1+\varepsilon)}{\varepsilon(\epsilon-1)} \int_0^1 dy\, y^{-1+\varepsilon}\,(1-y)^{-1-\varepsilon}\,, \end{aligned} \tag{5.28}$$

where in the second line we introduced Feynman parameters and in the third line we used the Dirac equation and we carried out the standard momentum integration. The integration over y yields $B(\varepsilon,-\varepsilon) = 0$ and hence the integral vanishes. More precisely, this is due to a cancellation between an IR pole (arising from the region $y \to 1$) and a UV pole (arising from the region $y \to 0$), as can be seen by looking at the second line of

Eq. (5.28). Since we are performing a renormalized calculation, we have to add $J^{(1)}_{V,CT}$ (the second diagram in Fig. 5.2), which equals minus the UV pole. Repeating the procedure described in Section 2.6 for the soft function, this can be easily identified by multiplying by $1 = (y + (1 - y))$. The UV counterterm is then given by the term which vanishes for $y \to 0$ (or equivalently minus the one for $y \to 1$), which yields

$$J^{(1)}_{V,CT} = \frac{\alpha_s}{2\pi} \left(4\pi\mu^2\right)^{\varepsilon} (-2p \cdot n)^{-\varepsilon} \frac{\Gamma(\varepsilon)\Gamma(1+\varepsilon)\Gamma(1-\varepsilon)}{\varepsilon(1-\varepsilon)} . \tag{5.29}$$

Therefore in this one-loop example we have proven that the bare contributions is scaleless and vanishes, while the counterterm reintroduces a $p \cdot n$ dependence.

In principle we could move on computing the other diagrams needed order by order in perturbation theory. At the end of such a procedure, we would end up with a final expression for the renormalized jet function that, when substituted into Eq. (5.27), will give a (hopefully simpler) factorization formula valid at a given loop order. Here, instead, we will use a shortcut that will simplify considerably the calculation. Moreover, we will get a simplified version of the factorized formula that will be still valid at all orders.

We note that the left-hand side of Eq. (5.27) is an on-shell scattering amplitude, and therefore it is a renormalization group (RG) invariant: all counterterms for $\mathcal{A}^\mu$ must cancel. The same can be stated for the non-radiative amplitude $\mathcal{A}$. Therefore, the first line on the right-hand side, which is made only of $\mathcal{A}$ (and no other function like J, $\mathcal{H}$ or $\overline{\mathcal{S}}$) is a RG invariant as well. To better exploit this property, we can rewrite Eq. (5.27) as

$$\begin{aligned} \mathcal{A}^\mu(p_j, k) = \sum_{i=1}^{2} \Bigg\{ & q_i \left(\frac{(2p_i - k)^\mu}{2p_i \cdot k - k^2} + G_i^{\nu\mu} \frac{\partial}{\partial p_i^\nu} \right) \\ & + G_i^{\nu\mu} \left[\frac{J_\nu(p_i, k, n_i)}{J(p_i, n_i)} - q_i \frac{\partial}{\partial p_i^\nu} \Big(\ln J(p_i, n_i) \Big) \right] \Bigg\} \mathcal{A}(p_i; p_j) . \end{aligned} \tag{5.30}$$

Now also the second line is a RG invariant. This means that the UV divergences of the radiative jet functions will be the same as those of the non-radiative one. Moreover, the ratio J^ν/J is free of UV divergences (and subsequently IR ones, thanks to the correspondence between them) and contains only collinear divergences. This remains true also if we work in a scheme different from dimensional regularization. In conclusion, we are free to neglect UV counterterms in the computation of the entire right-hand side of Eq. (5.27) or Eq. (5.30).

Now the advantage of working with $n^2 = 0$ (and with dimensional regularization) emerges: for light-like n^μ, radiative corrections to the *bare* jet function vanish at all-orders

in perturbation theory, so that we have[2]

$$J(p_i, n_i) = 1 \ , \qquad \frac{\partial}{\partial p_i^\nu} J(p_i, n_i) = 0 \ . \tag{5.31}$$

Thus in this scheme the above properties of the ratio J^ν/J are recovered by the radiative jet function itself, which contains only collinear poles, and the factorization formula takes the simple expression

$$\mathcal{A}^\mu(p_j, k) \ = \ \sum_{i=1}^{2} \left(q_i \, \frac{(2p_i - k)^\mu}{2p_i \cdot k - k^2} + q_i \, G_i^{\nu\mu} \frac{\partial}{\partial p_i^\nu} + G_i^{\nu\mu} J_\nu(p_i, k) \right) \mathcal{A}(p_i; p_j) \ . \tag{5.32}$$

This is the form of the LBKD theorem for $n^2 = 0$. We stress again that this formula holds at all orders in perturbation theory. Moreover, this form is valid only in dimensional regularization and for bare $J_\nu(p_i, k)$.

In order to implement it in a NNLO computation, we can simplify further this formula, expanding all its components at one-loop. While this is a process-dependent procedure for $\mathcal{A}$, the radiative jet function is universal. Its one-loop calculation is presented in the next section.

5.4 The theorem at one-loop

The main ingredient to be computed at one-loop is the radiative jet function. First introduced by Del Duca, this term was never computed explicitly before. For the reasons just explained we will perform a bare computation. As we have seen, this choice considerably simplified the calculation of the non-radiative jet function J, since, thanks to the absence of a scale that preserve the rescaling invariance, all radiative corrections vanish at all-order in perturbation theory. The same cannot be said for the radiative jet function J^μ. The emitted gluon brings an additional momentum k that can form new scales and makes the resulting integral non-vanishing. Finally, we recall that, working with $n^2 = 0$, also here we find the presence of spurious collinear singularities.

We start defining the perturbative expansion of the radiative jet function as

$$J_\nu \left(p, n, k \, ; \alpha_s, \varepsilon\right) \ = \ g_s \sum_{i=0}^{\infty} \left(\frac{\alpha_s}{4\pi} \right)^i J_\nu^{(i)} \left(p, n, k \, ; \varepsilon\right) \ . \tag{5.33}$$

The tree-level coefficient is easy to compute. Looking at the definition Eq. (5.11), the Wilson line can be set equal to the identity and the radiative jet is simply described by

[2]Strictly speaking, from now onward we should append a subscript "bare" to every jet and radiative jet function. However, this would make the notation rather heavy. Hence, we leave implicit that both J and J^μ in the following sections do not include their UV counterterms.

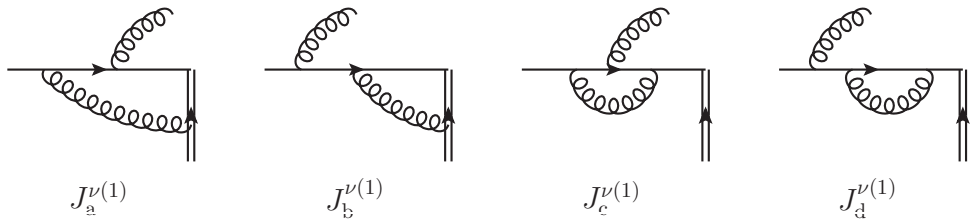

Figure 5.3: Diagrams contributing to the one-loop (bare) radiative jet function.

the emission form a quark line of momentum p. Neglecting terms of order $\mathcal{O}(k^2)$, one finds the (on-shell) effective vertices described in Eq. (3.10) and Eq. (3.13):

$$\begin{aligned} J^{\nu(0)}\left(p,n,k\right) &= -\frac{p^\nu}{p\cdot k}+\frac{k^\nu}{2p\cdot k}-\frac{\mathrm{i}\,k_\alpha \Sigma^{\alpha\nu}}{p\cdot k} \\ &= V_E^\mu(p,k)+V_{NE}^\mu(p,k), \end{aligned} \tag{5.34}$$

where the Lorentz generator $\Sigma^{\alpha\nu}$ is defined in Eq. (3.14).

At one-loop the calculation is more complicated, and one has to explicitly compute the diagrams depicted in Fig. 5.3. Self-energy corrections to the external legs (i.e. those where the radiated gluon is internal with respect to the virtual correction) are not included here since they are different from zero only after adding UV counterterms (which we do not do for this bare calculation). In this section we present only the results for the diagrams, postponing the details of the computation to Section 5.A.

Diagrams (c) and (d) are the standard radiative corrections to the emission amplitude: they belong only to the quark line and therefore carry no n^μ dependence. They yield

$$\begin{aligned} J^{\nu(1)}_{c+d}\left(p,n,k\,;\varepsilon\right) = (2p\cdot k)^{-\varepsilon}\Bigg[&\frac{1}{\varepsilon}\left(\frac{\not{k}\gamma^\nu}{p\cdot k}+\frac{k^\nu}{p\cdot k}\right)+\frac{5}{2}\,\frac{\not{k}\gamma^\nu}{p\cdot k}+\frac{k^\nu}{p\cdot k} \\ &+\ \varepsilon\left(5\,\frac{\not{k}\gamma^\nu}{p\cdot k}+2\,\frac{k^\nu}{p\cdot k}\right)\Bigg]. \end{aligned} \tag{5.35}$$

Note that in this one-loop computation we are also keeping terms of order ε. This is because when we use the next-to-soft factorization formula to reconstruct the NLP threshold logarithms by contracting the radiative jet function with a real emission diagram, the integration over the phase space will bring an additional $1/\varepsilon$ pole, whose combination with the $\mathcal{O}(\varepsilon)$ term in Eq. (5.35) yields finite contributions.

The calculation of diagrams (a) and (b) is considerably more involved, since there are gluons connecting the incoming quark with the Wilson line. Specifically, they represent

Feynman integrals with a combination of linear and quadratic propagators and therefore have a more intricate kinematic dependence. The result is

$$J^{\nu(1)}_{a+b}\,(p,n,k\,;\varepsilon) = (2p\cdot k)^{-\varepsilon}\left\{\left(\frac{2}{\varepsilon}+4+8\varepsilon\right)\left[\frac{n\cdot k}{p\cdot k}\frac{p^\nu}{p\cdot n}-\frac{\not{k}\gamma^\nu}{2p\cdot k}-\frac{n^\nu}{p\cdot n}\right]\right.$$
$$\left.+\;(1+3\varepsilon)\left(-\frac{2k^\nu}{p\cdot k}+\frac{\gamma^\nu\,\not{p}}{p\cdot n}-\frac{p^\nu\,\not{k}\,\not{p}}{p\cdot k\,p\cdot n}\right)\right\}. \tag{5.36}$$

We remark that while Eq. (5.36) has a only a single pole, individual diagrams have double pole which cancel in their combination.

Adding Eq. (5.35) and Eq. (5.36) we obtain the full result for the bare one-loop radiative jet function

$$J^{\nu(1)}\,(p,n,k\,;\varepsilon) = (2p\cdot k)^{-\varepsilon}\left[\left(\frac{2}{\varepsilon}+4+8\varepsilon\right)\left(\frac{n\cdot k}{p\cdot k}\frac{p^\nu}{p\cdot n}-\frac{n^\nu}{p\cdot n}\right)-(1+2\varepsilon)\,\frac{\mathrm{i}\,k_\alpha\Sigma^{\alpha\nu}}{p\cdot k}\right.$$
$$\left.+\left(\frac{1}{\varepsilon}-\frac{1}{2}-3\varepsilon\right)\frac{k^\nu}{p\cdot k}+(1+3\varepsilon)\left(\frac{\gamma^\nu\,\not{p}}{p\cdot n}-\frac{p^\nu\,\not{k}\,\not{p}}{p\cdot k\,p\cdot n}\right)\right]+\mathcal{O}(\varepsilon^2,k)\,, \tag{5.37}$$

where we used Eq. (3.14) to isolate the spin dependent part in the part without n^μ-dependence.

We can check the result for the tree level and one-loop jet functions by means of the Ward identity. From Eq. (5.34), Eq. (5.37) and Eq. (5.31) it is straightforward to verify that

$$k_\nu\,J^{\nu(0)}\,(p,n,k) \;=\; -\,J^{(0)}(p,n) \;=\; -1\,, \tag{5.38}$$
$$k_\nu\,J^{\nu(1)}\,(p,n,k) \;=\; -\,J^{(1)}(p,n) \;=\; 0\,. \tag{5.39}$$

Here we used the fact that the emitted gluon is assumed to be on-shell, and therefore the above identities have been verified neglecting terms of order $\mathcal{O}(k^2)$.

Finally, we note that the radiative jet function enters Eq. (5.30) and Eq. (5.32) only through the combination $G^{\nu\mu}J_\nu$, where the G-tensor has been defined in Eq. (5.20). One finds

$$G^{\nu\mu}J^{(0)}_\nu(p,n,k) \;=\; -\,\frac{\mathrm{i}\,k_\alpha\,\Sigma^{\alpha\mu}}{p\cdot k}\,, \tag{5.40}$$
$$G^{\nu\mu}J^{(1)}_\nu\,(p,n,k) \;=\; J^{\mu(1)}\,(p,n,k)\;, \tag{5.41}$$

where we used again Eq. (5.34) and Eq. (5.31). Therefore, for the tree level radiative jet the role of the G-tensor is to project out the pure spin dependent part of a full next-to-soft emission, represented by $J^{(0)}_\nu$. At one-loop instead it is remarkable that the radiative jet is an eigenfunction of G.

We have now all the ingredients to expand the next-to-soft factorization formula for the full radiative amplitude at one-loop. We start writing Eq. (5.32) as

$$\mathcal{A}^{\mu,(1)}(p_j,k) = \sum_{i=1}^{2}\left[\left(q_i\,\frac{(2p_i-k)^\mu}{2p_i\cdot k-k^2} + q_i\,G_i^{\nu\mu}\,\frac{\partial}{\partial p_i^\nu} + G_i^{\nu\mu}J_\nu^{(0)}(p_i,k)\right)\mathcal{A}^{(1)}(p_i;p_j)\right.$$
$$\left. +\; G_i^{\nu\mu}J_\nu^{(1)}(p_i,k)\mathcal{A}^{(0)}(p_i;p_j)\right], \tag{5.42}$$

where we have defined

$$\mathcal{A} = \sum_{n=0}^{\infty}\left(\frac{\alpha_s}{4\pi}\right)^n\mathcal{A}^{(n)}\,. \tag{5.43}$$

Next, we consider the first and the third term in the first line of Eq. (5.42). Making use of Eq. (5.40) and expanding up to $\mathcal{O}(k^2)$, for the quark line ($q_i=-1$) they yield

$$-\frac{(2p_i-k)^\mu}{2p_i\cdot k-k^2} - G_i^{\nu\mu}J_\nu^{(0)}(p_i,k) = -\frac{p_i^\mu}{p_i\cdot k} + \frac{\not{k}_2\gamma^\mu}{2p_i\cdot k}\,, \tag{5.44}$$

and similarly for the antiquark line. In the diagrammatic language of Chapter 3, this forms the sum of an eikonal and next-to-eikonal vertex. We then have

$$\mathcal{A}^{\mu,(1)}(p_j,k) = \sum_{i=1}^{2}\left[q_i\left(\frac{p_i^\mu}{p_i\cdot k} - \frac{\not{k}\gamma^\mu}{2p_i\cdot k}\right)\mathcal{A}^{(1)}(p_i;p_j) + q_i\left(G_i^{\nu\mu}\frac{\partial}{\partial p_i^\nu}\right)\mathcal{A}^{(1)}(p_i;p_j)\right.$$
$$\left. +\; J^{\mu\,(1)}(p_i,k)\mathcal{A}^{(0)}(p_i;p_j)\right], \tag{5.45}$$

where we left implicit that the order of the spinor matrices must be reversed for $q_i=-1$. This is the one-loop expanded form of the LBKD theorem for $n^2=0$, where $J^{\mu\,(1)}(p_i,k)$ is given by Eq. (5.37).

It is interesting to interpret this result in the light of the recently proposed next-to-soft theorems in gravity and gauge theories [93,96,100]. Focusing on the gauge theory case, these theorems state that the tree-level amplitude $\mathcal{A}_{n+1}$ for an emission of n-hard particles of momenta p_i and one (next-to-)soft gluon of momentum k can be factorized as

$$\begin{aligned}\mathcal{A}_{n+1}(\{p_i\},k) &= \mathcal{S}_n^0\,\mathcal{A}_n(\{p_i\})\,,\\ \mathcal{A}_{n+1}(\{p_i\},k) &= \mathcal{S}_n^1\,\mathcal{A}_n(\{p_i\})\,,\end{aligned} \tag{5.46}$$

where $\mathcal{S}_n^0$ and $\mathcal{S}_n^1$ are respectively the soft and next-to-soft factor, defined as

$$\mathcal{S}_n^0 \;=\; \sum_{i=1}^{n}\frac{\epsilon_\mu(k)\,p_i^\mu}{p_i\cdot k}\,,$$

$$\mathcal{S}_n^1 \;=\; \sum_{i=1}^{n} \frac{\epsilon_\mu(k)\, k_\alpha\, J^{(i)\mu\alpha}}{p_i \cdot k}\,, \tag{5.47}$$

where $J^{(i)\mu\alpha}$ is the total angular momentum of the i-th leg. Recent studies investigated the possibility of the extension of the theorem at loop level [95, 97]. Here we can shed light on this issue, looking at the one-loop form of the LBKD theorem in Eq. (5.45), and considering the antiquark terms. In particular, we note that the first two lines of Eq. (5.45), upon contracting with $\epsilon_\mu(k)$, can be rearranged as

$$\frac{\epsilon_\mu(k)\, p_i^\mu}{p_i \cdot k}\, \mathcal{A}^{(1)} \;+\; \frac{\mathrm{i}\, \epsilon_\mu(k)\, k^\nu}{p_i \cdot k}\, \left[L_{\mu\nu}^{(i)} + \Sigma_{\mu\nu}^{(i)}\right] \mathcal{A}^{(1)}\,, \tag{5.48}$$

where $\Sigma_{\mu\nu}^{(i)}$ is the spin part of the angular momentum of the leg i defined in Eq. (3.14), and $L_{\mu\nu}^{(i)}$ is the orbital angular momentum of the leg i, defined as

$$L_{\mu\nu}^{(i)} \;=\; x_{i\mu} p_{i\nu} - x_{i\nu} p_{i\mu} \;=\; \mathrm{i}\left(p_{i\mu}\, \frac{\partial}{\partial p_i^\nu} - p_{i\nu}\, \frac{\partial}{\partial p_i^\mu}\right)\,. \tag{5.49}$$

Clearly, we see that the terms in Eq. (5.48) correspond to Eq. (5.47). In particular, the next-to-soft term represents the coupling to the *total* angular momentum. However, looking at the second line of Eq. (5.45), we see that there is an additional term coupling to the spin angular momentum only. Indeed this term contains the one-loop radiative jet function that, as we discussed in Section 5.2, cannot be expressed as a derivative of the full form factor. In the following section we shall see that this is related to purely collinear effects. This shows the breakdown at loop level of the next-to-soft theorem in the form of Eq. (5.47).

Returning to Eq. (5.45), we see that we have a factorized amplitude that can be directly implemented in a NNLO calculation, upon contracting it with a real emission amplitude, and subsequently integrating over the phase space. This is therefore the version of the LBKD theorem that we will use in the next section to reconstruct the NLP threshold logarithms of the Drell-Yan K-factor.

5.5 Drell-Yan K-factor revisited

The theorems described in the previous sections are quite general and can be applied to several processes, as long as one takes into account some restrictions, such as having only two hard incoming lines. In this section, we are going to test this formalism in the case of the Drell-Yan production. In particular we will compute the C_F^2 part of the NNLO K-factor for real-virtual interference diagrams, already computed with other methods in Chapter 3 and Chapter 4.

The calculation will consist of contracting the amplitude of Eq. (5.45), which we call here $\mathcal{A}_{rv}$ as involves a real and a virtual gluon, with the real emission amplitude $\mathcal{A}_r$. Including the integration over the phase space, whose definition can be found in [73], the contribution to the K-factor can be written as

$$K_{\rm rv}^{(2)}(z) \,=\, \frac{1}{16\pi^2}\,\frac{(4\pi)^\varepsilon}{\Gamma(2-\varepsilon)}\,z^\varepsilon\,(1-z)^{1-2\varepsilon}\int_0^1 dy\,\Big[y(1-y)\Big]^{-\varepsilon}\,\Big[\mathcal{A}_{\rm rv}^\dagger\,\mathcal{A}_{\rm r}+\mathcal{A}_{\rm r}^\dagger\,\mathcal{A}_{\rm rv}\Big]\ , \quad (5.50)$$

where

$$y=\frac{k\cdot\bar{p}}{s(1-z)}\ , \quad (5.51)$$

and as usual $s=2p\cdot\bar{p}$ is the partonic center-of-mass energy, while $z=Q^2/s$ is the threshold variable. In order to reproduce the structure of NLP threshold logarithms, this formula has to be expanded at next-to-leading power in $(1-z)$. This is has to be done both in the phase space pre-factor

$$d\Phi = d\Phi_{LP}+d\Phi_{NLP}+\dots\ , \quad (5.52)$$

and in the integrand

$$\mathcal{A}_{\rm rv}^\dagger\,\mathcal{A}_{\rm r}+\mathcal{A}_{\rm r}^\dagger\,\mathcal{A}_{\rm rv}=\mathcal{P}_{LP}+\mathcal{P}_{NLP}+\dots\ . \quad (5.53)$$

With this notation, the contribution to the K-factor up to NLP will be of the form

$$K_{\rm rv}^{(2)}\ \sim\ d\Phi_{LP}\,(\mathcal{P}_{LP}+\mathcal{P}_{NLP})+d\Phi_{NLP}\mathcal{P}_{LP}\ . \quad (5.54)$$

Let us now we analyze the integrand $\mathcal{P}$, and in particular its main component $\mathcal{A}_{\rm rv}$, given by Eq. (5.45). First we note that the non-radiative amplitude for the Drell-Yan process is the well-known quark form factor, whose one-loop expression has been already calculated in the introduction. Then, most importantly, we observe that Eq. (5.45) can be decomposed in three contributions. For the i-th leg, they are in turn:

- a (next-to-)soft emission *external* to the form factor

$$\left(\frac{p_i^\mu}{p_i\cdot k_2}-\frac{\not{k}_2\gamma^\mu}{2p_i\cdot k_2}\right)\mathcal{A}^{(1)}(p_i;p_j)\ , \quad (5.55)$$

- a *derivative* of the form factor

$$\left(G_i^{\nu\mu}\frac{\partial}{\partial p_i^\nu}\right)\mathcal{A}^{(1)}(p_i;p_j)\ , \quad (5.56)$$

- the *radiative jet* contribution

$$J^{\mu\,(1)}(p_i,k)\mathcal{A}^{(0)}(p_i;p_j)\ . \quad (5.57)$$

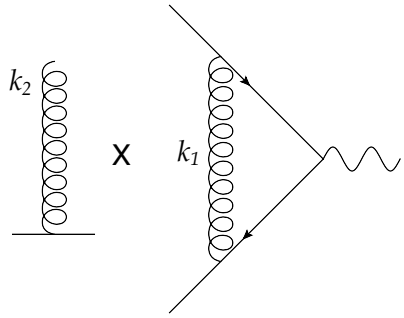

Figure 5.4: Schematic depiction of the external contribution. The next-to-soft emission is completely factorized from the form factor.

We define the contributions of these three terms to the K-factor to be respectively $K^{(2)}_{\rm ext}(z)$, $K^{(2)}_{\partial\mathcal{A}}(z)$ and $K^{(2)}_{\rm radJ}(z)$, such that

$$K^{(2)}_{\rm rv} = K^{(2)}_{\rm ext} + K^{(2)}_{\partial\mathcal{A}} + K^{(2)}_{\rm radJ} \,. \tag{5.58}$$

We now compute each term separately.

The external contribution

The external contribution is completely factorized from the one-loop form factor, as shown in Fig. 5.4. At NLP it belongs to the $\Sigma^{\alpha\mu}$ term of Eq. (5.48). This has been computed in the introduction, and reads

$$\mathcal{A}^{(1)}(z) \,=\, -\,\frac{\alpha_s}{4\pi}\, z^{\varepsilon}\, \frac{\Gamma^2(1-\varepsilon)\Gamma(1+\varepsilon)}{\Gamma(1-2\varepsilon)} \left(\frac{2}{\varepsilon^2} + \frac{3}{\varepsilon} + 8 + 16\varepsilon + \mathcal{O}(\varepsilon^2)\right) \,. \tag{5.59}$$

We recall that Eq. (5.59) has been evaluated with $\mu^2_{\overline{MS}} = Q^2$. The external gluon, instead, has to be contracted with its equivalent on the complex conjugated side, at the proper order in the $(1-z)$ expansion (LP or NLP). Specifically, at LP we have to square the real emission matrix element

$$\left|\mathcal{A}_{\rm r,LP}\right|^2 \,=\, 16\,(1-\epsilon)\, g_s^2\, \frac{s^2}{ut} \,, \tag{5.60}$$

where we introduced the Mandelstam invariants $t = -2k\cdot p$ and $u = -2k\cdot\bar{p}$. At NLP we have to consider only one of the two amplitudes to be subleading, as

$$\mathcal{A}^{\dagger}_{\rm r,NLP}\,\mathcal{A}_{\rm r,LP} + \mathcal{A}^{\dagger}_{\rm r,LP}\,\mathcal{A}_{\rm r,NLP} \,=\, 8\,(1-\varepsilon)\, g_s^2 \left(\frac{s}{t} + \frac{s}{u}\right) \,. \tag{5.61}$$

Combining Eq. (5.60) with both $d\Phi_{LP}$ and $d\Phi_{NLP}$ and Eq. (5.61) with only $d\Phi_{LP}$, we find the following contribution to the K-factor:

$$\begin{aligned} K^{(2)}_{\rm ext}(z) = \Big(\frac{\alpha_s}{4\pi}C_F\Big)^2 \Bigg\{ & \frac{32}{\varepsilon^3}\Big[\mathcal{D}_0(z)-1\Big] + \frac{8}{\varepsilon^2}\Big[-8\mathcal{D}_1(z)+6\mathcal{D}_0(z)+8L(z)-14\Big] \\ & + \frac{16}{\varepsilon}\Big[4\mathcal{D}_2(z)-6\mathcal{D}_1(z)+8\mathcal{D}_0(z)-4L^2(z)+14L(z)-14\Big] \\ & - \frac{128}{3}\mathcal{D}_3(z)+96\mathcal{D}_2(z)-256\mathcal{D}_1(z)+256\mathcal{D}_0(z) \\ & + \frac{128}{3}L^3(z)-224L^2(z)+448L(z)-512\Bigg\}\,. \end{aligned} \tag{5.62}$$

Comparing this result with the total result from the full QCD calculation in Eq. (3.36), we see that all LP logarithms are correctly reproduced. This is not surprising: we expect that plus distributions belong to the eikonal approximation, and we already verified in Chapter 3 that the use of effective eikonal Feynman rules correctly reproduces the LP structure. More precisely, we see that the result in Eq. (5.62) is the same as the contribution computed in Chapter 3 with the use of effective Feynman rules. Already at that point we concluded that LP logarithms were under control with simple diagrammatic techniques. Moreover, we recall that this result coincides with the factorizable contribution from the hard region of Chapter 4. Here, we recover that contribution as one of the terms coming from the LBKD theorem.

Thus we have verified that the next-to-soft factorization formula of the LBKD theorem does not spoil the well-known leading power soft factorization. We therefore expect the remaining two contributions ($K^{(2)}_{\partial\mathcal{A}}$ and $K^{(2)}_{\rm radJ}$) to be strictly NLP.

The derivative contribution

As we have seen in Eq. (5.49), the derivative contribution corresponds to the interaction of the emitted particle with the orbital angular momentum $L^{\mu\nu}$. The explicit computation of this contribution in the amplitude is straightforward, upon using Eq. (2.26). Considering for instance the derivative with respect to p, one gets

$$G^{\nu\mu}(p,k)\,\frac{\partial\mathcal{A}^{(1)}}{\partial p^\nu} \;=\; \left[-\frac{\varepsilon}{p\cdot\bar{p}}\left(-p^\mu+\frac{\bar{p}\cdot k}{p\cdot k}\,\bar{p}^\mu\right)\right]\mathcal{A}^{(1)}\,. \tag{5.63}$$

Of course, we have to include the contribution from both legs. Again we contract with the real emission amplitude and integrate over the phase space, at the correct order in the threshold expansion. The final contribution to the K-factor is

$$K^{(2)}_{\partial\mathcal{A}}(z) \;=\; \Big(\frac{\alpha_s}{4\pi}\,C_F\Big)^2\left\{\frac{32}{\varepsilon^2}+\frac{16}{\varepsilon}\Big[-4L(z)+3\Big]+64L^2(z)-96L(z)+128\right\}. \tag{5.64}$$

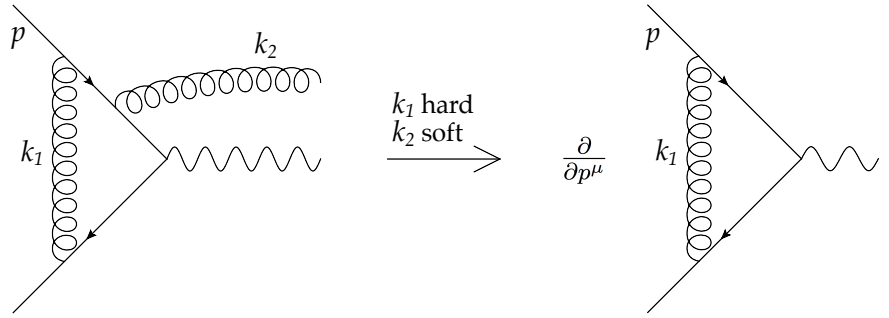

Figure 5.5: Schematic depiction of the derivative contribution. In Feynman gauge, it corresponds to the hard region of the diagram shown here.

We can now interpret this result in the light of the method-of-region calculation of Chapter 4. In particular, comparing with Eq. (4.31), we see that the derivative contribution catches the non-factorizable part of the hard region, as schematically depicted in Fig. 5.5.

We then conclude that the total hard region of the K-factor is reproduced by the sum of the external and the derivative contribution. Both contributions were part of the original analysis of Low, Burnett and Kroll and physically correspond to the interaction of the radiated gluon with the *total* angular momentum of the emitting fermion line.

However, there are still missing NLP logarithms, which must belong to the third and last contribution.

The radiative jet contribution

The two contributions computed so far have no dependence on the vector n. This is not the case for the radiative jet contribution, for which we have to discuss how to deal with this auxiliary vector.

At LP, it is possible to keep n^μ generic and to see explicitly at one-loop that its dependence cancels in the form factor. More precisely, the cancellation happens at pole level between the jets and the eikonal jets. In the finite part instead, one can define the hard coefficient by matching, and thus demanding that the total amplitude does not depend on n^μ.

At NLP the situation is more complicated, and carrying the vector n^μ completely generic increases considerably the difficulty of the calculation. This is why we already made a choice setting $n^2 = 0$. To achieve a full cancellation of the n-dependence we should introduce a further subtraction, replacing collinear poles in the direction n_i with those associated with the physical momentum of the parton colliding with parton i.

However, there is a shortcut. Motivated by the fact that the Wilson line in the direction n_i acts as a replacement for the parton colliding with parton i, we can rescale $n_i \to n_i Q/2$ and set

$$n = \bar{p}\,, \qquad \bar{n} = p\,. \tag{5.65}$$

This is also the standard choice made with a method of region calculation (and more generally in effective field theory approaches). One can generalize this procedure for processes with more legs, simply choosing n_i to be the anti-collinear direction of the leg i.

Therefore, using Eq. (5.65), we can compute the contribution to the K-factor, contracting with the real emission and integrating over the phase space, in the same way as it has been done for the external and the derivative contributions. One finds

$$K^{(2)}_{\rm radJ}(z) = \Big(\frac{\alpha_s}{4\pi}\,C_F\Big)^2 \left\{ -\frac{16}{\varepsilon^2} + \frac{4}{\varepsilon}\Big[12L(z) - 5\Big] - 72L^2(z) + 60L(z) - 24 \right\}. \tag{5.66}$$

As expected, the contribution is strictly NLP. Moreover, comparing with the method of region analysis, we see that this contribution is precisely identical to the collinear region of the K-factor, given by the sum of Eq. (4.19) and Eq. (4.20). This was again expected, since this term corresponds to the Del Duca modification of to the analysis of Low, Burnett and Kroll that takes into account also collinear effects.

Adding Eq. (5.62), Eq. (5.64) and Eq. (5.66) we reproduce the total result from the full QCD calculation, given in Eq. (3.36). Therefore, we conclude that with the LBKD theorem we have a factorization picture for *all* NLP logarithms at NNLO. We stress that, quite remarkably, this include also constant terms, which are not logarithmically enhanced.

5.6 Conclusions

In this chapter, building upon the work in [113], we have presented a theorem that extends the standard soft-collinear factorization formula at subleading level. In particular, using factorization techniques with modern definition of the universal hard, soft and jet functions, we carefully accounted for eikonal double counting in the jet contributions and addressed the dependence on auxiliary vector n. The crucial part of this analysis was the definition of a new object, the *radiative jet function*, which we computed for the first time at one-loop.

Implementing this theorem in the NNLO Drell-Yan K-factor, we found perfect agreement for *all* NLP threshold logarithms between the result given by this factorization formula and the one obtained from the threshold limit of a full QCD calculation. Moreover, we have been able to make a detailed comparison with the diagrammatic approach

of Chapter 3 and the method of regions of Chapter 4. Reproducing all NLP threshold logarithms by means of universal functions that are part of a factorization theorem introduces for the first time predictive power to this class of logarithms. It is therefore an important result that should pave the way for a full resummation formalism.

5.A The one-loop radiative jet function

In this appendix we compute the diagrams that contribute to the one-loop radiative jet function shown in Fig. 5.3. We recall here that this object depends only on the spin of the emitting particle and therefore the results presented here can be used for a variety of processes.

Diagram (a)

The contributions $J_a^{\nu(1)}$ and $J_b^{\nu(1)}$ evaluate to

$$2i\mu^{2\varepsilon}g_s^3\int\frac{d^dk_1}{(2\pi)^d}\left[\frac{(\not p-\not k_1-\not k_2)\gamma^\mu(\not p-\not k_1)\not n}{k_1^2(p-k_1-k_2)^2(p-k_1)^2 2n\cdot k_1}\right.$$
$$\left.+\frac{(\not p-\not k_1-\not k_2)\not n(\not p-\not k_2)\gamma^\mu}{k_1^2(p-k_1-k_2)^2(p-k_2)^2 2n\cdot k_1}\right]u(p) \tag{5.67}$$

respectively. Beginning with the first term, one must evaluate the scalar, vector and tensor integrals

$$\begin{aligned}
S_a &= 2\frac{d^dk_1}{(2\pi)^d}\frac{1}{k_1^2(p-k_1-k_2)^2(p-k_1)^2 2n\cdot k_1}\,,\\
V_a^\mu &= 2\frac{d^dk_1}{(2\pi)^d}\frac{k_1^\mu}{k_1^2(p-k_1-k_2)^2(p-k_1)^2 2n\cdot k_1}\,,\\
T_a^{\mu\nu} &= 2\frac{d^dk_1}{(2\pi)^d}\frac{k_1^\mu k_1^\nu}{k_1^2(p-k_1-k_2)^2(p-k_1)^2 2n\cdot k_1}\,.
\end{aligned} \tag{5.68}$$

Considering the scalar integral, one introduces Feynman parameters to obtain

$$\begin{aligned}
S_a &= 2\int\frac{d^dk_1}{(2\pi)^d}\frac{1}{k_1^2\,2n\cdot k_1\,(k_1-p)^2\,(p-k_1-k_2)^2}\\
&= 2\int\frac{d^d\tilde k_1}{(2\pi)^d}\left(\prod_{i=1}^4\int_0^1 d\alpha_i\right)\frac{6\delta(\sum\alpha_i-1)}{(\alpha_1+\alpha_3+\alpha_4)^4[\tilde k_1^2-M^2]^4},
\end{aligned} \tag{5.69}$$

where

$$\begin{aligned}
\tilde k_1 &= k_1+\frac{1}{(\alpha_1+\alpha_3+\alpha_4)}\left(\alpha_2 n+\alpha_3(k_2-p)-\alpha_4 p\right)\\
M^2 &= \frac{1}{(\alpha_1+\alpha_3+\alpha_4)^2}\left[\alpha_1\alpha_3(2k_2\cdot p)+\alpha_2\alpha_3(2n\cdot k_2)-\alpha_2(\alpha_3+\alpha_4)(2n\cdot p)\right].
\end{aligned} \tag{5.70}$$

One may now transform to the variables

$$\alpha_1=xy,\quad \alpha_2=x(1-y),\quad \alpha_3=(1-x)z,\quad \alpha_4=(1-x)(1-z), \tag{5.71}$$

with Jacobian

$$J = x(1-x). \tag{5.72}$$

Carrying out the momentum integral yields

$$S_a = \frac{2i}{(4\pi)^{d/2}}\Gamma(4-d/2)I(0,0,0), \tag{5.73}$$

where we have defined the master integral

$$\begin{aligned} I_a(n_1,n_2,n_3) = \int_0^1 dx \int_0^1 dy \int_0^1 dz\, x^{d/2-3+n_1}(1-x)^{d/2-3+n_2}(1-y)^{n_1} \\ \times z^{n_3}\ [1-x(1-y)]^{4-d-n_1-n_2} \\ \times \left[yz(2p\cdot k_2) + (1-y)z(2n\cdot k_2) - (1-y)(2p\cdot n)\right]^{d/2-4}, \end{aligned} \tag{5.74}$$

Likewise, one finds for the vector integral

$$\begin{aligned} V^\mu &= 2\int \frac{d^dk_1}{(2\pi)^d}\frac{k_1^\mu}{k_1^2\,2n\cdot k_1\,(k_1-p)^2\,(p-k_1-k_2)^2} \\ &= -\frac{2i}{(4\pi)^{d/2}}\Gamma(4-d/2)\left[I_a(1,0,0)n^\mu + I_a(0,1,1)k_2^\mu - I_a(0,1,0)p^\mu\right]. \end{aligned} \tag{5.75}$$

For the tensor integral, upon shifting the momentum variable according to eq. (5.70), there is a term that is quadratic in $\tilde{k}_1$ in the numerator. Using

$$\int \frac{d^d\tilde{k}_1}{(2\pi)^d}\frac{\tilde{k}_1^\mu\,\tilde{k}_1^\nu}{[\tilde{k}_1^2-M^2]^4} = \frac{\eta^{\mu\nu}}{6}\int \frac{d^d\tilde{k}_1}{(2\pi)^d}\frac{1}{[\tilde{k}_1^2-M^2]^3}\,, \tag{5.76}$$

one finds

$$T^{\mu\nu}|_{\text{quadratic}} = \frac{2i}{(4\pi)^{d/2}}\left(-\frac{\eta^{\mu\nu}}{2}\right)\Gamma(3-d/2)K_a\,, \tag{5.77}$$

where

$$\begin{aligned} K_a = \int_0^1 dx \int_0^1 dy \int_0^1 dz\,[x(1-x)]^{d/2-2}\,[1-x(1-y)]^{2-d} \\ \times \left[yz(2p\cdot k_2) + (1-y)z(2n\cdot k_2) - (1-y)(2p\cdot n)\right]^{d/2-3}. \end{aligned} \tag{5.78}$$

There is a second term with no $\tilde{k}_1$ dependence in the numerator, and this can be shown to be equal to

$$\begin{aligned} \frac{2i}{(4\pi)^{d/2}}\Gamma(4-d/2)\Big[I_a(2,0,0)n^\mu,n^\nu + I_a(0,2,0)p^\mu\,p^\nu + I_a(1,1,1)n^{(\mu}k_2^{\nu)} \\ -I_a(1,1,0)n^{(\mu}p^{\nu)} - I_a(0,2,1)k_2^{(\mu}p^{\nu)}\Big] + \ldots \end{aligned} \tag{5.79}$$

where the ellipsis denotes terms that are suppressed by two factors of soft momentum, and we have used the conventional notation

$$a^{(\mu}b^{\nu)} = a^\mu\, b^\nu + a^\nu\, b^\mu\ .$$

One must now calculate the master integrals $I_a(n_1, n_2, n_3)$ and K_a. For the former, we start by noticing that the x-integral can be carried out yielding a hypergeometric function:

$$\begin{aligned}
&\int_0^1 dx x^{n_1+d/2-3}(1-x)^{n_2+d/2-3}\left[1-x(1-y)\right]^{4-d-n_1-n_2} \\
&= \frac{\Gamma(n_1+d/2-2)\Gamma(n_2+d/2-2)}{\Gamma(d-4+n_1+n_2)} \\
&\times {}_2F_1\left(d-4+n_1+n_2, n_1+d/2-2; d-4+n_1+n_2; 1-y\right). \qquad (5.80)
\end{aligned}$$

Using the identity

$${}_2F_1(a,b;a;z) = (1-z)^{-b}, \qquad (5.81)$$

one then has

$$\begin{aligned}
I_a(n_1,n_2,n_3) = &\frac{\Gamma(n_1+d/2-2)\Gamma(n_2+d/2-2)}{\Gamma(d-4+n_1+n_2)} y^{2-d/2-n_1}(1-y)^{n_1} z^{n_3} \\
&\times \left[yz(2p\cdot k_2) + (1-y)(2n\cdot k_2) - (1-y)(2p\cdot n)\right]^{d/2-4}. \qquad (5.82)
\end{aligned}$$

At this point, it is better to separately consider different integer values of n_3. Beginning with $n_3 = 0$, the z-integral in this case is of the form

$$\int_0^1 dz[A-Bz]^{d/2-4} = -\frac{1}{B(d/2-3)}\left\{[A-B]^{d/2-3} - A^{d/2-3}\right\},$$

where

$$A = -(2p\cdot n)(1-y), \quad B = -(2n\cdot k_2)(1-y) - (2p\cdot k_2)y. \qquad (5.83)$$

One thus finds

$$\begin{aligned}
\int_0^1 dz[A-Bz]^{d/2-4} = &\frac{1}{(d/2-3)}\left[2n\cdot k_2(1-y) + 2p\cdot k_2 y\right]^{-1} \\
&\times \Big\{\left[2p\cdot k_2 y + 2n\cdot(k_2-p)(1-y)\right]^{d/2-3} \\
&- \left[-2p\cdot n(1-y)\right]^{d/2-3}\Big\}. \qquad (5.84)
\end{aligned}$$

The first term can be integrated to give

$$\frac{1}{d/2-3}\frac{C^{d/2-3}}{2n\cdot k_2}\frac{\Gamma(3-d/2-n_1)\Gamma(1+n_1)}{\Gamma(4-d/2)}$$

$$\times\ F_1\left(3-\frac{d}{2}-n_1;1,3-\frac{d}{2};4-\frac{d}{2};1-\frac{2p\cdot k_2}{2n\cdot k_2},\frac{D}{C}\right), \tag{5.85}$$

where F_1 is the Appell function, and we defined

$$C=2n\cdot(k_2-p),\quad D=C-2p\cdot k_2. \tag{5.86}$$

We may simplify this result using the identity

$$F_1(\alpha;\beta,\beta';\beta+\beta';x,y)=(1-y)^{-\alpha}{}_2F_1\left(\alpha;\beta;\beta+\beta';\frac{x-y}{1-y}\right). \tag{5.87}$$

The expression in Eq. (5.85) then becomes

$$\begin{aligned}&\frac{1}{d/2-3}\frac{\Gamma(3-d/2-n_1)\Gamma(1+n_1)}{\Gamma(4-d/2)}\frac{1}{2n\cdot k_2}(2p\cdot k_2)^{n_1+d/2-3}\left[2n\cdot(k_2-p)\right]^{-n_1}\\&\times{}_2F_1\left(3-\frac{d}{2}-n_1,1;4-\frac{d}{2};\frac{2n\cdot p}{2n\cdot k_2}\right).\end{aligned} \tag{5.88}$$

There is a problem here, in that the last argument of the hypergeometric function is singular as $k_2\to 0$, thus hampering the ability to perform the soft expansion. To circumvent this, one may transform the hypergeometric function using the identity

$$\begin{aligned}{}_2F_1(a,b;c;z)=&\frac{\Gamma(b-a)\Gamma(c)}{\Gamma(b)\Gamma(c-a)}(-z)^{-a}{}_2F_1(a,a-c+1;a-b+1;1/z)\\&+\frac{\Gamma(a-b)\Gamma(c)}{\Gamma(a)\Gamma(c-b)}(-z)^{-b}{}_2F_1(b,b-c+1;-a+b+1;1/z).\end{aligned} \tag{5.89}$$

Then Eq. (5.90) becomes

$$\begin{aligned}&\times\frac{1}{d/2-3}\frac{\Gamma(3-d/2-n_1)\Gamma(1+n_1)}{\Gamma(4-d/2)}\frac{1}{2n\cdot k_2}(2p\cdot k_2)^{n_1+d/2-3}\left[2n\cdot(k_2-p)\right]^{-n_1}\\&\left[\frac{\Gamma(d/2-2+n_1)\Gamma(4-d/2)}{\Gamma(n_1+1)}\left(-\frac{2n\cdot p}{2n\cdot k_2}\right)^{n_1+d/2-3}\left(1-\frac{2n\cdot k_2}{2n\cdot p}\right)^{n_1}\right.\\&\left.+\frac{\Gamma(2-d/2-n_1)(3-d/2)}{\Gamma(3-d/2-n_1)}\left(-\frac{2n\cdot p}{2n\cdot k_2}\right)^{-1}{}_2F_1\left(1,\frac{d}{2}-2;n_1+\frac{d}{2}-1;\frac{2n\cdot k_2}{2n\cdot p}\right)\right].\end{aligned} \tag{5.90}$$

One must also perform the y integral in the second term in Eq. (5.84), which gives

$$-\frac{1}{d/2-3}\frac{(-2p\cdot n)^{d/2-3}}{2n\cdot k_2}\Gamma(3-d/2-n_1)\Gamma(n_1+d/2-2)\left(\frac{2p\cdot k_2}{2n\cdot k_2}\right)^{n_1+d/2-3}, \tag{5.91}$$

where we have again used Eq. (5.81). Substituting Eq. (5.90) and Eq. (5.91) into Eq. (5.82), one finally finds

$$I_a(n_1,n_2,0)=\frac{\Gamma(n_1+d/2-2)\Gamma(n_2+d/2-2)\Gamma(2-d/2-n_1)\Gamma(1+n_1)}{\Gamma(4-d/2)\Gamma(d-4+n_1+n_2)}\frac{(2p\cdot k_2)^{n_1+d/2-3}}{2n\cdot p}$$

$$\times [2n\cdot(k_2-p)]^{-n_1}\,{}_2F_1\left(1,\frac{d}{2}-2;n_1+\frac{d}{2}-1;\frac{2n\cdot k_2}{2n\cdot p}\right). \tag{5.92}$$

Now we consider the case $n_3=1$. In this case the z integral is of the form

$$\int_0^1 dz\, z\,[A-Bz]^{d/2-4} = -\frac{(A-B)^{d/2-3}}{B(d/2-3)} - \frac{(A-B)^{d/2-2}}{B^2(d/2-3)(d/2-2)} + \frac{A^{d/2-2}}{B^2(d/2-3)(d/2-2)}, \tag{5.93}$$

where A and B have already been defined in eq. (5.83). From now on, all integrals can be carried out in a similar fashion to the previous section. The answer is

$$\begin{aligned}
I_a(n_1,n_2,1) = {}& \frac{\Gamma(n_1+d/2-2)\Gamma(n_2+d/2-2)}{\Gamma(d-4+n_1+n_2)}\left\{\frac{\Gamma(3-d/2-n_1)\Gamma(d/2-2+n_1)}{d/2-3}\right.\\
&\times (2n\cdot k_2)^{2-d/2-n_1}(2p\cdot k_2)^{n_1+d/2-3}(-2n\cdot p)^{d/2-3} - \frac{\Gamma(2-d/2-n_1)\Gamma(1+n_1)}{\Gamma(4-d/2)}\\
&\times(2p\cdot k_2)^{n_1+d/2-3}\frac{[2n\cdot(k_2-p)]^{-n_1}}{(-2n\cdot p)}\,{}_2F_1\left(1,\frac{d}{2}-2;n_1+\frac{d}{2}-1;\frac{2n\cdot k_2}{2n\cdot p}\right)\\
&-\frac{1}{(d/2-3)(d/2-2)}\frac{[2n\cdot(k_2-p)]^{1-n_1}}{(2n\cdot k_2)^2}(2p\cdot k_2)^{n_1+d/2-3}\\
&\times\frac{\Gamma(3-d/2-n_1)\Gamma(1+n_1)}{\Gamma(4-d/2)}\left[\frac{\Gamma(n_1+d/2-1)\Gamma(4-d/2)}{\Gamma(1+n_1)}\right.\\
&\times\left(-\frac{2n\cdot p}{2n\cdot k_2}\right)^{n_1+d/2-3}{}_2F_1\left(3-\frac{d}{2}-n_1,-n_1;2-\frac{d}{2}-n_1;\frac{2n\cdot k_2}{2n\cdot p}\right)\\
&+\frac{\Gamma(1-d/2-n_1)\Gamma(4-d/2)}{\Gamma(3-d/2-n_1)\Gamma(2-d/2)}\\
&\left.\times\left(-\frac{2n\cdot p}{2n\cdot k_2}\right)^{-2}{}_2F_1\left(2,\frac{d}{2}-1;n_1+\frac{d}{2};\frac{2n\cdot k_2}{2n\cdot p}\right)\right] + \frac{1}{(d/2-3)(d/2-2)}\\
&\left.\times\frac{(-2p\cdot n)^{d/2-2}}{(2n\cdot k_2)^2}\Gamma(3-d/2-n_1)\Gamma(n_1+d/2-1)\left(\frac{2p\cdot k_2}{2n\cdot k_2}\right)^{n_1+d/2-3}\right\}.
\end{aligned} \tag{5.94}$$

We also need to determine the integral in Eq. (5.78). This can be carried out similarly to the scalar integral $I_a(0,0,0)$, and the answer is

$$K_a = \frac{1}{(d/2-2)}\frac{\Gamma^2(d/2-1)\Gamma(1-d/2)}{\Gamma(d-2)\Gamma(2-d/2)}\frac{(2p\cdot k_2)^{d/2-2}}{(-2p\cdot n)}\,{}_2F_1\left(1,\frac{d}{2}-1;\frac{d}{2};\frac{2n\cdot k_2}{2n\cdot p}\right). \tag{5.95}$$

One may substitute the results of eqs. (5.92, 5.94, 5.95) into eqs. (5.73, 5.75, 5.77, 5.79), before using these in eq. (5.67).

Diagram (b)

For diagram (b), one defines the scalar and vector integrals

$$S_b = 2\int \frac{1}{k_1^2(k_1+k_2-p)^2 2n\cdot k_1};$$
$$V_b^\mu = 2\int \frac{k_1^\mu}{k_1^2(k_1+k_2-p)^2 2n\cdot k_1}. \tag{5.96}$$

For the scalar integral, one may introduce Feynman parameters to get

$$S_b = 2\int \frac{d^d\tilde{k}_1}{(2\pi)^d}\int_0^1 dx\int_0^1 dy \frac{2y}{[\tilde{k}_1^2 - M^2]^3}, \tag{5.97}$$

where

$$\begin{aligned}\tilde{k}_1 &= k_1 + (1-x)(k_2-p) + \frac{(1-y)}{y}n,\\ M^2 &= -(1-x)^2(2p\cdot k_2) + 2n\cdot(k_2-p)(1-x)\frac{(1-y)}{y} + 2(1-x)p\cdot k_2\\ &= (1-x)\left[\frac{2(1-y)}{y}n\cdot(k_2-p) + 2xp\cdot k_2\right].\end{aligned} \tag{5.98}$$

Performing the momentum integration in eq. (5.97) then gives

$$S_b = -\frac{2i\Gamma(3-d/2)}{(4\pi)^{d/2}} I_b(0,0), \tag{5.99}$$

where we have defined the master integral

$$\begin{aligned}I_b(n_1,n_2) = \int_0^1 dx\int_0^1 dy\, y^{1-d/2-n_1}(1-y)^{n_1}(1-x)^{n_2+d/2-3}\\ \times\ [2n\cdot(k_2-p)(1-y) + 2xyp\cdot k_2]\,.\end{aligned} \tag{5.100}$$

For the vector integral one finds

$$V_b^\mu = -\frac{2i\Gamma(3-d/2)}{(4\pi)^{d/2}}\left[-I_b(0,1)(k_2-p)^\mu - I_b(1,0)n^\mu\right]. \tag{5.101}$$

The master integral in this case is relatively straightforward to calculate. First one performs the y integral, which has form

$$\int_0^1 y^{1-d/2-n_1}(1-y)^{n_1}\left[\tilde{A}-\tilde{B}y\right]^{d/2-3}, \tag{5.102}$$

where

$$\tilde{A} = 2n\cdot(k_2-p), \quad \tilde{B} = \tilde{A} - 2xp\cdot k_2. \tag{5.103}$$

The integral is hypergeometric, and using the identity of eq. (5.81) one finds

$$\int_0^1 y^{1-d/2-n_1}(1-y)^{n_1}\left[\tilde{A}-\tilde{B}y\right]^{d/2-3} = \frac{\Gamma(2-d/2-n_1)\Gamma(1+n_1)}{\Gamma(3-d/2)}[2n\cdot(k_2-p)]^{-1-n_1} \times (2p\cdot k_2)^{n_1+d/2-2}x^{n_1+d/2-2}. \tag{5.104}$$

The remaining x integral is a simple beta-function, and one finds after restoring all prefactors

$$I_b(n_1,n_2) = \frac{\Gamma(n_1+d/2-1)\Gamma(n_2+d/2-2)\Gamma(2-d/2-n_1)\Gamma(1+n_1)}{\Gamma(n_1+n_2+d-3)\Gamma(3-d/2)} \times [2n\cdot(k_2-p)]^{-1-n_1}(2p\cdot k_2)^{n_1+d/2-2}. \tag{5.105}$$

Substituting this into Eq. (5.99) and Eq. (5.101), one may combine results with diagram (a) before expanding in k_2, to give the result quoted in Eq. (5.36).

Diagram (c)

The sum of $J_c^{\nu(1)}$ and $J_d^{\nu(1)}$ reads Fig. 5.3 reads

$$i\mu^{2\varepsilon}g_s^3\int\frac{d^dk_1}{(2\pi)^d}\left[\frac{(\not{p}-\not{k}_2)\gamma^\mu(\not{p}-\not{k}_1-\not{k}_2)\gamma^\nu(\not{p}-\not{k}_1)\gamma_\mu}{k_1^2(p-k_1-k_2)^2(p-k_1)^2(p-k_2)^2} + \frac{(\not{p}-k_2)\gamma^\mu(\not{p}-\not{k}_1-\not{k}_2)\gamma_\mu(\not{p}-\not{k}_2)\gamma^\nu}{k_1^2(p-k_1-k_2)^2(p-k_2)^4}\right]u(p)\,. \tag{5.106}$$

For diagram (c), one needs the scalar, vector and tensor integrals

$$\begin{aligned} S_c &= \int\frac{d^dk_1}{(2\pi)^d}\frac{1}{k_1^2(k_1-p)^2(k_1+k_2-p)^2};\\ V_c &= \int\frac{d^dk_1}{(2\pi)^d}\frac{k_1^\mu}{k_1^2(k_1-p)^2(k_1+k_2-p)^2};\\ T_c^{\mu\nu} &= \int\frac{d^dk_1}{(2\pi)^d}\frac{k_1^\mu k_1^\nu}{k_1^2(k_1-p)^2(k_1+k_2-p)^2}. \end{aligned} \tag{5.107}$$

One may introduce Feynman parameters to obtain

$$S_c = \int\frac{d^d\tilde{k}_1}{(2\pi)^d}\int_0^1 dx\int_0^1 dy\frac{2y}{[\tilde{k}_1^2-M^2]^3}, \tag{5.108}$$

where

$$\tilde{k}_1^\mu = k_1^\mu-(1-xy)p^\mu+(1-y)k_2^\mu,\quad M^2=(2p\cdot k_2)xy(1-y). \tag{5.109}$$

Carrying out the momentum integral, one then finds

$$S_c = -\frac{i}{(4\pi)^{d/2}}(2p\cdot k_2)^{d/2-3}\Gamma(3-d/2)I_c(0,0), \tag{5.110}$$

where we defined the master integral

$$\begin{aligned} I_c(n_1,n_2) &= \int_0^1 dx \int_0^1 dy x^{d/2-3+n_1} y^{d/2-2+n_1}(1-y)^{d/2-3+n_2} \\ &= \frac{\Gamma(d/2-2+n_1)\Gamma(d/2-2+n_2)}{\Gamma(d-3+n_1+n_2)}. \end{aligned} \tag{5.111}$$

Likewise, one finds

$$V_c^\mu = -\frac{i}{(4\pi)^{d/2}}(2p\cdot k_2)^{d/2-3}\Gamma(3-d/2)\left[p^\mu\left(I_c(0,0)-I_c(1,0)\right)-k_2^\mu I_c(0,1)\right]. \tag{5.112}$$

For the tensor integral, after shifting the integration variable there is a term whose numerator is quadratic in $\tilde{k}_1^\mu$. Using the result,

$$\int d^d\tilde{k}_1 \frac{\tilde{k}_1^\mu \tilde{k}_1^\nu}{[\tilde{k}_1^2-M^2]^3} = \frac{\eta^{\mu\nu}}{4}\int d^d\tilde{k}_1 \frac{1}{[\tilde{k}_1^2-M^2]^2}, \tag{5.113}$$

one may carry out the momentum and Feynman parameter integrations to get

$$T_c^{\mu\nu}|_{\text{quad.}} = \frac{i}{(4\pi)^{d/2}}(2p\cdot k_2)^{d/2-2}\frac{\eta^{\mu\nu}}{2}\frac{\Gamma(2-d/2)\Gamma^2(d/2-1)}{\Gamma(d-1)}. \tag{5.114}$$

There is also a contribution to $T_c^{\mu\nu}$ whose numerator does not depend on $\tilde{k}_1^\mu$. For this one finds

$$\begin{aligned} T_c^{\mu\nu}|_{\text{non-quad.}} = \frac{i}{(4\pi)^{d/2}}(2p\cdot k_2)^{d/2-3}\Gamma(3-d/2)\Big[&p^\mu p^\nu\left(I_c(0,0)-2I_c(1,0)+I_c(2,0)\right) \\ &-p^{(\mu}k_2^{\nu)}\left(I_c(0,1)-I_c(1,1)\right)+k_2^\mu k_2^\nu I_c(0,2)\Big]. \end{aligned} \tag{5.115}$$

Expanding the first term in Eq. (5.106) into its scalar, vector and tensor components, one may then use Eqs. (5.110), (5.112), (5.114) and (5.115) to obtain the contribution of diagram (c) to Eq. (5.35), after expanding in k_2.

Diagram (d)

For diagram (d) one needs the scalar and vector integrals

$$S_d = \int \frac{d^dk_1}{(2\pi)^d}\int_0^1 dx \frac{1}{k_1^2(k_1+k_2-p)^2},$$

$$V_d^\mu = \int \frac{d^d k_1}{(2\pi)^{d/2}} \int_0^1 dx \frac{k_1^\mu}{k_1^2 (k_1 + k_2 - p)^2}. \tag{5.116}$$

Introducing a Feynman parameter, one obtains

$$S_d = \int \frac{d^d \tilde{k}_1}{(2\pi)^d} \int_0^1 \frac{1}{[\tilde{k}_1^2 - M^2]^2}, \tag{5.117}$$

where

$$\tilde{k}_1^\mu = k_1^\mu + x(k_2 - p)^\mu, \quad M^2 = (2p \cdot k_2) x(1-x). \tag{5.118}$$

Carrying out the momentum integral in eq. (5.117) then gives

$$S_d = \frac{i}{(4\pi)^{d/2}} \Gamma(2 - d/2)(2p \cdot k_2)(2p \cdot k_2)^{d/2-2} I_d(0), \tag{5.119}$$

with

$$\begin{aligned} I_d(n) &= \int_0^1 dx x^{n+d/2-2} (1-x)^{d/2-2} \\ &= \frac{\Gamma(n + d/2 - 1)\Gamma(d/2 - 1)}{\Gamma(n + d - 2)}. \end{aligned} \tag{5.120}$$

Likewise, one finds for the vector integral

$$V^\mu = \frac{i}{(4\pi)^{d/2}} \Gamma(2 - d/2)(2p \cdot k_2)^{d/2-2} (p - k_2)^\mu I_d(1). \tag{5.121}$$

Using these results, together with those of the previous section, in Eq. (5.106) yields the expression quoted in Eq. (5.35).

CHAPTER 6

Drell-Yan moments with unitary cuts

The Drell-Yan process has been the main application of the techniques developed so far in this thesis. In particular, we have used it as a case study to investigate the subleading behaviour in the threshold expansion around $z = 1$, where threshold logarithms dominate the cross-section and need to be organized in an all-order framework. In this chapter, we will consider once again an expansion in z, but this time around $z = \infty$ and without any truncation at finite order. Despite this similarity, the purpose is totally different: we are not interested in all-order properties but rather in the development of a novel, efficient method to perform fixed-order computations.

Specifically, we will investigate how the use of unitarity, which in the form of the optical theorem turned out to be successful for the fully inclusive DIS up to three loops [125–130], can be extended to the Drell-Yan case. In this regard, we will relate the Mellin moments of the cross-section with the series coefficients of the forward amplitude expanded in powers of $1/z$. The main feature that makes this generalization highly non-trivial is the semi-inclusiveness of the process, which implies the presence of unphysical cuts. To tackle this problem, we will move from the optical theorem to the more general use of unitarity cuts.

The structure of this chapter is the following. We begin by reviewing how unitarity can be implemented in Mellin space to work out cross sections of fully inclusive processes. Then, in Section 6.2 we discuss how this can be generalized to single-particle inclusive cross-sections. The key aspect is to move to a diagram-by-diagram approach and to deal with unphysical cuts. In Section 6.3 we explain how these cuts can be efficiently removed directly in Mellin space. In order to exhibit the main features of the method, in Section 6.4 we will apply these techniques in the computation of the one-loop Drell-Yan K-factor. Although we discuss this case in detail, the method works also beyond one-loop. Therefore in Section 6.5 we briefly describe how it can be implemented in two-loop

cases.

6.1 The optical theorem in Mellin Space

The optical theorem relates the cross section $\sigma_{a+b\to X}$ of a fully inclusive process to the imaginary part of its corresponding forward amplitude $\mathcal{M}_{a+b\to a+b}$:

$$\sigma_{a+b\to X} = 2\, E_{\text{cm}}\, p_{\text{cm}}\, \text{Im}\, \mathcal{M}_{a+b\to a+b}\ , \tag{6.1}$$

where E_{cm} is the total center-of-mass energy and p_{cm} is the momentum of both particles in the center-of-mass frame. The inclusiveness is a crucial property to prove Eq. (6.1), because when summing over all intermediate states X one uses $\sum_X |X\rangle \langle X| = 1$. The most straightforward application of the theorem can be done in fully inclusive DIS, which at parton level is described as the scattering of an electron e of momentum l off a quark q of momentum p through the exchange of a photon of (space-like) momentum q:

$$e(l) + q(p) \longrightarrow e(l-q) + X\ , \tag{6.2}$$

where X represents any QCD final states allowed by current conservation. It is well-known [58] that the cross-section can be written in terms of a leptonic and an hadronic tensor $L^{\mu\nu}$ and $W^{\mu\nu}$. The latter collects QCD corrections and can be expressed in term of two scalar functions $W_i(x, Q^2)$, with $i = 1, 2$, which are function of

$$Q^2 = -q^2, \qquad x = \frac{Q^2}{2p\cdot q}\ . \tag{6.3}$$

Thanks to the inclusiveness of the process, we can use the optical theorem and relate $W_i(x, Q^2)$ to the imaginary part of the forward Compton amplitude $T^{\mu\nu}$ which describes the scattering of an off-shell photon and a quark:

$$\gamma^*(q) + q(p) \longrightarrow \gamma^*(q) + q(p)\ . \tag{6.4}$$

Since $T^{\mu\nu}$ has the same tensor structure of $W^{\mu\nu}$ [58], it can be also expressed in term of two scalar functions

$$T_i\left(\omega = \frac{1}{x}, Q^2\right)\ , \tag{6.5}$$

where we introduced the variable ω for later purposes. The optical theorem can now be expressed in term of scalar functions and reads

$$W_i\left(x, Q^2\right) = 2\,\text{Im}\, T_i\left(\omega, Q^2\right)\ . \tag{6.6}$$

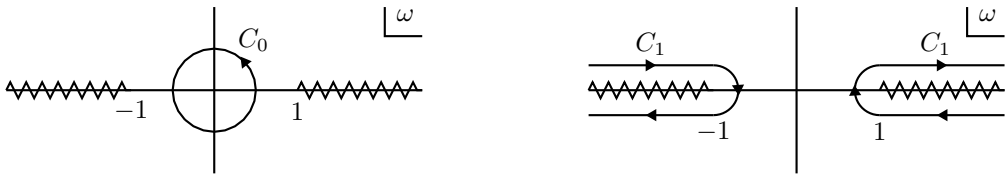

(a) (b)

Figure 6.1: Branch cut structure of $T(\omega)$ with the two contours used for $T^{(n)}$. On the left the contour C_0 wraps around the origin, while on the right the contour C_1 encloses the two branch cuts. Note that the combination $\omega^{-n-1}T(\omega)$ in Eq. (6.10) has an additional pole at the origin.

Before moving to Mellin space, we have to stress the analytic properties of the forward amplitude in the ω-plane. In particular, it can be shown [58] that T_i has two branch cuts along the intervals $[1, +\infty)$ and $(-\infty, -1]$, and satisfies the property

$$T_i\left(\omega, Q^2\right) = T_i\left(-\omega, Q^2\right) \ . \tag{6.7}$$

This branch cut structure guarantees that the imaginary part can be written in term of the discontinuity of the amplitude $\text{Disc}\, T_i(\omega)$ across one of the branch cut

$$2\,\text{Im}\, T_i\left(\omega, Q^2\right) = -i\,\text{Disc}_\omega\, T_i\left(\omega, Q^2\right) \ , \tag{6.8}$$

where we defined the discontinuity of a function f in the variable x as

$$\text{Disc}_x\, f(x) = \lim_{\eta \to 0} \left(f(x + i\eta) - f(x - i\eta)\right) \ . \tag{6.9}$$

Now we will explore how this can be translated to Mellin space. Specifically, we will see that it is possible to relate the Mellin moments of $W_i\left(x, Q^2\right)$ with the series coefficients of $T_i\left(\omega, Q^2\right)$. We start expanding the forward amplitude around $\omega = 0$ and considering its series coefficient $T_i^{(n)}(Q^2)$, defined as

$$T_i^{(n)}(Q^2) \equiv \frac{1}{n!} \frac{d^n T_i(\omega, Q^2)}{d\omega^n}\bigg|_{\omega=0} = \oint_{C_0} \frac{d\omega}{2\pi i} \omega^{-n-1} T_i(\omega, Q^2) \ , \tag{6.10}$$

where in the second equation we used the Cauchy's differentiation formula and the contour C_0 wraps around the origin. Then we can deform the contour C_0 into C_1, as depicted in Fig. 6.1. This yields

$$
\begin{aligned}
T_i^{(n)}(Q^2) &= \frac{1}{2\pi i}\int_{-\infty}^{-1} d\omega\, \omega^{-n-1}\left(T_i(\omega+i\eta,Q^2)-T_i(\omega-i\eta,Q^2)\right)\\
&+\frac{1}{2\pi i}\int_{1}^{\infty} d\omega\, \omega^{-n-1}\left(T_i(\omega+i\eta,Q^2)-T_i(\omega-i\eta,Q^2)\right)\\
&=(1+(-1)^n)\,\frac{1}{2\pi i}\int_1^{+\infty} d\omega\,\omega^{-n-1}\text{Disc}_\omega\, T_i(\omega,Q^2)\,, \qquad (6.11)
\end{aligned}
$$

where in the last line we used Eq. (6.7). The presence of the factor $(1+(-1)^n)$ implies that only *even* moments are non-vanishing. Now we can move from ω to x, defined in Eq. (6.5), relate the discontinuity with the imaginary part via Eq. (6.8) and use the optical theorem of Eq. (6.6). One finds

$$
\begin{cases}
T_i^{(n)}(Q^2)=0 \qquad \text{for odd } n\,,\\
T_i^{(n)}(Q^2)=\dfrac{1}{\pi}\displaystyle\int_0^1 dx\, x^{n-1}W_i(x,Q^2) \qquad \text{for even } n\,.
\end{cases} \qquad (6.12)
$$

Defining the Mellin transform $\mathcal{M}_n$ as

$$
\mathcal{M}_n[f(x)]\equiv\int_0^1 x^{n-1}\,f(x)\,, \qquad (6.13)
$$

we finally have

$$
T_i^{(n)}(Q^2)=\frac{1}{\pi}\mathcal{M}_n\big[W_i(Q^2)\big]\ . \qquad (6.14)
$$

This proves that, for a forward amplitude with branch cut structure as the one shown in Fig. 6.1, the Mellin moments of a fully inclusive cross section can be reconstructed from the series coefficients of the forward amplitude. Translating back the result to momentum space can be easily done, and up to three loops produces combinations of Harmonic Polylogarithms (HPL's) [111].

6.2 From the optical theorem to unitary cuts

Now we move to the central issue of this chapter, which is whether this approach can be used for the computation of the cross-sections for single-particle inclusive processes like Drell-Yan or Higgs production. Specifically, we will focus again on the (partonic) Drell-Yan process, which reads

$$
q(p)+\bar{q}(\bar{p})\longrightarrow V(Q)\,+\,X\,, \qquad (6.15)
$$

and on the corresponding forward amplitude

$$
q(p)+\bar{q}(\bar{p})\longrightarrow q(p)+\bar{q}(\bar{p})\,. \qquad (6.16)
$$

Here we introduce

$$\omega = \frac{1}{z}\,, \tag{6.17}$$

where $z = Q^2/s$ is the threshold variable we used in the previous chapters and s is the squared partonic center-of-mass energy. The variable z is the analogous to the Bjorken variable x for DIS.

The differences between Drell-Yan and DIS are numerous, and listing them all is not the goal of this chapter. Here, we limit ourselves to observe those differences at the parton level that are relevant for using unitarity and Mellin moments. We begin with very general observations that do not specifically belong to Mellin space.

The Drell-Yan amplitudes can be obtained from the DIS ones by crossing the exchanged off-shell photon to the final state, and the outgoing quark to the initial state. This simple procedure has important consequences. First, the momentum of the photon becomes time-like and therefore its off-shellness can be effectively regarded as a mass. Hence, the forward amplitude will contain a massive propagator. Then, there is another important difference. The presence of this massive boson in the final state implies that the process is not fully inclusive but only single-particle inclusive. Indeed, unlike DIS, there are cut diagrams that do not contribute to the Drell-Yan cross-section. This implies that the optical theorem cannot used here and the imaginary part of the forward amplitude does not give the cross-section.

When moving to Mellin space further complications arise. We note that the physical branch cut in the ω plane lies along the interval $[1, +\infty)$ only and no symmetry relates the forward amplitude with opposite values of ω. Hence, we expect that, if it is still possible to reconstruct the Mellin moments from the series coefficient of the forward amplitude, those will be both odd and even. However, there is a further complication. Besides the physical cut, other (unphysical) branch cuts are present and may have a branch point at the origin. This is clearly an obstacle for expanding the forward amplitude around $\omega = 0$.

These problems can be solved after moving from the optical theorem to the more general use of unitarity through the cutting equation. Using Cutkosky rules, it is possible to interpret the sum over intermediate states of the optical theorem as a sum over all possible branch cut discontinuities of the forward amplitude in the s-channel. More precisely, in the optical theorem every cut is a phase space integration of squared matrix elements, and all these cut diagrams contribute to the cross section. When we move to a single-particle inclusive process, some of these cuts do not contribute to the cross-section. Therefore we leave the optical theorem approach and we move to a diagram-by-diagram analysis.

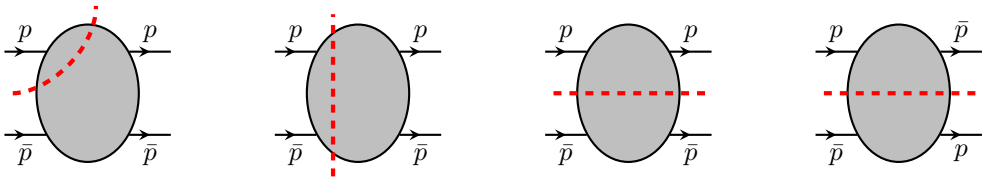

(a) vertex cut (b) s-channel cut (c) t-channel cut (d) u-channel cut

Figure 6.2: Generic cuts of forward amplitudes with two initial massless particles with momenta p and $\bar{p}$. The cuts of type (a) and (c) vanish for $p^2 = \bar{p}^2 = 0$. Note that the u-channel cut differs from the t-channel cut by interchange of the two outgoing momenta.

A priori, given a generic Feynman diagram $\mathcal{F}$, we can consider a different discontinuity for each channel. This can be an s-channel (i.e. a phase space integration) or another channel formed with kinematical invariants. For a generic x-channel, we can compute the discontinuity in the variable x using [131]

$$\text{Disc}_x \mathcal{F} = \sum_{k \in x\text{-ch}} \text{Cut}_k \mathcal{F} \,, \tag{6.18}$$

where the subscript $k \in x$-ch means that the sum is restricted to cuts in the x-channel. However, when looking at forward amplitudes, and in particular in a two-scale problem like Drell-Yan, there is one dimensionless variable only (e.g. ω) and therefore all the cuts of a diagram will contribute to the same discontinuity. In particular, for each forward Feynman diagram $f(\omega)$ the discontinuity in the variable ω is given by the sum over all possible cuts of the diagram, as follows

$$\text{Disc}_\omega f(\omega) = \sum_k \text{Cut}_k f(\omega) \,. \tag{6.19}$$

Let us now discuss in more detail how to organize the possible cuts of a generic forward diagram $f(\omega)$. Let us assume for a moment that the amplitude is not actually forward, but that outgoing external momenta can be different from the incoming ones, such that we have different channels given by the Mandelstam variables s, t, u and the off-shellness of the external legs. Then, we can measure the discontinuity in each channel, cutting the diagram in all possible ways as shown in Fig. 6.2. Now we return to the forward on-shell amplitude but we keep the same terminology to classify all cuts. Clearly in a forward amplitude the only kinematical invariant is s, (or equivalently ω, assuming that the mass Q^2 is fixed). Therefore, despite our terminology, all these cuts measure the discontinuity in the s-channel. The physical cuts are those contributing to the cross-section and therefore are only of the s-channel type and must cut the massive

boson propagator. Accordingly to whether the cut passes through the massive line or not we define the cut to be *massive* or *massless* respectively.

With this set-up, it seems that the number of unphysical cut diagrams might increase considerably with the order of the computation. However, we can observe that most of them actually vanish. Indeed, if we consider the vertex-type diagram of Fig. 6.2, we note that it isolates a single external leg of momentum p^2, and therefore it measure the discontinuity of the cross-section in this channel. Since the cross-section does not depend on $p^2 = 0$, we can conclude that this type of cut vanishes. Following the same arguments, t-channel cuts isolate on one side of the cut two legs with same momentum and therefore vanish. In conclusion, the only non-vanishing unphysical cuts are the massless s-channel cuts and the (massive and massless) u-channel cuts.

The method we want to present aims to reconstruct the cross section from the forward amplitude making use of Eq. (6.19). In order to do that, we should remove from the discontinuity of the forward amplitude all unphysical cuts.[1] At first glance, this approach does not seem very efficient, as one should compute unphysical cuts on top of the forward amplitude, and these might be even more complicated than the physical ones. However, we will see that moving to Mellin space, it is possible to define a set of prescriptions that select automatically the physical branch cut. Once unphysical branch cuts are removed, the procedure described for DIS in Eq. (6.10) and Eq. (6.11) and shown in Fig. 6.1 can be repeated. One finds

$$f_{\text{phys}}^{(n)} = \frac{1}{2\pi i}\mathcal{M}_n\left[\text{Cut}_{\text{phys}}\,\mathcal{F}\right] \ , \tag{6.20}$$

where $\mathcal{F}$ is the forward Feynman diagram and $f_{\text{phys}}^{(n)}$ are the series coefficients of the modified forward amplitude without unphysical cuts. Therefore, the Mellin moments of the cross-section can be reconstructed from the forward amplitude.

Let us now discuss how the unphysical cuts can be removed.

6.3 Removing unphysical cuts

From the previous section, we have seen that the only unphysical cuts that need a special treatment are the massless s-channel cut and the u-channel cut (both massive and massless). The prescription to remove these unphysical cuts passes through the analysis of the analytic properties of the forward amplitude. Hence, before discussing

[1] Clearly, a diagram-by-diagram approach that makes use of Eq. (6.19) can be applied also to fully inclusive processes like DIS: for a given diagram, the discontinuity across the physical cut can be reconstructed from the forward amplitude after removing the unphysical cuts in different channels. However, for DIS, the optical theorem is a shortcut that allows us not to deal with them: leaving a diagram-by-diagram approach and considering the full amplitude we get only cuts that contribute to the cross-section.

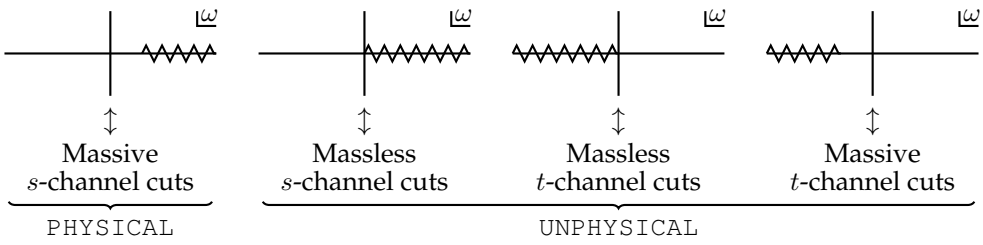

Figure 6.3: Branch cut structures of the NNLO forward diagrams. Only the first type of cut is physical, i.e. contributes to the Drell-Yan cross-section. The remaining three types of cuts are unphysical.

the prescription in Mellin space, we start by observing general properties of the branch cut structure of the forward amplitude.

Different cut diagrams correspond to different branch cuts in the ω-plane. Considering diagrams up to NNLO, this classification is shown in Fig. 6.3. We will now analyze these cuts in turn.

- **Massive *s*-channel** cuts are the only physical ones. Replacing the massive boson propagator with a delta function $\delta(q^2 - Q^2)$ fixes the off-shellness of the photon to be Q^2. They correspond to the phase space integration of matrix elements with one massive particle plus zero, one or two real massless particles. As it is well-known, this phase space integration carries a $\theta(s - Q^2)$. Looking at the ω-plane, these diagrams have a branch cut in the semi-axis $\omega > 1$.

- **Massless *s*-channel** cuts can be regarded as phase space integrations as well. However, since no massive line is cut, they contain a $\theta(s)$. Their branch point in the ω-plane is shifted from $\omega = 1$ to the origin. The presence of this kind of cuts in the forward amplitude is due to factors of $(-\omega)^{k\varepsilon}$. This clearly prevents the forward amplitude to be expanded around $\omega = 0$. We will solve this issue by a method that we call *shifting procedure*.

- **Massless *u*-channel** cuts cannot be naively regarded as phase space integrations, since the integration measure contains a $\theta(-s)$. This corresponds to a branch cut in the negative semi-axis in ω-plane. In the forward amplitude, the presence of this kind of cuts emerges with factors of $(+\omega)^{k\varepsilon}$. Therefore, these kinds of cuts are similar to the massless s-channel cuts described above and can be treated with the same shifting procedure.

- At one-loop, the only unphysical cuts are those described above. At two-loop we have to deal also with the **massive *u*-channel cuts**. The presence of a cut massive line shifts the branch point of the massless u-channel cut from the origin to $\omega = -1$. As such, we will see that the shifting procedure cannot remove this unphysical cut. Our solution involves the definition of a set of *replacement rules* in Mellin space.

The general strategy we follow is to re-define the forward amplitude such that it contains the physical branch cut only. Indeed this is a perfectly allowed procedure as long as the discontinuity across the physical branch cut remains the same. This is achieved through several steps. First we make the following observation. Let us assume that the forward amplitude may be expanded as

$$f(\omega) = \sum_{n=n_0}^{\infty} c_n \, \omega^n \,, \quad n_0 > 0 \,. \tag{6.21}$$

Considering a new lower bound $n_1 > 0$ is equivalent to adding polynomials in ω to the original function. These do not contain any singularity and therefore the discontinuity of $f(\omega)$ is not affected. Also a negative original lower bound is not a problem, as this would correspond to (unphysical) isolated poles at the origin that must be removed. In other words, the physical information in the series coefficients of the forward amplitude is carried only by their n-dependence and not by the lowest moment. Therefore, in the following when writing series coefficients we will omit the lower bound of the sum, unless when strictly necessary, assuming that this is a finite positive integer.

The idea of modifying the forward amplitude might be further exploited, and is at the basis of the shifting procedure, required for massless unphysical cuts, and the replacement procedure, required for the massive unphysical cuts. Now we discuss in turn these two methods. We start with the former.

Shifting procedure

The goal of the shifting procedure is to redefine the forward amplitude such that it contains no factor of $(\pm\omega)^{k\varepsilon}$, with k integer. To illustrate the method, let us consider the function

$$f(\omega) = \omega^{k\varepsilon} g(\omega) \,, \tag{6.22}$$

where $g(\omega)$ is an analytic function. Expanding $g(\omega)$ around $\omega = 0$ yields

$$f(\omega) = \sum_{n=n_0}^{\infty} c_n \, \omega^{n+k\varepsilon} = \sum_{n=n_0+k\varepsilon}^{\infty} c_{n-k\varepsilon} \, \omega^n \,, \tag{6.23}$$

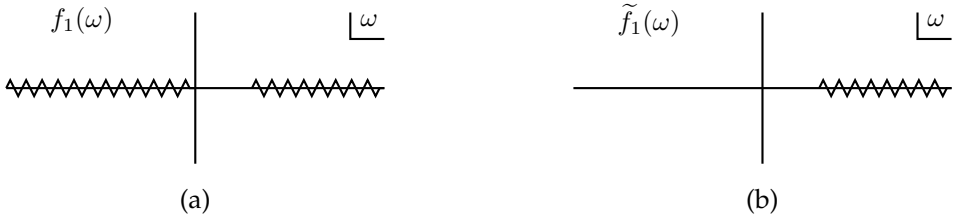

Figure 6.4: Analytic structure of the functions $f_1(\omega)$ and $\widetilde{f}_1(\omega)$, related by the shifting procedure.

where in the last equation we formally defined a sum starting at non-integer value $\alpha \in \mathbb{C}$ as $\sum_{n=\alpha}^{\infty} c_n = (c_\alpha + c_{\alpha+1} + \dots)$. The shifting procedure consists in setting $\varepsilon = 0$ in the lower bound of the sum. This defined a *new* function $\widetilde{f}(\omega)$

$$\widetilde{f}(\omega) \equiv \sum_{n=n_0}^{\infty} c_{n-k\varepsilon}\, \omega^n \equiv \sum_{n=n_0}^{\infty} \widetilde{c}_n\, \omega^n \,, \tag{6.24}$$

with no branch cut starting in the origin.

To see that the physical cut is not altered by this procedure, we consider a toy example, also illustrated in Fig. 6.4. Consider

$$f_1(\omega) = \log(1-\omega)\omega^{-\varepsilon} = -\sum_{n=1}^{\infty} \frac{1}{n}\omega^{n-\varepsilon} \,. \tag{6.25}$$

The shifting procedure yields

$$\widetilde{f}_1(\omega) = -\sum_{n=1}^{\infty} \frac{1}{n+\varepsilon}\omega^n \,. \tag{6.26}$$

The discontinuity can be easily computed order by order in ε. We first write

$$f_1(\omega) = \log(1-\omega) \sum_{k=0}^{\infty} (-\varepsilon)^k \frac{\log^k \omega}{k!} \,, \tag{6.27}$$

$$\widetilde{f}_1(\omega) = -\sum_{k=0}^{\infty} (-\varepsilon)^k \mathrm{Li}_{k+1}\omega \,, \tag{6.28}$$

where $\mathrm{Li}_s(\omega)$ is the polylogarithm function. Then, we can verify that for each k-th term in the ε-expansion we have

$$\mathrm{Disc}_{\omega\geq 1} f_1^{(k)}(\omega) = \mathrm{Disc}_{\omega\geq 1} \widetilde{f}_1^{(k)}(\omega) = -2\pi i \frac{\log^k \omega}{k!} \,, \tag{6.29}$$

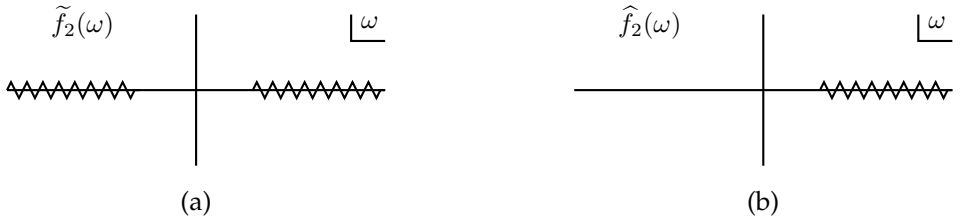

Figure 6.5: Analytic structure of the functions $\widetilde{f}_2(\omega)$ and $\widehat{f}_2(\omega)$, related by the replacement procedure.

and therefore the discontinuity across the physical branch cut is not altered by the shifting procedure.

This method can be applied to the massless unphysical cuts described above. For these indeed the non-analyticity of $f(\omega)$ can be captured only by overall factors of $(\pm\omega)^{k\varepsilon}$, as can be argued by dimensional analysis [49]. We claim that up to NNLO for a generic forward diagram $\mathcal{F}$ containing only massless unphysical branch cuts we have

$$\widetilde{c}_n\left[\mathcal{F}\right] = \frac{1}{2\pi i}\mathcal{M}_n\left[\sum_{\substack{\text{phys}\\ \text{cuts } k}} \text{Cut}_k\,\mathcal{F}\right] , \tag{6.30}$$

as required by Eq. (6.20).

Replacement procedure

At two-loop the shifting procedure is not sufficient for every diagram, as massive u-channel cuts might be present. For this case, we shall replace the forward amplitude by a new function $\widehat{f}(\omega)$ whose branch cut along $\omega \in (-\infty, 1]$ is removed while its branch cut discontinuity around the physical region $\omega \in (1, \infty]$ remains unchanged.

To illustrate the method, let us consider a generic function $\widetilde{f}(\omega)$ whose discontinuity is given by

$$\text{Disc}_\omega \widetilde{f}(\omega) = g_{\text{unphys}}(\omega)\,\theta(-\omega - 1) + g_{\text{phys}}(\omega)\,\theta(\omega - 1) , \tag{6.31}$$

where, thanks to the theta functions, $g_{\text{unphys}}(\omega)$ and $g_{\text{phys}}(\omega)$ are the discontinuities across the physical and unphysical branch cut respectively, as illustrated in Fig. 6.5. The tilde notation for $\widetilde{f}(\omega)$ suggests that this function might be the result of the shifting procedure and that no unphysical branch cut other than $(-\infty, 1]$ is present. The method consists of

defining a new function

$$\widehat{f}(\omega) = \sum_n \widehat{c}_n \, \omega^n \, , \tag{6.32}$$

where the coefficients $\widehat{c}_n$ can be determined by following the same procedure carried out in Section 6.1. One finds

$$\widehat{c}_n = \frac{1}{2\pi i} \mathcal{M}_n \left[g_{\text{phys}}(\omega) \right] \, . \tag{6.33}$$

Comparing $\widehat{c}_n$ and $\widetilde{c}_n$, and focusing on the case where the functions are constructed with HPLs (as it is the case up to two-loop), the replacement $\widetilde{c}_n \to \widehat{c}_n$ involves a replacement of only harmonic sums with negative indices [111], as these are the only one giving rise to a branch cut at $(-\infty, 1]$. This defines a "dictionary" of replacement rules for harmonic sums that may then be applied to any diagram.

As we did for the shifting procedure, the method is best illustrated with a toy example. Let us consider

$$\widetilde{f}_2(\omega) = \log(1+\omega) \log(1-\omega) \, , \tag{6.34}$$

whose discontinuity is given by

$$\text{Disc}_\omega \widetilde{f}_2(\omega) = 2\pi i \log(1-\omega)\theta(-\omega-1) - 2\pi i \log(1+\omega)\theta(\omega-1) \, . \tag{6.35}$$

We define a new function $\widetilde{f}_2(\omega)$ with series coefficients

$$\begin{aligned} \widehat{c}_n &= -\int_0^1 z^{n-1} \, \log\left(1+\frac{1}{z}\right) \\ &= -\frac{1}{n^2} + \frac{(-1)^n S_{-1}(n)}{n} + \frac{((-1)^n - 1)\log 2}{n} \, , \end{aligned} \tag{6.36}$$

where $S_\ell(n)$ is the harmonic sum, whose definition for multiple indices can be found in [132]. Upon reorganizing harmonic sums into a convenient basis [133] we can resum the coefficients to get an expression for $\widehat{f}(\omega)$ in terms of HPLs [111]. One finds

$$\widehat{f}_2(\omega) = -\text{Li}_2\left(\frac{1+\omega}{2}\right) + \log 2 \, \log(1-\omega) - \frac{\log^2 2}{2} + \frac{\pi^2}{12} \, , \tag{6.37}$$

which has the required branch cut discontinuity, as one can check explicitly.

This method can be applied to more complicated cases which exhibit massive u-channel cuts. We claim that for a generic forward diagram $\mathcal{F}$ up to NNLO we have

$$\widehat{c}_n[\mathcal{F}] = \frac{1}{2\pi i} \mathcal{M}_n \left[\sum_{\substack{\text{phys} \\ \text{cuts } k}} \text{Cut}_k \, \mathcal{F} \right] \, , \tag{6.38}$$

as required by Eq. (6.20).

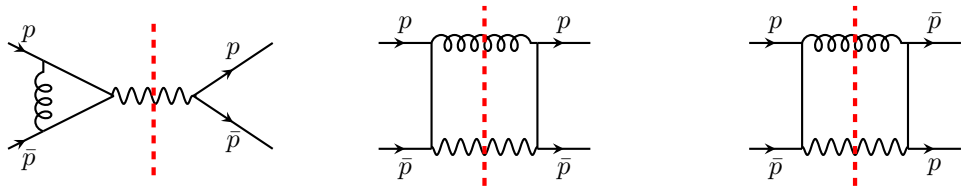

Figure 6.6: Diagrams needed for the one-loop DY cross sections. From left to right: $\mathrm{Cut}_{\mathrm{phys}}\, T$, $\mathrm{Cut}_{\mathrm{phys}}\, B_1$ and $\mathrm{Cut}_{\mathrm{phys}}\, B_2$. Diagrams obtained by complex conjugation or exchanging $p \leftrightarrow \bar{p}$ are omitted. Arrows on the lines indicate momentum flow.

6.4 The one-loop cross-section

In this section we apply the methods described in the previous sections to the one-loop Drell-Yan cross-section. The diagrams required for this calculations are shown in Fig. 6.6. They involve the phase space integration of matrix elements for real and virtual corrections. The former are given by the cut triangle $\mathrm{Cut}_{\mathrm{phys}}\, T$, the latter by the normal-box and crossed-box cut diagrams $\mathrm{Cut}_{\mathrm{phys}}\, B_1$ and $\mathrm{Cut}_{\mathrm{phys}}\, B_2$. Since they contribute to the cross-section, these cut diagrams are all physical (as stressed in the subscript) and, using the language of Section 6.2, they are massive s-channel cuts. Similarly to what was done in the other chapters, we will work with the one-loop K-factor

$$K^{(1)} = \frac{1}{\sigma_B}\frac{d\sigma^{(1)}}{dz}\,, \tag{6.39}$$

where σ_B is the tree level cross-section. Therefore, in the results presented in this section we will assume that both forward and cut diagrams have this normalization (i.e. divided by σ_B). The contributions of the diagrams of Fig. 6.6 to the one-loop cross-section, including complex conjugated diagrams and diagrams related by $p \leftrightarrow \bar{p}$ symmetry, reads

$$K^{(1)} = 2\,\Re e\left(\mathrm{Cut}_{\mathrm{phys}}\, T\right) + 2\ \mathrm{Cut}_{\mathrm{phys}}\, B_1 + 2\ \mathrm{Cut}_{\mathrm{phys}}\, B_2\,. \tag{6.40}$$

In this section, we will compute these three contributions in turn, following the method described in the previous sections: from the series coefficients of the forward amplitudes T, B_1 and B_2, we will extract the Mellin moments of the physical cuts, removing unphysical cuts when necessary. In particular, the triangle diagram T has a non-vanishing massless s-channel cut while the crossed-box diagram B_2 has a non-vanishing massless u-channel cut. As we have discussed, both kinds of cuts can be removed in Mellin space by the shifting procedure.

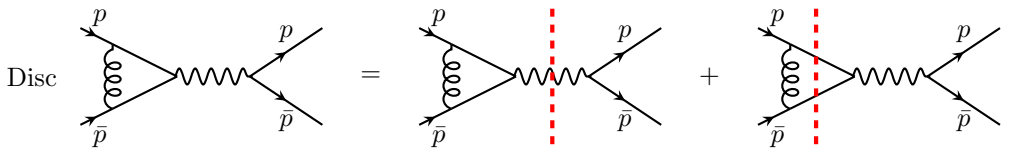

Figure 6.7: Cutting equation for the forward triangle diagram T. The right-hand side features both a physical massive s-channel cut ($\mathrm{Cut}_{\mathrm{phys}}\, T$) and an unphysical massless s-channel cut ($\mathrm{Cut}_{\mathrm{unphys}}\, T$).

Finally, we observe that, given the simplicity of this one-loop calculations, it is possible to perform a calculation exactly in ε. For simplicity, in the following we will set $\bar{\mu}^2 = Q^2$, where $\bar{\mu}^2 = 4\pi e^{-\gamma_E}\mu^2$.

Triangle diagram

The cutting equation for the triangle diagram is depicted in Fig. 6.7. It shows the presence of an unphysical massless s-channel cut $\mathrm{Cut}_{\mathrm{unphys}}\, T$. Both the forward amplitude and the physical cut involve the computation of the same loop integral. This is the one-loop form factor $\Gamma^{(1)}$ that was already evaluated in Eq. (2.26). With the notation of this chapter, it reads

$$\Gamma^{(1)}(\omega,\varepsilon) = \frac{\alpha_s\, C_F}{4\pi}\, \mathcal{C}(\varepsilon)\, (-\omega)^{-\varepsilon}\,, \tag{6.41}$$

where we expressed the result as a function of $\omega = 1/z = s/Q^2$ and we defined

$$\mathcal{C}(\varepsilon) = \frac{\Gamma^2(1-\varepsilon)\Gamma(1+\varepsilon)}{\Gamma(1-2\varepsilon)}\, \frac{2-\varepsilon+2\varepsilon^2}{\varepsilon^2(2\varepsilon-1)}\,. \tag{6.42}$$

Then, the evaluation of both the forward amplitude and the cut diagram follows straightforwardly. From direct evaluation over the one-particle phase space one has

$$\begin{aligned} \mathrm{Cut}_{\mathrm{phys}}\, T &= \Gamma^{(1)}(\omega,\varepsilon)\, \delta(1-z) \\ &= \frac{\alpha_s\, C_F}{4\pi}\, \mathcal{C}(\varepsilon)\, (-z)^{\varepsilon}\, \delta(1-z)\,. \end{aligned} \tag{6.43}$$

The forward amplitude can be computed by simple application of the Cutkosky cutting rule. It yields

$$\begin{aligned} T &= -\frac{1}{2\pi i}\Gamma^{(1)}(\omega,\varepsilon)\, \frac{s}{s-Q^2} \\ &= \frac{\alpha_s\, C_F}{4\pi}\, \mathcal{C}(\varepsilon)\, \frac{1}{2\pi i}\, (-\omega)^{-\varepsilon}\, \frac{\omega}{1-\omega}\,. \end{aligned} \tag{6.44}$$

At this point the presence of an unphysical cut is manifest, due to the factor $(-\omega)^{-\varepsilon}$ in Eq. (6.44). Upon computing also the unphysical cut $\mathrm{Cut}_{\text{unphys}}\, T$, one can explicitly check that

$$\mathrm{Disc}_\omega\, T = \mathrm{Cut}_{\text{phys}}\, T + \mathrm{Cut}_{\text{unphys}}\, T\ . \tag{6.45}$$

Therefore, to reconstruct the physical cut in z-space from the forward amplitude, one should subtract (and thus compute) the unphysical cut.

In Mellin space the procedure is simpler. One first writes a series representation for the forward amplitude as

$$T = \frac{\alpha_s\, C_F}{4\pi}\, \mathcal{C}(\varepsilon)\, \frac{1}{2\pi i}\, (-\omega)^{-\varepsilon} \sum_{n=1}^{\infty} \omega^n\ . \tag{6.46}$$

The presence of $(-\omega)^{-\varepsilon}$ prevents us from expanding the entire amplitude around $\omega = 0$ as $T = \sum_n c_n \omega^n$. Therefore we apply the shifting procedure of Section 6.3, which yields a new function

$$\widetilde{T} = \frac{\alpha_s\, C_F}{4\pi}\, \mathcal{C}(\varepsilon)\, \frac{1}{2\pi i} \sum_{n=1}^{\infty} \omega^n\ , \tag{6.47}$$

whose series coefficients are

$$\widetilde{c}_n[T] = \frac{\alpha_s\, C_F}{4\pi}\, \mathcal{C}(\varepsilon)\, \frac{1}{2\pi i}\ . \tag{6.48}$$

The Mellin moments of the physical cut can be easily computed as well. They read

$$\begin{aligned} \mathcal{M}_n\big[\mathrm{Cut}_{\text{phys}}\, T\big] &= \frac{\alpha_s\, C_F}{4\pi}\, \mathcal{C}(\varepsilon) \int_0^1 dz\, (-z)^{\varepsilon}\, \delta(1-z) \\ &= \frac{\alpha_s\, C_F}{4\pi}\, \mathcal{C}(\varepsilon)\ . \end{aligned} \tag{6.49}$$

Comparing Eq. (6.48) and Eq. (6.49) we see that

$$\widetilde{c}_n[T] = \frac{1}{2\pi i} \mathcal{M}_n\big[\mathrm{Cut}_{\text{phys}}\, T\big]\ , \tag{6.50}$$

which verifies the cutting equation in Mellin space in the form of Eq. (6.20).

In this example we have seen how the shifting procedure removes the unphysical cut and yields the correct Mellin moments. However, the application has been quite simple, since the moments are constant. In the next diagram we will have instead a non-trivial n-dependence.

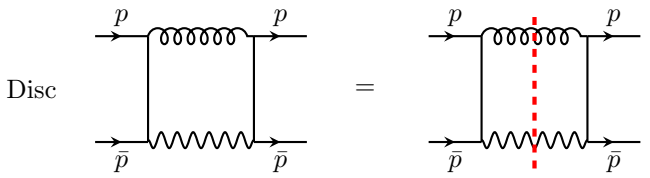

Figure 6.8: Cutting equation for the one-loop box diagram.

Normal box diagram

The cutting equation for the normal box diagram B_1 involves only a physical massive s-channel cut, as shown in Fig. 6.8. The forward diagrams can be easily computed with standard techniques and reads

$$B_1 = -\frac{\alpha_s C_F}{4\pi}\,\frac{1}{2\pi i}\,\frac{2(1-\varepsilon)^2\Gamma(\varepsilon)\Gamma(1-\varepsilon)}{\Gamma(1-2\varepsilon)}\Big[{}_2F_1(1,\varepsilon,2-\varepsilon;\omega) + (\omega-1)\;{}_2F_1(1,1+\varepsilon,2-\varepsilon;\omega)\Big]\,. \tag{6.51}$$

As expected, the function is analytical in $\omega = 0$. The physical cut can be easily computed as well. The result exact in ε is

$$\text{Cut}_{\text{phys}} B_1 = -\frac{\alpha_s C_F}{4\pi}\, z^{\varepsilon}(1-z)^{1-2\varepsilon}\,\frac{2\,(1-\varepsilon)^2\,\Gamma(1-\varepsilon)}{\varepsilon\,(1-2\varepsilon)\,\Gamma(1-2\varepsilon)}\,. \tag{6.52}$$

After expanding in ε one can explicitly check that Eq. (6.52) matches the known expression in the literature [39].

As for the triangle diagram, it is possible to verify the cutting equation in z-space, showing that $\text{Disc}_\omega\, B_1 = \text{Cut}_{\text{phys}} B_1$. We will now translate this in Mellin space. We start expanding the forward amplitude around $\omega = 0$ as $B_1 = \sum_n c_n \omega^n$. This yields the following series coefficients

$$c_n[B_1] = -\frac{\alpha_s C_F}{4\pi}\,\frac{1}{2\pi i}\,\frac{2\,(1-\varepsilon)^2\,\Gamma(1-\varepsilon)}{\varepsilon}\,\frac{\Gamma(n+\varepsilon)}{\Gamma(n+2-\varepsilon)}\,. \tag{6.53}$$

Then we compute the Mellin moments of the physical cuts. One finds

$$\mathcal{M}_n\big[\text{Cut}_{\text{phys}} B_1\big] = -\frac{\alpha_s C_F}{4\pi}\,\frac{2\,(1-\varepsilon)^2\,\Gamma(1-\varepsilon)}{\varepsilon\,(1-2\varepsilon)\,\Gamma(1-2\varepsilon)}\int_0^1 dz\, z^{n-1+\varepsilon}(1-z)^{1-2\varepsilon} \tag{6.54}$$

$$= -\frac{\alpha_s C_F}{4\pi}\,\frac{2\,(1-\varepsilon)^2\Gamma(1-\varepsilon)}{\varepsilon}\,\frac{\Gamma(n+\varepsilon)}{\Gamma(n+2-\varepsilon)} \tag{6.55}$$

Comparing Eq. (6.53) and Eq. (6.55) yields

$$c_n[B_1] = \frac{1}{2\pi i}\mathcal{M}_n\big[\text{Cut}_{\text{phys}} B_1\big]\,, \tag{6.56}$$

which verifies the cutting equation in Mellin space in the form of Eq. (6.20). Once again we stress that this relation is exact in ε.

Crossed box diagram

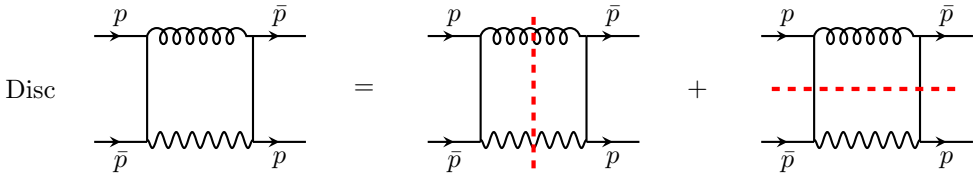

Figure 6.9: Cutting equation for the one-loop crossed-box diagram B_2, featuring on the right-hand side both the physical s-channel cut ($\mathrm{Cut}_{\mathrm{phys}}\, B_2$) and the unphysical u-channel cut ($\mathrm{Cut}_{\mathrm{unphys}}\, B_2$).

The crossed box B_2 is the most difficult diagram that enters the one-loop cross-section, since it exhibits both a non-physical cut and a non-trivial n-dependence in Mellin space, as shown in Fig. 6.9. Now we will compute in turn the forward amplitude and the physical cut to show that the cutting equation can be verified in Mellin space by means of the shifting procedure.

The forward diagram can be computed with the same techniques used for the triangle and normal-box diagrams. The algebra is however slightly more complicated. The final result is

$$
\begin{aligned}
B_1 = \frac{\alpha_s\, C_F}{4\pi}\frac{1}{2\pi i}\frac{\Gamma(1-\varepsilon)}{\Gamma(1-2\varepsilon)}\Bigg[&\frac{2\omega^{1-\varepsilon}\Gamma(1-\varepsilon)\Gamma(\varepsilon+1)\,{}_2F_1(1,1-\varepsilon;1-2\varepsilon;\omega)}{\varepsilon^2}\\
&-\frac{2\omega\Gamma(1-2\varepsilon)\Gamma(\varepsilon+1)\,{}_2F_1(1,1;1-\varepsilon;\omega)}{\varepsilon^2\Gamma(1-\varepsilon)}\\
&+\frac{2\omega\Gamma(1-2\varepsilon)\Gamma(\varepsilon+1)\,{}_2F_1(1,\varepsilon+1;1-\varepsilon;\omega)}{\varepsilon^2\Gamma(1-\varepsilon)}\\
&-\frac{2\omega^{-\varepsilon}\Gamma(1-2\varepsilon)\Gamma(1-\varepsilon)\Gamma(\varepsilon+1)\,{}_2F_1(1,1-\varepsilon;2-2\varepsilon;\omega)}{\Gamma(2-2\varepsilon)}\\
&+\frac{4\omega\Gamma(1-2\varepsilon)\Gamma(\varepsilon+1)\,{}_2F_1(1,\varepsilon+1;2-\varepsilon;\omega)}{\varepsilon\Gamma(2-\varepsilon)}\\
&+\frac{2\Gamma(1-2\varepsilon)\Gamma(\varepsilon+1)\,{}_2F_1(1,1;2-\varepsilon;\omega)}{\Gamma(2-\varepsilon)}\\
&-\frac{2\varepsilon\Gamma(1-2\varepsilon)\Gamma(\varepsilon)\,{}_2F_1(1,\varepsilon;2-\varepsilon;\omega)}{\Gamma(2-\varepsilon)}+\frac{2\varepsilon\omega^{-\varepsilon}\Gamma(1-2\varepsilon)\Gamma(1-\varepsilon)\Gamma(\varepsilon)}{\Gamma(2-2\varepsilon)}\Bigg]\,. \qquad (6.57)
\end{aligned}
$$

As for the triangle diagram, the presence of unphysical cuts is revealed by non-integer powers of ω. To be able to expand the result around $\omega = 0$, we make use of the shifting procedure, which yields the following series coefficients

$$\widetilde{c}_n[B_2] = \frac{\alpha_s\, C_F}{4\pi} \frac{1}{\pi i} \frac{\left(-\varepsilon(-1+\varepsilon+\varepsilon^2)+n+n^2\right)\,\Gamma(1-\varepsilon)\,\Gamma(n+\varepsilon)}{\varepsilon^2\,\Gamma(2-\varepsilon+n)}\,. \tag{6.58}$$

Now we move to the computation of the physical cut diagram $\mathrm{Cut}_{\mathrm{phys}}\, B_2$. In this regard we need to perform the phase space integration with one massive and one massless particle in the final state. The result, exact in ε, reads

$$\mathrm{Cut}_{\mathrm{phys}}\, B_2 = -\frac{\alpha_s\, C_F}{4\pi} \frac{2}{\varepsilon} \frac{\Gamma(1-\varepsilon)}{\Gamma(1-2\varepsilon)} z^{\varepsilon} \left[2z(1-z)^{-1-2\varepsilon} + \frac{\varepsilon^2}{1-2\varepsilon}(1-z)^{1-2\varepsilon} \right], \tag{6.59}$$

which, as for the normal box, matches the known result [39] after expanding in ε and making use of Eq. (3.2).

The Mellin moments can now be computed easily and read

$$\begin{aligned}
\mathcal{M}_n\big[\mathrm{Cut}_{\mathrm{phys}}\, B_2\big] &= -\frac{\alpha_s\, C_F}{4\pi} \frac{4}{\varepsilon} \frac{\Gamma(1-\varepsilon)}{\Gamma(1-2\varepsilon)} \left[\int_0^1 dz\, z^{n+\varepsilon}(1-z)^{-1-2\varepsilon} \right. \\
&\qquad \left. - \frac{2\varepsilon}{1-2\varepsilon} \int_0^1 dz\, z^{n-1+\varepsilon}(1-z)^{1-2\varepsilon} \right] \\
&= \frac{\alpha_s\, C_F}{4\pi} \frac{2\left(-\varepsilon(-1+\varepsilon+\varepsilon^2)+n+n^2\right)\,\Gamma(1-\varepsilon)\Gamma(n+\varepsilon)}{\varepsilon^2\,\Gamma(2-\varepsilon+n)}\,.
\end{aligned} \tag{6.60}$$

Comparing Eq. (6.58) and Eq. (6.60) we conclude that

$$\widetilde{c}_n[B_2] = \frac{1}{2\pi i} \mathcal{M}_n\big[\mathrm{Cut}_{\mathrm{phys}}\, B_2\big]\,, \tag{6.61}$$

which verifies the cutting equation in Mellin space in the form of Eq. (6.20). As for the triangle and the normal box, this relation holds exactly in ε.

In conclusion, with the shifting procedure we have been able to remove all unphysical cut from the forward amplitudes and we reproduced the correct Mellin moments of the physical cuts. These can then be easily converted to z-space and yields order by order in ε the well-known coefficient and splitting functions [39]. Hence, this provides an alternative method to compute the one-loop Drell-Yan cross-section. Admittedly, this one-loop correction is long known and the method, which turns phase space integrations into loop integrals, does not seem to offer a great simplification. The value of this approach becomes manifest beyond one-loop, as we will discuss in the next section.

6.5 The method at two-loop

In the previous section we have been able to test our method exactly in ε. This is not feasible at higher loops, where it is customary to compute results as Laurent series in ε. To this end, we first note that a powerful tool for computing higher loop diagrams is given by the so-called integration by parts identities (IBPs). These relate different diagrams, once a common topology is identified (i.e. a integral representation where propagators are elevated to a symbolic power). By means of these relations it is possible to decompose a diagram into a finite sum of master integrals.

The idea of relating different diagrams with a common topology can be taken further and new relations can be found by introducing derivatives with respect to the kinematical invariants of the process. This turns the above relations into *differential* equations that, supplemented by suitable boundary conditions, yield the solutions to the unknown master integrals. Computing Feynman diagrams via differential equations is now a mature field where many insights have been achieved (for a recent review see [134]).

For the purposes of the method described in the previous section, we note that we are interested in computing the series coefficients of the forward amplitude. As we discussed, this has to take into account the possibility that the function has a branch point at $\omega = 0$. Therefore, we assume that the each forward amplitude can be described by the following two-loop ansatz

$$f(\omega) = \sum_n c_n \omega^n + \sum_n d_n \omega^{n-\varepsilon} + \sum_n e_n \omega^{n-2\varepsilon} \,, \tag{6.62}$$

where c_n, d_n and e_n are functions of ε. The ansatz for the one-loop case amounts to dropping the last term in Eq. (6.62). Substituting this ansatz into the differential equation and equating equal powers of ω produces a set of *difference* equations for the series coefficients c_n, d_n and e_n. Such a difference equation in general reads

$$a_1(n,\varepsilon)\, c_n + a_2(n,\varepsilon)\, c_{n+1} + \cdots + a_r(n,\varepsilon)\, c_{n+r} = F(n,\varepsilon) \,, \tag{6.63}$$

and similarly for d_n and e_n. If $r = 1$ the difference equation becomes simply a recursion relation and the coefficients can be found exactly in ε. For $r > 1$, as it happens in two-loop examples, one should first expand in ε the unknown c_n and then find a solution order-by-order in ε. To simplify further this task, we observe that at a given order in ε we expect the unknown coefficients c_n to be made out of combinations of harmonic sums $S_\ell(n)$ with different values of ℓ and shifted argument. Therefore, we find solutions to the difference equations of the form

$$c_n = \sum_{k,\ell,m} A_{k,\ell,m}\, \varepsilon^k\, S_\ell(n-m) \,, \tag{6.64}$$

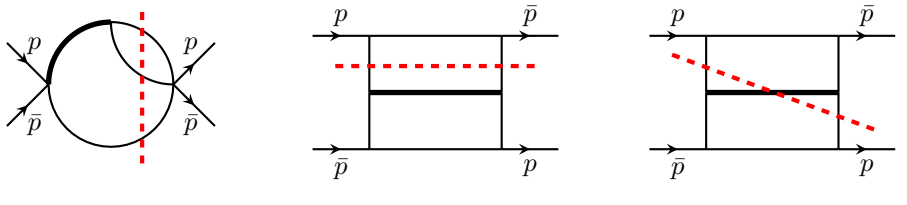

Figure 6.10: Representative examples for the unphysical cuts appearing at two loops: (a) massless s-channel cut; (b) massless u-channel cut; (c) massive u-channel cut.

for reasonable choice of k, ℓ and m.

After c_n, d_n and e_n are found by following these prescriptions, we can apply the shifting procedure of Section 6.3, which yields the series coefficients of $\widetilde{f}(\omega)$

$$\widetilde{c}_n = c_n + d_{n+\varepsilon} + e_{n+2\varepsilon} \,. \tag{6.65}$$

Clearly, if no massless cut is present, the shifting procedure is unnecessary and one can deal with c_n only. Then, if massive unphysical cuts are present, one has also to apply the replacement procedure described in Section 6.3, which amounts to perform $\widetilde{f}(\omega) \to \widehat{f}(\omega)$.

This set of routines has been successfully applied to the three diagrams shown in Fig. 6.10 in [49], where it is shown that the Mellin moments of the physical cut are indeed correctly reproduced. Hence the method also works at two-loop order.

6.6 Conclusions

In this chapter we presented a method to compute the Mellin moments of the Drell-Yan process making use of unitary cuts of forward amplitudes. As such, this method generalizes the optical theorem approach for DIS to a diagram-by-diagram approach. The key feature of this procedure is the removal of unphysical cuts from the discontinuity of the forward amplitude. This has been achieved through a shifting prescription in Mellin space for unphysical massless cuts. For unphysical massive cuts instead, which appear only from two-loop onwards, we defined a replacement procedure which yields the Mellin moments of the physical cut.

With this method we have been able to recompute the one loop Drell-Yan K-factor, where we saw that only massless unphysical cuts need to be removed, and therefore the shifting procedure was sufficient. Moreover, in [49] it has been shown that this method works also for representative two-loop cases.

Being based on forward amplitudes (turning cut integrals into loop integrals), this method is particularly suitable for phase space integrations, while it does not bring any new insight for purely virtual corrections. Moreover, a key element is the presence of a single dimensionless scale, as it is the case for Higgs or Drell-Yan production, that allowed us to deal with just a single Mellin variable. Finally, we note that an underlying assumption in the method consists of the knowledge of the analytic structure of the amplitude and its functional dependence given by combinations of HPLs. Although these assumptions need to be revisited at higher loops, the method seems a promising tool for the computation of cross-sections at N^3LO.

CHAPTER 7

Conclusions

In this thesis we have considered perturbative aspects of the Drell-Yan process to investigate two different topics: the search for a next-to-soft factorization formalism to organize NLP threshold logarithms, and the development of new methods based on unitarity to efficiently compute cross sections of single-particle inclusive processes.

Specifically, next-to-soft corrections have been investigated considering the abelian part of the real-virtual interference diagrams of the two-loop Drell-Yan K-factor. We have first computed this in full QCD after expanding at next-to-leading power in the threshold variable, such that the result contained both LP and NLP terms. Then we have compared this with the result given by three different approaches. The first one (in Chapter 3) is a diagrammatic approach that built upon the work of [73], by means of which it is possible to correctly identify all LP terms and the NLP term with highest power. Then in Chapter 4 we moved to an approach based on the expansion by regions. With this method we correctly reproduced all NLP terms, achieving a precise undertanding of each contribution to the K-factor from the hard, soft and collinear regions [45]. This however did not bring any information towards higher orders, as it is required for any formalism that leads to resummation. Therefore in Chapter 5 we moved to a factorization approach based on the LBKD theorem and the soft-collinear factorization formula. With this approach we have been able to correctly reproduce all NLP terms, thus introducing for the first time predictive power to this class of logarithms and paving the way for a full resummation formalism [46]. Progress in this direction is underway, and needs the inclusion of non-abelian terms into the formalism and all-order analysis of phase-space corrections to generalize the factorization formula at cross-section level.

In Chapter 6 instead we have proposed a new method to compute the Drell-Yan process by means of unitary cuts in Mellin space. Specifically, we have generalized the optical theorem approach for DIS to a diagram-by-diagram approach based on unitary

cuts. Crucial to this analysis has been the removal of unphysical cuts by means of a diagram-independent prescription in Mellin space. We presented the details of the calculation here for the one-loop K-factor. However, as shown in [49], the method works also at two-loop level. Although specific features of the Drell-Yan process have been fundamental in the definition of the method (such as the presence of a single dimensionless scale and the knowledge of the functional class of the solution) this seems a promising tool for the computation of inclusive cross-sections at $\mathrm{N^3LO}$.

In conclusion, we have seen that the Drell-Yan process, even though it has a long history, can still reveal surprising new insights in theoretical developments for perturbative quantum field theory, both at fixed and all orders, which are interesting both for phenomenological applications and for more formal contexts.

Summary

In this summary I aim to give a description of the themes of this thesis without discussing technical details. In particular, I hope that it offers the reader a more intuitive insight at least into the meaning of three keywords that compose the title of this thesis: the Drell-Yan process, (next-to-soft) factorization and unitarity.

A different way of seeing

The field of particle physics, to some extent, can be seen as a branch of microscopy, in the sense that it is aimed at viewing things that cannot be seen with the naked eye. In general, the process of observing requires different instruments according to the size of the object we want to study. Normally, in everyday life, we simply use our eyes. Already when we wish to observe human cells we need an artificial instrument like an optical microscope. For nanostructures we have to leave the idea of using light in the common sense and we need more powerful instruments like an atomic-force microscope. For elementary particles we need to go even further and build a particle accelerator. And the smaller the size we want to test, the larger the accelator (and thereby its energy) should be.

All these instrument seems very different from one another. However, they are all based on a scattering process. The idea is quite straightforward and can be intuitively understood thinking about a mysterious object, of which we want to reconstruct the shape. This can be reconstructed throwing another object against it and seeing how it bounces. This we can repeat again and again until, from the pattern of the scattering, we can reconstruct the shape. Even if might be odd, our sight is based on the same principle. When we look at an object illuminated by the sunshine or the light from a bulb, our eye is detecting photons scattered by the surface of this object. Then according to the intensity,

the direction and the color (i.e. the frequency) our brain reconstructs from the detected image the shape of the object. High energy experiments are based on exactly the same idea.

Clearly, for actual proton collisions like those that happen at the CERN Large Hadron Collider (LHC) we have to modify a little bit the picture described above. The entangled effect of special relativity and quantum mechanics makes it possible that new particles are created during these scattering processes, and the role of particle physicists is to understand the mechanism that governs the interactions among these particles. In this regard, we can distinguish experimentalists, who take part in the actual measurements of cross-sections (i.e. how these particles are scattered), and theorists, who predict these cross-sections based on a mathematical well-defined framework. Among theorists efforts we can discriminate those that predict the cross-sections in presence of new particles still to be discovered, and those that predict the so-called background, i.e. the cross-section for known effects due to pure Quantum Chromodynamical effects (the theory that governs the nuclear interactions, shortly indicated as QCD). The work presented in this thesis is set in the last group, as it computes QCD corrections to one particular cross-section known as Drell-Yan process.

Feynman diagrams and the Drell-Yan process

In a particle accelerator like the LHC at CERN protons collide and many particles are created and detected as final states. The Drell-Yan process describes a particular outcome for such collisions when among the final particles there is a lepton-antilepton pair. These are two particles that are insensitive to the nuclear force like muons and electrons. This production mechanism can be explained in the context of the parton model. This assumes that protons are made of elementary particles called quarks and gluons collectively called partons. In the Drell-Yan process, when two protons collide at very high energy, a parton from one proton annihilates with another parton in the other proton, creating a photon. However, this photon is not a physical one (whose mass is zero) but has a virtual mass less or equal to the incoming energy of the two partons. This might sounds a bit strange but, thanks to the magic of quantum mechanics, in Feynman diagrams particles can violate some constraint typical of physical particles, provided they do so for the briefest of moments (technically they are called off-shell particles). Therefore, this unphysical photon is an unstable particle and it decays in the lepton pair described above.

To predict the occurrence rate for this process one makes use of the so-called Feynman diagrams, like the one shown on the cover of this thesis. Apart from getting an intuitive picture of how particles interact, we can associate to each of these diagrams a number, which represents the probability that the process will happen through this specified

diagram. Computing this number is the goal of a particle theorists because this number can be compared with an experimental measurement. However this task might be very complicated. In particular, the higher the number of particles in a diagram, the more complicated the calculation will be.

The reason why it is convenient to compute cross-sections with Feynman diagrams is the fact that partons are almost free at high energy, and therefore diagrams with many interactions are unlikely and can be neglected. Therefore, we can approximate the probability for the entire cross-section with a subset of easier-to-compute diagrams. Mathematically speaking, we are using perturbation theory and we are approximating the exact result with the first terms of the series. Experiments demand very precise predictions, hence sometimes cross sections have been calculated with many of these Feynman diagrams.

In this thesis we have investigated these computations for the Drell-Yan process both when it is possible to consider only a *few* diagrams (by means of unitarity methods) and when one is forced to take into account a specific effect from *all* diagrams (by means of factorization methods). Let us now discuss them in turn.

Next-to-soft factorization

In a collider experiment the energy of the final particles will clearly depend on the energy of the particles we want to collide. In particular, the incoming energy should be greater than the mass of the particle we want to create. When we accelerate protons we typically control the energy of the protons, but we cannot have control of the energy of its components (quarks and gluons). Hence, we have to take into account the possibility that the energy of these might be very close to the threshold energy required to produce the final particles. For the Drell-Yan case, this corresponds to the situation when the energy is sufficient to produce the lepton-antilepton pair, and all other particles produced are soft (particles with little energy are called soft, while very energetic ones are called hard).

In this limiting situation, the approximation of taking only a few diagrams is not valid anymore and one has to take into account all diagrams with many soft gluons. Mathematically speaking, when we are close to the threshold limit the results of the computations are plagued by logarithms that need to be resummed to all orders. This process can be achieved through a so-called factorization. Indeed, after factorizing the effects of soft gluons, the soft part of the process becomes independent from the hard part and can be organized such that it gives predictions for more complicated diagrams (higher order terms). This well-known procedure called soft-gluon resummation is a well-established field and many cross sections have been computed including these

effects.

In this thesis we have extended this factorization procedure to a considerably more precise level, known as next-to-soft. In this case the emitted gluons are less soft than the purely soft case, and the hard particle recoils somewhat after the emission. Specifically, we have studied these next-to-soft effects with three different approaches (a diagrammatic one, the method of regions, and the soft-collinear factorization formula) and we have shown that it is possible to organize the logarithms due to next-to-soft effects to all orders. With this preliminary work the door is now open to more research that can be done, as eventually we would like to use this factorization to compute a full resummed result.

Unitarity

In the last chapter of this thesis we have investigated how to develop new methods for computing Feynman diagrams of the Drell-Yan process. Some of these methods made use of a property called unitarity. The name of this feature comes from the fact that, in a consistent theory, the sum of all probabilities (which as we discussed are related to Feynman diagrams) should be equal to one. With more mathematical precision, for some processes this is defined through a theorem, called the optical theorem.

For the Drell-Yan process this theorem cannot be used at face value and thus we might think that these types of methods cannot be used. However, in this thesis we have shown that it is indeed possible, after moving from the optical theorem to the more general use of cuts of a diagram. This consists in literally cutting a diagrams in two parts with a separator line, and making every particle cut by this line physical (technically, putting it on-shell). The virtue of this perhaps somewhat mysterious procedure is that upon summing over all possible cuts of a diagram, it is possible to reconstruct the full cross-section. For some processes, this is intimately connected to the optical theorem, and hence these cuts are called unitarity cuts. With this method we have shown that it is possible to recompute the Drell-Yan cross sections (and thereby related cross sections such as for Higgs boson production), thus providing a new method for fixed order-computation.

This concludes the summary, where I hope I gave a glimpse of what has been presented in this thesis, omitting technical details. For a more rigorous discussion, the interested reader can simply begin reading the introduction of this thesis.

Samenvatting

In deze samenvatting probeer ik een beschrijving te geven van de thema's in dit proefschrift zonder technische details te bespreken. In het bijzonder hoop ik dat het een intuïtief inzicht verschaft aan de lezer, tenminste met betrekking de drie sleutelwoorden in de titel van dit proefschrift: het Drell-Yan proces, (één-na-zacht) factorisatie en unitariteit.

Een andere manier van kijken

Het vakgebied van deeltjesfysica kan gezien worden als een tak van microscopie, met dien verstande dat het gericht is op het bekijken van dingen die voor het blote oog onzichtbaar zijn. In het algemeen vereist het proces van observatie verschillende instrumenten, al naar gelang de grootte van het te bestuderen object. Normaal gesproken, in het alledaagse leven, gebruiken we simpelweg onze ogen. Maar wanneer we bijvoorbeeld een menselijke cel willen observeren hebben we al een kunstmatig instrument nodig zoals een optische microscoop. Voor nano-structuren moeten we zelfs het idee laten varen om normaal licht te gebruiken en hebben we krachtigere instrumenten nodig zoals een atoomkrachtmicroscoop. Voor elementaire deeltjes gaan we nog een stap verder en bouwen we een deeltjesversneller. Hoe kleiner de schaal van wat we willen testen, des te groter moet de versneller zijn (en daarmee diens energie).

Al deze instrumenten lijken heel verschillend van elkaar. Desalniettemin zijn ze allemaal gebaseerd op een verstrooiingsproces. Het onderliggende idee is simpel en kan intuïtief begrepen worden door te denken aan een mysterieus voorwerp waarvan we de vorm willen reconstrueren. Dit kan gedaan worden door er een ander voorwerp tegenaan te schieten en te bekijken hoe dat terugkaatst. Dit kunnen we keer op keer herhalen, totdat we uit het verstrooiingspatroon de vorm kunnen reconstrueren. Ook al klinkt dit

misschien gek, ons zicht is gebaseerd op hetzelfde principe. Wanneer we kijken naar een object dat verlicht wordt door de zon of door het licht van een gloeilamp, dan detecteert ons oog de fotonen die verstrooid worden door het oppervlak van het object. Al naar gelang de intensiteit, de richting en de kleur (ofwel frequentie) reconstrueren onze hersenen de vorm van het object uit het gevormde beeld. Hoge energie experimenten zijn gebaseerd op precies hetzelfde idee.

Vanzelfsprekend moeten we deze beschrijving een beetje aanpassen voor daadwerkelijke botsingen tussen protonen, zoals die plaatsvinden in de CERN Large Hadron Collider (LHC). Het gecombineerde effect van speciale relativiteitstheorie en kwantummechanica maken het mogelijk dat nieuwe deeltjes worden gecreëerd tijdens deze verstrooiingsprocessen, en de rol van de deeltjesfysicus is om de mechanismen te begrijpen die de interacties tussen deze deeltjes dicteren. In dit verband kunnen we onderscheid maken tussen experimentatoren, die deelnemen aan het daadwerkelijk meten van werkzame doorsneden (hoe deeltjes verstrooid worden), en theoretici, die deze werkzame doorsneden voorspellen op basis van een solide wiskundig bouwwerk. Binnen de inspanningen van theoretici kunnen we verder onderscheid maken tussen zij die werkzame doorsneden berekenen van nieuwe onontdekte deeltjes, en zij die een voorspelling doen van de zogenaamde achtergrond, oftewel de werkzame doorsnede ten gevolge van zuivere kwantumchromodynamische effecten (de theorie welke de nucleaire interacties beschrijft, kortweg aangeduid met QCD). Het werk dat gepresenteerd wordt in dit proefschrift valt binnen de laatste categorie, aangezien het berekeningen bevat van QCD correcties op een specifieke werkzame doorsnede, bekend als het Drell-Yan proces.

Feynman diagrammen en het Drell-Yan proces

In een deeltjesversneller, zoals de LHC op CERN, botsen protonen en daarbij worden veel deeltjes geproduceerd en gedetecteerd als eindtoestand. Het Drell-Yan proces beschrijft een specifieke uitkomst voor zulke botsingen waarbij zich een lepton-antilepton paar bevindt in de eindtoestand. Dit zijn twee deeltjes die ongevoelig zijn voor de sterke kernkracht, zoals bijvoorbeeld muonen of elektronen. Het productiemechanisme kan beschreven worden in de context van het parton model. Dit model neemt aan dat protonen opgebouwd zijn uit elementaire deeltjes genaamd quarks en gluonen, tezamen partonen genaamd. In het Drell-Yan proces zal, wanneer twee protonen met hoge energie op elkaar botsen, een parton van het ene proton samenkomen met een parton uit het andere proton, waarna ze elkaar wederzijds vernietigen en daarbij een foton produceren. Dit foton is echter geen fysisch deeltje (wiens massa nul is), maar het heeft een massa kleiner of gelijk aan de inkomende energie van de twee partonen. Dit klinkt misschien vreemd, maar dankzij de magie van de kwantummechanica kunnen deeltjes in Feynman

diagrammen sommige behoudswetten schenden die typisch gelden voor fysische deeltjes, mits ze dat doen gedurende een zeer korte tijd (technische gesproken heten dit off-shell deeltjes). Daarom is dit on-fysische foton een instabiel deeltje en zal het vervallen tot het bovengenoemde lepton paar.

Om de kans op dit proces te voorspellen gebruikt men zogenaamde Feynman diagrammen, zoals bijvoorbeeld die op de omslag van dit proefschrift. Afgezien van het verkrijgen van een gevoelsmatig beeld van de interacties tussen de deeltjes kunnen we bovendien aan zulke diagrammen getallen toewijzen, welke staan voor de kans waarmee het proces kan plaatsvinden volgens het betreffende diagram. Het berekenen van dit getal is de taak van de deeltjestheoreticus, omdat dit getal kan worden vergeleken met een experimentele meting. Deze taak kan echter zeer moeilijk zijn. In het bijzonder zal de berekening moeilijker zijn naarmate er zich meer deeltjes in het diagram bevinden.

De reden waarom Feynman diagrammen zo geschikt zijn om werkzame doorsneden uit te rekenen is vanwege het feit dat partonen zich bijna vrij kunnen bewegen bij hoge energie, zodat diagrammen met veel interacties onwaarschijnlijk zijn en dus mogen worden verwaarloosd. Dientengevolge kunnen we de waarschijnlijkheid voor de gehele werkzame doorsnede benaderen met een deelverzameling van gemakkelijk-te-berekenen diagrammen. Wiskundig gesproken maken we gebruik van storingstheorie en benaderen we het exacte resultaat met de eerste paar termen in een serie. De experimenten vereisen heel nauwkeurige voorspellingen, dus zijn sommige werkzame doorsneden uitgerekend met veel van deze Feynman diagrammen.

In dit proefschrift hebben we deze berekeningen onderzocht voor het Drell-Yan proces, zowel in het geval waarbij het mogelijk is om slechts *enkele* diagrammen te beschouwen (met behulp van unitariteit methoden), als ook in het geval dat men gedwongen wordt om een specifiek effect van *alle* diagrammen in aanmerking dient te nemen (met behulp van factorisatie methoden). We zullen deze methoden om de beurt nader bespreken.

Eén-na-zacht factorisatie

In een botsingsexperiment zal de energie van de eindtoestand deeltjes uiteraard afhangen van de energie van de deeltjes die we willen laten botsen. In het bijzonder zal de energie van de inkomende deeltjes groter moeten zijn dan de massa van het deeltje wat we willen produceren. Wanneer we protonen accelereren, dan hebben we de energie van de protonen onder controle, maar niet de energie van diens partonen (quarks en gluonen). Daarom moeten we rekening houden met de mogelijkheid dat de partonen slechts net genoeg energie hebben om de eindtoestand deeltjes te produceren. Voor het Drell-Yan proces correspondeert dit met de situatie waarbij de energie net genoeg is om het lepton-antilepton paar te produceren, terwijl alle andere geproduceerde deeltjes zacht zijn

(deeltjes met weinig energie worden zachte deeltjes genoemd, terwijl zeer energetische deeltjes hard zijn).

In dit grensgeval is het beschouwen van enkele diagrammen geen goede benadering meer en moet men alle diagrammen met veel zachte gluonen in aanmerking nemen. Wiskundig gesproken worden de resultaten van de berekeningen rond dit grensgeval geplaagd door logarithmen, welke hersommeerd moeten worden tot alle orden. Dit kan worden bereikt door een zogenaamde factorisatie. Inderdaad, na het factoriseren van de effecten van zachte gluonen, wordt het zachte deel van het proces onafhankelijk van het harde deel, en kan het zo worden georganiseerd dat het voorspellingen geeft van meer ingewikkelde diagrammen (hogere orde termen). Deze welbekende procedure heet zachte-gluon hersommatie en is een gevestigd terrein en veel werkzame doorsneden zijn berekend met inbegrip van deze effecten.

In dit proefschrift hebben we deze factorisatie procedure uitgebreid tot een aanzienlijk nauwkeuriger niveau, bekend als één-na-zacht. In dit geval zijn de uitgestraalde gluonen minder zacht dan in het zuiver zachte geval, en ervaren de harde deeltjes iets van terugslag na uitstraling van zachte gluonen. In het bijzonder hebben we deze één-na-zacht effecten bestudeerd met drie verschillende aanpakken (een diagrammatische aanpak, de methode van regio's, alsmede de zacht-collineaire factorisatie formule) en hebben we laten zien dat het mogelijk is om de logarithmen ten gevolge van deze één-na-zacht effecten te organiseren tot op alle orden. Met dit voorbereidend werk staat nu de deur open tot meer onderzoek wat gedaan kan worden, aangezien we uiteindelijk deze factorisatie willen gebruiken om een volledig hersommeerd resultaat te berekenen.

Unitariteit

In het laatste hoofdstuk van dit proefschrift hebben we onderzoek gedaan naar nieuwe methoden om Feynman diagrammen voor het Drell-Yan proces te berekenen. Sommige van deze methoden maken gebruik van een eigenschap genaamd unitariteit. De naam van deze eigenschap komt voort uit het feit dat in een consistente theorie de som van waarschijnlijkheden (welke zoals besproken gerelateerd zijn aan Feynman diagrammen) gelijk is aan één. Wiskundig nauwkeuriger gesproken is dit gedefinieerd als een stelling, genaamd de optische stelling.

Op het Drell-Yan proces kan deze stelling op het eerste gezicht echter niet worden gebruikt, waardoor we zouden denken dat dit type methoden niet van toepassing is. Maar in dit proefschrift hebben we laten zien dat dit toch mogelijk is, nadat we overgaan van de optische stelling naar het meer algemene gebruik van snedes van diagrammen. Dit bestaat uit het letterlijk snijden van diagrammen in twee stukken door middel van een scheidingslijn, waarbij alle deeltjes die door deze lijn worden gesneden fysische

deeltjes zijn (technisch, on-shell). De deugd van deze wellicht mysterieuze procedure is dat de gehele werkzame doorsnede gereconstrueerd wordt door het optellen van alle mogelijke sneden. Voor sommige processen is dit innig verbonden met de optische stelling, waardoor aan deze sneden gerefereerd wordt als unitariteits sneden. Met deze methode hebben we laten zien dat het mogelijk is om de Drell-Yan werkzame doorsnede te herberekenen (en daarmee gerelateerde werkzame doorsneden zoals voor Higgs boson productie), waardoor een nieuwe methode is geleverd voor het doen van gefixeerde orde berekeningen.

Dit concludeert deze samenvatting, waarbij ik hoop dat ik een glimp gaf van wat er gepresenteerd is in dit proefschrift, zonder technische details. Voor een meer rigoureuze discussie kan de geïnteresseerde lezer simpelweg beginnen met lezen van de introductie in dit proefschrift.

Acknowledgements

This thesis is the result of the research carried out over four years, during which I interacted with many people that I wish to thank.

First of all I would like to express my sincere gratitude to my supervisor Eric Laenen for giving me the opportunity to be a PhD student at Nikhef, for the possibility to work in this field and for the patient guidance and encouragement he has provided during these years. Then I would like to thank my co-promotor Chris White for the enthusiasm he transmitted to me when working together and for the huge amount of time he devoted to help me. My sincere gratitude goes also to Lorenzo Magnea for the inspiring discussions we had during our collaboration and for the deep insights and clean explanations he has provided during these years. Then, I would like to thank Leonardo Vernazza for the time we spent together during our collaboration and the help he has given in the most difficult parts of the projects. A special thanks goes to Robbert Rietkerk for the nice collaboration we had together, for sharing his inspiring precise methodology and also for the translation in Dutch of the summary of this thesis. I would like to thank other people with whom I had nice discussions specifically related to the projects presented in this thesis, in particular Stacey Melville, Marco Volponi and Davide Melini. I also would like to thank Wim Beenakker for important feedback he gave me on this manuscript.

Three out of four years of this PhD project have been founded by the LHCPhenoNet network, where I have been an ESR fellow. I want to thank the LHCPhenoNet board for the excellent schools they organized and the friendly environment created. I wish to thank all the people I met at the meetings. I also thank the network for the opportunity to spend three months in the US for an internship at Wolfram Res.

During these years, I had the opportunity to visit several times the School of Physics and Astronomy in Glasgow and Higgs Center for Theoretical Physics in Edinburgh, where crucial parts of the results presented in this thesis were done. I thank both

institutes for the warm hospitality.

Finally, a big thanks to Nikhef for the lively environment and for the efficiency of the services provided. In particular, I thank all members of the theory group, from whom I benefitted of many discussions and with whom I shared many activities that made these four years special.

Domenico Bonocore,
5 April 2016.

Bibliography

[1] **ATLAS** Collaboration, G. Aad *et al.*, "Observation of a new particle in the search for the Standard Model Higgs boson with the ATLAS detector at the LHC," *Phys. Lett.* **B716** (2012) 1–29, arXiv:1207.7214 [hep-ex].

[2] **CMS** Collaboration, S. Chatrchyan *et al.*, "Observation of a new boson at a mass of 125 GeV with the CMS experiment at the LHC," *Phys. Lett.* **B716** (2012) 30–61, arXiv:1207.7235 [hep-ex].

[3] L. Magnea, "The growing toolbox of perturbative QCD," in *Physics Prospects for Linear and other Future Colliders after the Discovery of the Higgs (LFC15) Trento, Italy, September 7-11, 2015*. 2016. arXiv:1601.02113 [hep-ph]. http://inspirehep.net/record/1414796/files/arXiv:1601.02113.pdf.

[4] S. Forte *et al.*, "The Standard Model from LHC to future colliders," *Eur. Phys. J.* **C75** no. 11, (2015) 554, arXiv:1505.01279 [hep-ph].

[5] G. Zanderighi, "QCD and High Energy Interactions: Moriond 2015 Theory Summary," arXiv:1507.01693 [hep-ph].

[6] J. Butterworth *et al.*, "PDF4LHC recommendations for LHC Run II," *J. Phys.* **G43** (2016) 023001, arXiv:1510.03865 [hep-ph].

[7] **NNPDF** Collaboration, R. D. Ball *et al.*, "Parton distributions for the LHC Run II," *JHEP* **04** (2015) 040, arXiv:1410.8849 [hep-ph].

[8] M. Dasgupta, A. Fregoso, S. Marzani, and G. P. Salam, "Towards an understanding of jet substructure," *JHEP* **09** (2013) 029, arXiv:1307.0007 [hep-ph].

[9] J. Alwall, R. Frederix, S. Frixione, V. Hirschi, F. Maltoni, O. Mattelaer, H. S. Shao, T. Stelzer, P. Torrielli, and M. Zaro, "The automated computation of tree-level and next-to-leading order differential cross sections, and their matching to parton shower simulations," *JHEP* **07** (2014) 079, arXiv:1405.0301 [hep-ph].

[10] M. Czakon and D. Heymes, "Four-dimensional formulation of the sector-improved residue subtraction scheme," *Nucl. Phys.* **B890** (2014) 152–227, arXiv:1408.2500 [hep-ph].

[11] L. Hartgring, E. Laenen, and P. Skands, "Antenna Showers with One-Loop Matrix Elements," *JHEP* **10** (2013) 127, arXiv:1303.4974 [hep-ph].

[12] R. Bonciani, S. Catani, M. Grazzini, H. Sargsyan, and A. Torre, "The q_T subtraction method for top quark production at hadron colliders," *Eur. Phys. J.* **C75** no. 12, (2015) 581, arXiv:1508.03585 [hep-ph].

[13] C. Duhr, "Hopf algebras, coproducts and symbols: an application to Higgs boson amplitudes," *JHEP* **08** (2012) 043, arXiv:1203.0454 [hep-ph].

[14] J. M. Henn, "Multiloop integrals in dimensional regularization made simple," *Phys. Rev. Lett.* **110** (2013) 251601, arXiv:1304.1806 [hep-th].

[15] S. Abreu, R. Britto, C. Duhr, and E. Gardi, "From multiple unitarity cuts to the coproduct of Feynman integrals," *JHEP* **10** (2014) 125, arXiv:1401.3546 [hep-th].

[16] C. Anastasiou, C. Duhr, F. Dulat, E. Furlan, T. Gehrmann, F. Herzog, and B. Mistlberger, "Higgs boson gluon-fusion production beyond threshold in N^3LO QCD," *JHEP* **03** (2015) 091, arXiv:1411.3584 [hep-ph].

[17] T. Gehrmann and E. Remiddi, "Differential equations for two loop four point functions," *Nucl. Phys.* **B580** (2000) 485–518, arXiv:hep-ph/9912329 [hep-ph].

[18] S. J. Parke and T. R. Taylor, "An Amplitude for n Gluon Scattering," *Phys. Rev. Lett.* **56** (1986) 2459.

[19] E. Witten, "Perturbative gauge theory as a string theory in twistor space," *Commun. Math. Phys.* **252** (2004) 189–258, arXiv:hep-th/0312171 [hep-th].

[20] Z. Bern, L. J. Dixon, D. C. Dunbar, and D. A. Kosower, "One loop n point gauge theory amplitudes, unitarity and collinear limits," *Nucl. Phys.* **B425** (1994) 217–260, arXiv:hep-ph/9403226 [hep-ph].

[21] Z. Bern, L. J. Dixon, D. C. Dunbar, and D. A. Kosower, "Fusing gauge theory tree amplitudes into loop amplitudes," *Nucl. Phys.* **B435** (1995) 59–101, arXiv:hep-ph/9409265 [hep-ph].

[22] R. Britto, F. Cachazo, B. Feng, and E. Witten, "Direct proof of tree-level recursion relation in Yang-Mills theory," *Phys. Rev. Lett.* **94** (2005) 181602, arXiv:hep-th/0501052 [hep-th].

[23] C. F. Berger, Z. Bern, L. J. Dixon, F. Febres Cordero, D. Forde, H. Ita, D. A. Kosower, and D. Maitre, "An Automated Implementation of On-Shell Methods for One-Loop Amplitudes," *Phys. Rev.* **D78** (2008) 036003, arXiv:0803.4180 [hep-ph].

[24] J. M. Drummond, J. Henn, G. P. Korchemsky, and E. Sokatchev, "Dual superconformal symmetry of scattering amplitudes in N=4 super-Yang-Mills theory," *Nucl. Phys.* **B828** (2010) 317–374, arXiv:0807.1095 [hep-th].

[25] A. Brandhuber, P. Heslop, and G. Travaglini, "A Note on dual superconformal symmetry of the N=4 super Yang-Mills S-matrix," *Phys. Rev.* **D78** (2008) 125005, arXiv:0807.4097 [hep-th].

[26] A. Brandhuber, P. Heslop, and G. Travaglini, "MHV amplitudes in N=4 super Yang-Mills and Wilson loops," *Nucl. Phys.* **B794** (2008) 231–243, arXiv:0707.1153 [hep-th].

[27] J. M. Drummond, J. M. Henn, and J. Plefka, "Yangian symmetry of scattering amplitudes in N=4 super Yang-Mills theory," *JHEP* **05** (2009) 046, arXiv:0902.2987 [hep-th].

[28] Z. Bern, J. J. Carrasco, L. J. Dixon, H. Johansson, and R. Roiban, "The Ultraviolet Behavior of N=8 Supergravity at Four Loops," *Phys. Rev. Lett.* **103** (2009) 081301, arXiv:0905.2326 [hep-th].

[29] Z. Bern, J. J. M. Carrasco, and H. Johansson, "Perturbative Quantum Gravity as a Double Copy of Gauge Theory," *Phys.Rev.Lett.* **105** (2010) 061602, arXiv:1004.0476 [hep-th].

[30] F. Cachazo, S. He, and E. Y. Yuan, "Scattering of Massless Particles in Arbitrary Dimensions," *Phys. Rev. Lett.* **113** no. 17, (2014) 171601, arXiv:1307.2199 [hep-th].

[31] **CMS Collaboration** Collaboration, S. Chatrchyan *et al.*, "Performance of CMS muon reconstruction in pp collision events at $\sqrt{s} = 7$ TeV," *JINST* **7** (2012) P10002, arXiv:1206.4071 [physics.ins-det].

[32] S. D. Drell and T.-M. Yan, "Massive Lepton Pair Production in Hadron-Hadron Collisions at High-Energies," *Phys. Rev. Lett.* **25** (1970) 316–320. [Erratum: Phys. Rev. Lett.25,902(1970)].

[33] **E598** Collaboration, J. J. Aubert *et al.*, "Experimental Observation of a Heavy Particle J," *Phys. Rev. Lett.* **33** (1974) 1404–1406.

[34] S. W. Herb *et al.*, "Observation of a Dimuon Resonance at 9.5-GeV in 400-GeV Proton-Nucleus Collisions," *Phys. Rev. Lett.* **39** (1977) 252–255.

[35] **UA1** Collaboration, G. Arnison *et al.*, "Experimental Observation of Isolated Large Transverse Energy Electrons with Associated Missing Energy at s**(1/2) = 540-GeV," *Phys. Lett.* **B122** (1983) 103–116. [,611(1983)].

[36] **UA1** Collaboration, G. Arnison *et al.*, "Experimental Observation of Lepton Pairs of Invariant Mass Around 95-GeV/c**2 at the CERN SPS Collider," *Phys. Lett.* **B126** (1983) 398–410.

[37] **UA2** Collaboration, M. Banner *et al.*, "Observation of Single Isolated Electrons of High Transverse Momentum in Events with Missing Transverse Energy at the CERN anti-p p Collider," *Phys. Lett.* **B122** (1983) 476–485.

[38] **UA2** Collaboration, P. Bagnaia *et al.*, "Evidence for Z0 —> e+ e- at the CERN anti-p p Collider," *Phys. Lett.* **B129** (1983) 130–140.

[39] G. Altarelli, R. K. Ellis, and G. Martinelli, "Large Perturbative Corrections to the Drell-Yan Process in QCD," *Nucl. Phys.* **B157** (1979) 461.

[40] T. Matsuura, S. C. van der Marck, and W. L. van Neerven, "The Calculation of the Second Order Soft and Virtual Contributions to the Drell-Yan Cross-Section," *Nucl. Phys.* **B319** (1989) 570.

[41] R. Hamberg, W. L. van Neerven, and T. Matsuura, "A Complete calculation of the order $\alpha - s^2$ correction to the Drell-Yan K factor," *Nucl. Phys.* **B359** (1991) 343–405. [Erratum: Nucl. Phys.B644,403(2002)].

[42] C. Anastasiou, L. J. Dixon, K. Melnikov, and F. Petriello, "High precision QCD at hadron colliders: Electroweak gauge boson rapidity distributions at NNLO," *Phys. Rev.* **D69** (2004) 094008, arXiv:hep-ph/0312266 [hep-ph].

[43] K. Melnikov and F. Petriello, "Electroweak gauge boson production at hadron colliders through O(alpha(s)**2)," *Phys. Rev.* **D74** (2006) 114017, arXiv:hep-ph/0609070 [hep-ph].

[44] S. Catani, L. Cieri, G. Ferrera, D. de Florian, and M. Grazzini, "Vector boson production at hadron colliders: a fully exclusive QCD calculation at NNLO," *Phys. Rev. Lett.* **103** (2009) 082001, arXiv:0903.2120 [hep-ph].

[45] D. Bonocore, E. Laenen, L. Magnea, L. Vernazza, and C. D. White, "The method of regions and next-to-soft corrections in Drell-Yan production," *Phys.Lett.* **B742** (2015) 375–382, arXiv:1410.6406 [hep-ph].

[46] D. Bonocore, E. Laenen, L. Magnea, S. Melville, L. Vernazza, *et al.*, "A factorization approach to next-to-leading-power threshold logarithms," *JHEP* **1506** (2015) 008, arXiv:1503.05156 [hep-ph].

[47] D. Bonocore, "Universal structure of the Drell-Yan process beyond threshold," 2015. arXiv:1512.05364 [hep-ph]. http://inspirehep.net/record/1410099/files/arXiv:1512.05364.pdf.

[48] D. Bonocore, E. Laenen, L. Magnea, S. Melville, L. Vernazza, and C. White, "Next-to-leading power threshold logarithms: a status report," in *Proceedings, 12th International Symposium on Radiative Corrections (Radcor 2015) and LoopFest XIV (Radiative Corrections for the LHC and Future Colliders)*. 2016. arXiv:1602.01988 [hep-ph]. http://inspirehep.net/record/1419984/files/arXiv:1602.01988.pdf.

[49] D. Bonocore, E. Laenen, and R. Rietkerk, "Unitarity methods for Mellin moments of Drell-Yan cross sections," arXiv:1603.05252 [hep-ph].

[50] J. C. Collins, D. E. Soper, and G. F. Sterman, "Factorization for Short Distance Hadron - Hadron Scattering," *Nucl. Phys.* **B261** (1985) 104.

[51] J. C. Collins, D. E. Soper, and G. F. Sterman, "Factorization of Hard Processes in QCD," *Adv. Ser. Direct. High Energy Phys.* **5** (1989) 1–91, arXiv:hep-ph/0409313 [hep-ph].

[52] J. C. Collins, D. E. Soper, and G. F. Sterman, "Transverse Momentum Distribution in Drell-Yan Pair and W and Z Boson Production," *Nucl. Phys.* **B250** (1985) 199.

[53] G. F. Sterman, "Summation of Large Corrections to Short Distance Hadronic Cross-Sections," *Nucl. Phys.* **B281** (1987) 310.

[54] C. W. Bauer, S. Fleming, D. Pirjol, and I. W. Stewart, "An Effective field theory for collinear and soft gluons: Heavy to light decays," *Phys. Rev.* **D63** (2001) 114020, arXiv:hep-ph/0011336 [hep-ph].

[55] C. W. Bauer, D. Pirjol, and I. W. Stewart, "Soft collinear factorization in effective field theory," *Phys. Rev.* **D65** (2002) 054022, arXiv:hep-ph/0109045 [hep-ph].

[56] M. Beneke, A. P. Chapovsky, M. Diehl, and T. Feldmann, "Soft collinear effective theory and heavy to light currents beyond leading power," *Nucl. Phys.* **B643** (2002) 431–476, arXiv:hep-ph/0206152 [hep-ph].

[57] T. Becher, A. Broggio, and A. Ferroglia, "Introduction to Soft-Collinear Effective Theory," arXiv:1410.1892 [hep-ph].

[58] G. F. Sterman, *An Introduction to quantum field theory*. Cambridge University Press, 1993.

[59] G. F. Sterman, "Partons, factorization and resummation, TASI 95," in *QCD and beyond. Proceedings, Theoretical Advanced Study Institute in Elementary Particle Physics, TASI-95, Boulder, USA, June 4-30, 1995*. 1995. arXiv:hep-ph/9606312 [hep-ph].

[60] J. C. Collins, "Sudakov form-factors," *Adv. Ser. Direct. High Energy Phys.* **5** (1989) 573–614, arXiv:hep-ph/0312336 [hep-ph].

[61] L. Magnea, "Advanced Lectures on the Infrared structure of Perturbative QCD,". https://people.phys.ethz.ch/~banfi/gaugetheory/program.html.

[62] L. D. Landau, "On analytic properties of vertex parts in quantum field theory," *Nucl. Phys.* **13** (1959) 181–192.

[63] S. Coleman and R. E. Norton, "Singularities in the physical region," *Nuovo Cim.* **38** (1965) 438–442.

[64] L. Magnea and G. F. Sterman, "Analytic continuation of the Sudakov form-factor in QCD," *Phys. Rev.* **D42** (1990) 4222–4227.

[65] L. Magnea, "Analytic resummation for the quark form-factor in QCD," *Nucl. Phys.* **B593** (2001) 269–288, arXiv:hep-ph/0006255 [hep-ph].

[66] G. F. Sterman, "Mass Divergences in Annihilation Processes. 1. Origin and Nature of Divergences in Cut Vacuum Polarization Diagrams," *Phys. Rev.* **D17** (1978) 2773.

[67] L. J. Dixon, E. Gardi, and L. Magnea, "On soft singularities at three loops and beyond," *JHEP* **02** (2010) 081, arXiv:0910.3653 [hep-ph].

[68] S. Catani, D. de Florian, and G. Rodrigo, "Space-like (versus time-like) collinear limits in QCD: Is factorization violated?," *JHEP* **07** (2012) 026, arXiv:1112.4405 [hep-ph].

[69] J. R. Forshaw, M. H. Seymour, and A. Siodmok, "On the Breaking of Collinear Factorization in QCD," *JHEP* **11** (2012) 066, arXiv:1206.6363 [hep-ph].

[70] I. Z. Rothstein and I. W. Stewart, "An Effective Field Theory for Forward Scattering and Factorization Violation," arXiv:1601.04695 [hep-ph].

[71] E. Gardi and L. Magnea, "Factorization constraints for soft anomalous dimensions in QCD scattering amplitudes," *JHEP* **03** (2009) 079, arXiv:0901.1091 [hep-ph].

[72] L. J. Dixon, L. Magnea, and G. F. Sterman, "Universal structure of subleading infrared poles in gauge theory amplitudes," *JHEP* **0808** (2008) 022, arXiv:0805.3515 [hep-ph].

[73] E. Laenen, L. Magnea, G. Stavenga, and C. D. White, "Next-to-eikonal corrections to soft gluon radiation: a diagrammatic approach," *JHEP* **1101** (2011) 141, arXiv:1010.1860 [hep-ph].

[74] F. E. Low, "Bremsstrahlung of very low-energy quanta in elementary particle collisions," *Phys. Rev.* **110** (1958) 974–977.

[75] S. Catani and L. Trentadue, "Resummation of the QCD Perturbative Series for Hard Processes," *Nucl. Phys.* **B327** (1989) 323.

[76] G. P. Korchemsky and G. Marchesini, "Resummation of large infrared corrections using Wilson loops," *Phys. Lett.* **B313** (1993) 433–440.

[77] H. Contopanagos, E. Laenen, and G. F. Sterman, "Sudakov factorization and resummation," *Nucl. Phys.* **B484** (1997) 303–330, arXiv:hep-ph/9604313 [hep-ph].

[78] S. Forte and G. Ridolfi, "Renormalization group approach to soft gluon resummation," *Nucl. Phys.* **B650** (2003) 229–270, arXiv:hep-ph/0209154 [hep-ph].

[79] T. Becher and M. Neubert, "Threshold resummation in momentum space from effective field theory," *Phys. Rev. Lett.* **97** (2006) 082001, arXiv:hep-ph/0605050 [hep-ph].

[80] M. D. Schwartz, "Resummation and NLO matching of event shapes with effective field theory," *Phys. Rev.* **D77** (2008) 014026, arXiv:0709.2709 [hep-ph].

[81] M. Kramer, E. Laenen, and M. Spira, "Soft gluon radiation in Higgs boson production at the LHC," *Nucl.Phys.* **B511** (1998) 523–549, arXiv:hep-ph/9611272 [hep-ph].

[82] S. Catani, D. de Florian, M. Grazzini, and P. Nason, "Soft gluon resummation for Higgs boson production at hadron colliders," *JHEP* **07** (2003) 028, arXiv:hep-ph/0306211 [hep-ph].

[83] R. D. Ball, M. Bonvini, S. Forte, S. Marzani, and G. Ridolfi, "Higgs production in gluon fusion beyond NNLO," *Nucl. Phys.* **B874** (2013) 746–772, arXiv:1303.3590 [hep-ph].

[84] M. Bonvini and S. Marzani, "Resummed Higgs cross section at N^3LL," *JHEP* **09** (2014) 007, arXiv:1405.3654 [hep-ph].

[85] E. Laenen, L. Magnea, and G. Stavenga, "On next-to-eikonal corrections to threshold resummation for the Drell-Yan and DIS cross sections," *Phys. Lett.* **B669** (2008) 173–179, arXiv:0807.4412 [hep-ph].

[86] E. Laenen, G. Stavenga, and C. D. White, "Path integral approach to eikonal and next-to-eikonal exponentiation," *JHEP* **0903** (2009) 054, arXiv:0811.2067 [hep-ph].

[87] S. Moch and A. Vogt, "On non-singlet physical evolution kernels and large-x coefficient functions in perturbative QCD," *JHEP* **11** (2009) 099, arXiv:0909.2124 [hep-ph].

[88] S. Moch and A. Vogt, "Threshold Resummation of the Structure Function F(L)," *JHEP* **04** (2009) 081, arXiv:0902.2342 [hep-ph].

[89] G. Grunberg and V. Ravindran, "On threshold resummation beyond leading 1-x order," *JHEP* **10** (2009) 055, arXiv:0902.2702 [hep-ph].

[90] L. Apolinário, N. Armesto, J. G. Milhano, and C. A. Salgado, "Medium-induced gluon radiation and colour decoherence beyond the soft approximation," *JHEP* **02** (2015) 119, arXiv:1407.0599 [hep-ph].

[91] A. A. Almasy, N. A. Lo Presti, and A. Vogt, "Generalized threshold resummation in inclusive DIS and semi-inclusive electron-positron annihilation," arXiv:1511.08612 [hep-ph].

[92] S. Weinberg, "Infrared photons and gravitons," *Phys. Rev.* **140** (1965) B516–B524.

[93] F. Cachazo and A. Strominger, "Evidence for a New Soft Graviton Theorem," arXiv:1404.4091 [hep-th].

[94] C. D. White, "Factorization Properties of Soft Graviton Amplitudes," *JHEP* **05** (2011) 060, arXiv:1103.2981 [hep-th].

[95] F. Cachazo and E. Y. Yuan, "Are Soft Theorems Renormalized?," arXiv:1405.3413 [hep-th].

[96] E. Casali, "Soft sub-leading divergences in Yang-Mills amplitudes," *JHEP* **08** (2014) 077, arXiv:1404.5551 [hep-th].

[97] Z. Bern, S. Davies, and J. Nohle, "On Loop Corrections to Subleading Soft Behavior of Gluons and Gravitons," *Phys.Rev.* **D90** no. 8, (2014) 085015, arXiv:1405.1015 [hep-th].

[98] H. Luo, P. Mastrolia, and W. J. Torres Bobadilla, "Subleading soft behavior of QCD amplitudes," *Phys. Rev.* **D91** no. 6, (2015) 065018, arXiv:1411.1669 [hep-th].

[99] A. J. Larkoski, "Conformal Invariance of the Subleading Soft Theorem in Gauge Theory," *Phys. Rev.* **D90** no. 8, (2014) 087701, arXiv:1405.2346 [hep-th].

[100] C. White, "Diagrammatic insights into next-to-soft corrections," *Phys.Lett.* **B737** (2014) 216–222, arXiv:1406.7184 [hep-th].

[101] Z. Bern, S. Davies, P. Di Vecchia, and J. Nohle, "Low-Energy Behavior of Gluons and Gravitons from Gauge Invariance," *Phys. Rev.* **D90** no. 8, (2014) 084035, arXiv:1406.6987 [hep-th].

[102] J. Broedel, M. de Leeuw, J. Plefka, and M. Rosso, "Constraining subleading soft gluon and graviton theorems," *Phys. Rev.* **D90** no. 6, (2014) 065024, arXiv:1406.6574 [hep-th].

[103] A. Brandhuber, E. Hughes, B. Spence, and G. Travaglini, "One-Loop Soft Theorems via Dual Superconformal Symmetry," arXiv:1511.06716 [hep-th].

[104] A. J. Larkoski, D. Neill, and I. W. Stewart, "Soft Theorems from Effective Field Theory," *JHEP* **06** (2015) 077, arXiv:1412.3108 [hep-th].

[105] D. R. Yennie, S. C. Frautschi, and H. Suura, "The infrared divergence phenomena and high-energy processes," *Annals Phys.* **13** (1961) 379–452.

[106] J. G. M. Gatheral, "Exponentiation of Eikonal Cross-sections in Nonabelian Gauge Theories," *Phys. Lett.* **B133** (1983) 90.

[107] J. Frenkel and J. C. Taylor, "Nonabelian Eikonal Exponentiation," *Nucl. Phys.* **B246** (1984) 231.

[108] E. Gardi, E. Laenen, G. Stavenga, and C. D. White, "Webs in multiparton scattering using the replica trick," *JHEP* **11** (2010) 155, arXiv:1008.0098 [hep-ph].

[109] C. D. White, "An Introduction to Webs," *J. Phys.* **G43** no. 3, (2016) 033002, arXiv:1507.02167 [hep-ph].

[110] T. O. Eynck, E. Laenen, and L. Magnea, "Exponentiation of the Drell-Yan cross-section near partonic threshold in the DIS and MS-bar schemes," *JHEP* **06** (2003) 057, arXiv:hep-ph/0305179 [hep-ph].

[111] E. Remiddi and J. A. M. Vermaseren, "Harmonic polylogarithms," *Int. J. Mod. Phys.* **A15** (2000) 725–754, arXiv:hep-ph/9905237 [hep-ph].

[112] T. H. Burnett and N. M. Kroll, "Extension of the low soft photon theorem," *Phys. Rev. Lett.* **20** (1968) 86.

[113] V. Del Duca, "High-energy bremsstrahlung theorems for soft photons," *Nucl. Phys.* **B345** (1990) 369–388.

[114] M. Beneke and V. A. Smirnov, "Asymptotic expansion of Feynman integrals near threshold," *Nucl.Phys.* **B522** (1998) 321–344, arXiv:hep-ph/9711391 [hep-ph].

[115] V. A. Smirnov, "Analytic tools for Feynman integrals," *Springer Tracts Mod. Phys.* **250** (2012) 1–296.

[116] B. Jantzen, "Foundation and generalization of the expansion by regions," *JHEP* **12** (2011) 076, arXiv:1111.2589 [hep-ph].

[117] V. A. Smirnov, "Asymptotic expansions in limits of large momenta and masses," *Commun. Math. Phys.* **134** (1990) 109–137.

[118] C. Anastasiou, C. Duhr, F. Dulat, F. Herzog, and B. Mistlberger, "Real-virtual contributions to the inclusive Higgs cross-section at N^3LO," *JHEP* **1312** (2013) 088, arXiv:1311.1425 [hep-ph].

[119] C. Anastasiou, C. Duhr, F. Dulat, F. Herzog, and B. Mistlberger, "Higgs Boson Gluon-Fusion Production in QCD at Three Loops," *Phys. Rev. Lett.* **114** (2015) 212001, arXiv:1503.06056 [hep-ph].

[120] T. Becher, M. Neubert, and G. Xu, "Dynamical Threshold Enhancement and Resummation in Drell-Yan Production," *JHEP* **07** (2008) 030, arXiv:0710.0680 [hep-ph].

[121] M. Beneke and T. Feldmann, "Factorization of heavy to light form-factors in soft collinear effective theory," *Nucl. Phys.* **B685** (2004) 249–296, arXiv:hep-ph/0311335 [hep-ph].

[122] A. Pak and A. Smirnov, "Geometric approach to asymptotic expansion of Feynman integrals," *Eur. Phys. J.* **C71** (2011) 1626, arXiv:1011.4863 [hep-ph].

[123] B. Jantzen, A. V. Smirnov, and V. A. Smirnov, "Expansion by regions: revealing potential and Glauber regions automatically," *Eur. Phys. J.* **C72** (2012) 2139, arXiv:1206.0546 [hep-ph].

[124] G. Grammer, Jr. and D. R. Yennie, "Improved treatment for the infrared divergence problem in quantum electrodynamics," *Phys. Rev.* **D8** (1973) 4332–4344.

[125] J. A. M. Vermaseren, A. Vogt, and S. Moch, "The Third-order QCD corrections to deep-inelastic scattering by photon exchange," *Nucl. Phys.* **B724** (2005) 3–182, arXiv:hep-ph/0504242 [hep-ph].

[126] A. Vogt, S. Moch, and J. Vermaseren, "The Three-loop splitting functions in QCD: The Singlet case," *Nucl.Phys.* **B691** (2004) 129–181, arXiv:hep-ph/0404111 [hep-ph].

[127] S. Moch, J. Vermaseren, and A. Vogt, "The Three loop splitting functions in QCD: The Nonsinglet case," *Nucl.Phys.* **B688** (2004) 101–134, arXiv:hep-ph/0403192 [hep-ph].

[128] S. Moch and J. A. M. Vermaseren, "Deep Inelastic Structure Functions at Two Loops," *Nucl. Phys.* **B573** (2000) 853–907, arXiv:hep-ph/9912355 [hep-ph].

[129] A. Mitov, "A New Method for Calculating Differential Distributions Directly in Mellin Space," *Phys. Lett.* **B643** (2006) 366–373, arXiv:hep-ph/0511340 [hep-ph].

[130] A. Mitov and S.-O. Moch, "QCD Corrections to Semi-Inclusive Hadron Production in Electron-Positron Annihilation at Two Loops," *Nucl. Phys.* **B751** (2006) 18–52, arXiv:hep-ph/0604160 [hep-ph].

[131] M. J. G. Veltman, "Diagrammatica: The Path to Feynman rules," *Cambridge Lect. Notes Phys.* **4** (1994) 1–284.

[132] J. A. M. Vermaseren, "Harmonic Sums, Mellin Transforms and Integrals," *Int. J. Mod. Phys.* **A14** (1999) 2037–2076, arXiv:hep-ph/9806280 [hep-ph].

[133] J. A. M. Vermaseren and S. Moch, "Mathematics for Structure Functions," *Nucl. Phys. Proc. Suppl.* **89** (2000) 131–136, arXiv:hep-ph/0004235 [hep-ph].

[134] J. M. Henn, "Lectures on differential equations for Feynman integrals," *J. Phys.* **A48** (2015) 153001, arXiv:1412.2296 [hep-ph].